***Model Membranes as a tool for biological studies and biosensor applications***

By

Kevin P. Armendariz

Submitted to the graduate degree program in Department of Chemisty and the Graduate Faculty of the University of Kansas in partial fulfillment of the requirements for the degree of Doctor of Philosophy.

_____

Chairperson: Dr. Robert Dunn

_____

Dr. Susan Lunte

_____

Dr. Craig Lunte

_____

Dr. Cindy Berrie

_____

Dr. Scott Hefty

Date Defended: 12/11/2013

The Dissertation Committee for Kevin P. Armendariz

certifies that this is the approved version of the following dissertation:

***Model Membranes as a tool for biological studies and biosensor applications***

_____

Chairperson: Dr. Robert Dunn

Date approved: 12/16/2013

***Model membranes as a tool for biological studies and biosensor applications***

By

Kevin P. Armendariz

## Abstract –

The biological membrane is a fundamental cellular structure which forms the natural selective barrier separating cells from their environment. Model membranes have long been employed to study these complicated structures in controlled environments. Within this dissertation we report the use of a defocused single molecule fluorescence imaging approach for examining the molecular level structure of model membranes which incorporate biological lipid components. Through these single molecule studies, an optimal single molecule probe of membrane structure was determined. Using this probe the influence of a minor biological membrane component, ganglioside GM1 (GM1), on membrane structure was examined. In addition to structural studies, we also report the use of model membranes as coatings for whispering gallery mode (WGM) label-free biosensors. Using Langmuir-Blodgett/Langmuir-Schaffer deposited bilayers we were able to demonstrate the specific detection of cholera toxin with a membrane containing the glycosphingolipid, GM1. Further studies of lipid coated WGM sensor showed polyethylene glycol (PEG) functionalized lipid bilayers are capable of reducing nonspecific adsorption on sensor surfaces while maintaining functional sites for specific analyte detection. Finally, preliminary studies for expanding the single molecule orientation approach to investigate antibody orientation on sensor surfaces are also reported. Through these studies the utility of both the defocused single molecule imaging technique and model membranes as a tool for biological and sensor applications is demonstrated.

**Acknowledgements –**

I would like to thank all to the past and current members of the of Dunn group who have contributed to the work presented in this dissertation. Thank you to Dr. Philip Livanec, Dr. Heath Huckabay, Sarah Borland (Wildgen), and Daniel Kim who have all contributed to co-authored publications. Thank you to my graduate advisor, Dr. Robert Dunn, for his contributions and guidance over the past five years. I would like to thank all of the professors and students at the University of Kansas who have shared their thoughts and time discussing chemistry and research with me.

I would like to thank those organizations that provided financial support for my research over the past five years including the KU Department of Chemistry, the NIH Dynamic Aspects of Chemical Biology Training Grant (T32 GM08545), the Bill and Melinda Gates Foundation, and the NSF (CBET 1133814).

Thank you to my mother and father, Susan and Jose Armendariz, and my mother and father-in-law, Kathie and John Coleman, for their encouragement and continued support over the years and their enthusiasm as I neared my goal.

Most of all I would like to thank my wife, Sarah. Her support, assistance, and patience through my graduate career have been pivotal to all my accomplishments. But most of all, thank you for being my best friend. I owe you everything.

**Dissertation Outline**

# Chapter 1: Introduction

## 1.1 - Biological membranes

Biological membranes serve a well-known and vital role within living organisms forming the natural selective barrier for individual cells. Not only do biological membranes separate a cell from its chemical and biological environment, but they are responsible for controlling communication across this boundary. This requires that the biological membrane be more than a simple barrier, but rather a complex structure which can regulate both transport and signaling across the barrier. Additionally, biological membranes also serve to compartmentalize organelles within the cell. Given the importance of biological membranes as a fundamental structural and functional element of living cells, membranes have been the subject of significant scientific investigation. For several decades researchers have studied biological and model systems to elucidate the principles which relate structure and function within cellular membranes.

Biological membranes are highly heterogeneous and dynamic structures which are composed of a wide assortment of lipids, proteins, and sterols. Together these components constitute the functional membranes observed in biology. The aggregation of these components into the formation of a membrane is largely driven by the hydrophobic effect, which is the known effect of nonpolar molecules in an aqueous environment to naturally aggregate to limit their surface area exposure to surrounding water molecules. Lipids are amphiphilic molecules which contain a nonpolar tailgroup and a polar headgroup, which spontaneously form lipid bilayers to limit unfavorable interactions between lipid tail groups and the surrounding aqueous environment. While lipid bilayers were originally thought to form a passive matrix for holding the protein components of biological membranes, it is now understood that lipids influence organization and events at the cellular membrane [1, 2].

Lipidomic studies have identified thousands of unique naturally occurring lipids incorporated into cellular membranes [3]. While all lipids are amphiphilic in nature, there is great structural diversity among naturally occurring lipids. These lipids contain various headgroups and tailgroups of numerous lengths and levels of saturation. An example of the utility of this lipid diversity is exemplified by two common lipid types, phosphatidylcholines and phosphatidylserines. These lipids are structurally different in that phosphatidylcholines contain zwitterionic headgroups, which overall carry no net charge, while phosphotidylserines contain negatively charged headgroups. Phosphatidylcholines are found within both leaflets of cell membranes, while phosphotidylserines are typically located on the inner leaflet of cell membranes in healthy cells. Phosphotidylserines begin to populate the outer leaflet of cell membranes following cellular apoptosis. When phosphotidylserines are presented on the outer surface of a cell, the cell is detected and degraded by macrophages [4]. Therefore, this example demonstrates how various lipid components can be utilized for signaling on the cell surface. **Table 1.1** demonstrates some of the structural diversity observed within naturally occurring biological membranes. This table also shows the percent composition of lipids with commonly occurring headgroups including phosphatidylcholine (PC), phosphatidylethanolamine

**Table 1.1 - Lipid Composition of Plasma and Subcellular Membranes**

| | Phospholipid Percentage | | | | | | | |
|---|---|---|---|---|---|---|---|---|
| | PC | PE | PS | PI | PA | CL | LGP | SM |
| Rectal Gland Plasma Membrane | 50.4 | 35.5 | 8.4 | <1 | | | | 5.7 |
| Brush border membrane | 33.3 | 35.6 | 7.4 | 8.2 | 1.2 | | 4.1 | 10.3 |
| Cholinergic receptor membranes | 37 | 40.6 | 17 | | <1 | | <1 | <1 |
| Plasma Membrane | 39 | 23 | 9 | 8 | 1 | 1 | 2 | 16 |
| Microsomes | 40 | 35 | 1 | 5 | | 18 | 1 | 1 |
| Mitochondria | 58 | 22 | 2 | 10 | 1 | 1 | 11 | 1 |
| Lysosomes | 40 | 14 | 2 | 5 | 1 | 1 | 7 | 20 |
| Nuclear Membrane | 55 | 13 | 3 | 10 | 2 | 4 | 3 | 3 |
| Gogli membrane | 50 | 20 | 6 | 12 | <1 | 1 | 3 | 8 |
| Sarcoplasmic reticulum | 72 | 13.5 | 1.8 | 8.7 | <1 | <1 | | 1 |

(PE), phosphatidylserine (PS), phosphatidylinositol (PI), phosphatidic acid (PA), cardiolipin (CL), lysoglycerophospholipid (LGP) and sphingomyelin (SM) from various types of membranes [5]. **Table. 1.1** shows how the lipid composition of plasma and subcellular membranes from different biological sources varies significantly [5]. Through this abundant diversity of lipids, cells are capable of fine tuning their membrane structure and functional properties.

Given the importance of the biological membrane, it has been the focus of countless studies, all of which cannot be recounted within the scope of this dissertation. One of the key studies which has helped shape the current understanding of membrane structure and function was the introduction of the fluid mosaic model of the lipid membrane. As described by Singer and Nicolson in 1972, this model described the lipid bilayer containing various proteins and other membrane components, which were free to move laterally within the membrane, shown in **Fig. 1.1** [6]. This structural fluidity within the membrane is vital for cellular transport and recognition. Following these studies the heterogeneous nature of membranes begun to be elucidated through several studies of model membranes. Various imaging techniques have demonstrated the formation of regions, termed domains, within the membrane which are enriched in certain membrane components while excluding others. Examples of the formation and imaging of these domains are recounted in several reviews [7-9]. The formation of these domains is not surprising, considering the complex mixture of lipids, proteins, and sterols which compose a biological membrane.

When considering the diverse array of molecular species comprising a biological membrane, it becomes evident that these complex matrices make it difficult to elucidate the functional role of individual molecular species within the membrane. Within a unique system the possible number of phases that may coexist is described by the Gibbs' Phase Rule:

$$P = C - F + 2 \qquad \textbf{Eq. 1.1}$$

where P describes the number of coexisting phases in equilibrium, C is the number of components, and F described degrees of freedom within the system. Therefore, given the abundant diversity of lipids, proteins, and sterols within biological membranes the possible phase complexity within the membrane becomes exceedingly high. In order to probe the functional role of individual biological components that comprise these membranes there is the need study them in simpler and more controlled systems. Thus, there has been a long standing history of utilizing model membranes to elucidate the structural and functional roles of individual membrane components.

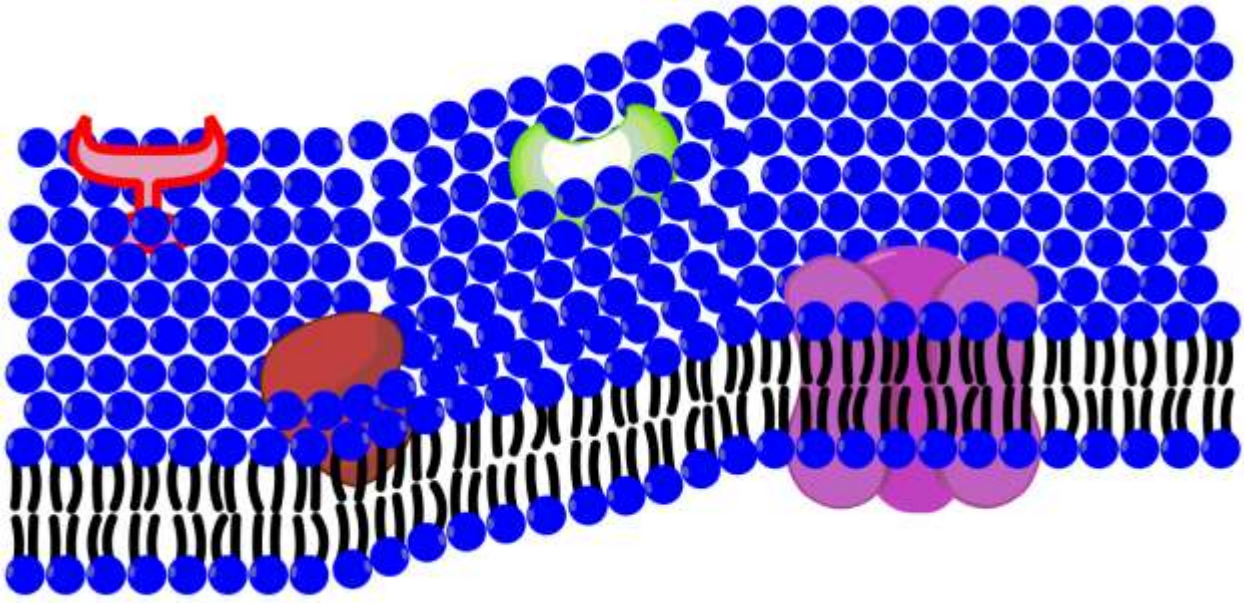

**Figure 1.1** –The fluid mosaic model of membrane structure proposes that the proteins and other membrane components are free to move laterally within a sea of lipids which comprises the biological membrane.

### 1.2 - Model Membranes

Model membranes can be fabricated through several well established techniques, including Langmuir-Blodgett (LB) deposition, Langmuir-Schaffer (LS) deposition, vesicle formation and fusion, and self-assembled monolayers (SAMs), all of which allow for control of

membrane composition. This control allows specific components of the membrane to be probed individually and more accurately than in biological systems. Thus, model membranes have been used extensively to elucidate the physical, chemical, and biological effect of membrane components.

Each of these techniques offers unique advantages for various research applications. For example, the Langmuir-Blodgett method not only allows a monolayer to be transferred to a solid substrate, but allows for control of thermodynamic parameters through temperature and surface pressure control during deposition. Other methods, such as vesicle fusion, also allow for the transfer of membranes to solid substrate. Vesicle fusion results in the transfer of a bilayer to a substrate resulting in a more relevant membrane model for many applications. Preparation of model membranes will be discussed in further detail in Chapter 2.

### 1.3- Studies of Biological Membranes

While the presence of domains within model membranes has been well established, there are proposed nanometric structures within biological membranes which have been difficult to probe. These domains, called lipid rafts, are proposed to be nanometric condensed domains within biological membranes, which are highly enriched in cholesterol. They are implicated in trafficking membrane proteins and cellular signaling, among other functions [10, 11]. Thus, the formation of lipid rafts in biological system is thought to contribute to complex structure of natural membranes which can regulate both transport and signaling across the cellular barrier.

Early evidence for possible lipid raft formation was reported as glycosylphosphatidylinositol (GPI)-anchored proteins were found to partition within membranes and form complexes [12, 13]. In 1997, Simons and Ikonen presented evidence for the formation of lipid rafts enriched in sphingolipids and cholesterol [1]. These domains were discovered by

their resistance to the detergent Triton x-100, and they provided evidence for the selective transport of proteins and intracellular signaling through lipid domain formation. These membrane heterogeneities became known as detergent resistant membranes (DRMs), which had been synonymous with the term lipid raft for many years. Further studies of DRM's found receptor proteins within these fractions leading to the conclusion that lipid rafts were specialized membrane domains associated in signaling events [14-17]. A schematic representation of the proposed lipid raft is shown in **Fig. 1.2.**

However, one issue which has caused considerable skepticism toward the lipid raft theory is related to difficulties visualizing raft formation in biological systems. In model systems, domains within lipid films can be generated on the microscopic scale and stabilized for long periods of time to allow them to be accurately measured [18]. However, in biological systems lipid rafts are proposed to exist on the nanometric scale on a timescale from tens to hundreds of milliseconds [19]. Thus, the dynamic nature and diminutive size of these domains have caused their existence and potential function to be highly debated[1, 10, 11, 18, 20, 21].

While obviously a valuable tool, the use of detergent extraction methods to isolate raft components has also contributed to some of the skepticism toward the lipid raft theory[11]. Several studies have used detergent resistance as the main criterion for raft associated activity of membrane components [22, 23]. Other methods identified raft components by treating membranes with cyclodextrin, which results in cholesterol depletion and lateral protein immobilization [24, 25]. Therefore, it is possible that these may have led to erroneous conclusions regarding the membrane components which contribute to raft formation. Thus, while it is presently common to not consider all DRMs as functional lipid rafts, in general lipid rafts exhibit detergent resistance. Given the significant biological implications of lipid rafts there have been significant research efforts toward further understanding their formation and composition.

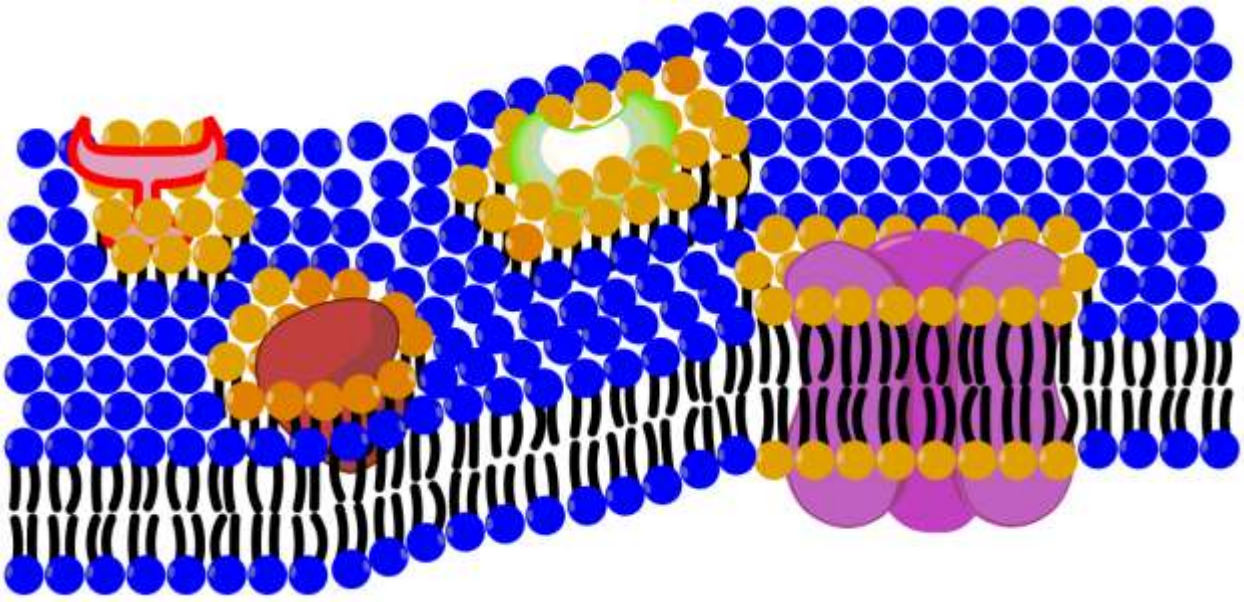

**Figure 1.2** – An artistic rendering of a lipid raft within a lipid bilayer is provided above. Within the bilayer condensed nanometric domains enriched in cholesterol and sphingomyelin, shown in orange, are capable of protein trafficking and affecting intracellular signaling.

### 1.4 - Methods for Membrane Interrogation

The biological significance and vast complexity exhibited by natural membranes has promoted significant research efforts of these structures for several decades utilizing a vast array of traditional techniques. These techniques encompass several imaging methods, such as fluorescence microscopy, atomic force microscopy (AFM) and electron microscopy (EM) as well as non-imaging methods, including nuclear magnetic resonance (NMR), calorimetry, and X-ray diffraction. Each of these techniques has proven useful for probing structural features of biological and model membranes. However, each method is not without its unique disadvantages as well.

For instance, electron microscopy provides far superior resolution relative to opitcal imaging techniques. The use of EM has provided several interesting findings regarding the structure and partitioning of various components within membranes [26-28]. A representative image from an EM study of model membranes containing ganglioside GM1, a minor natural membrane component, which has been labeled with cholera toxin is shown in **Fig. 1.3** [26]. The resolution provided by EM allows GM1/cholera toxin partitioning within the membrane to be examined. Unfortunately, a drawback to using EM is that the samples cannot be imaged at biological conditions. These samples are required to be placed in a vacuum and often times require staining. This detracts from the ability to relate findings made from EM studies to functioning biological systems.

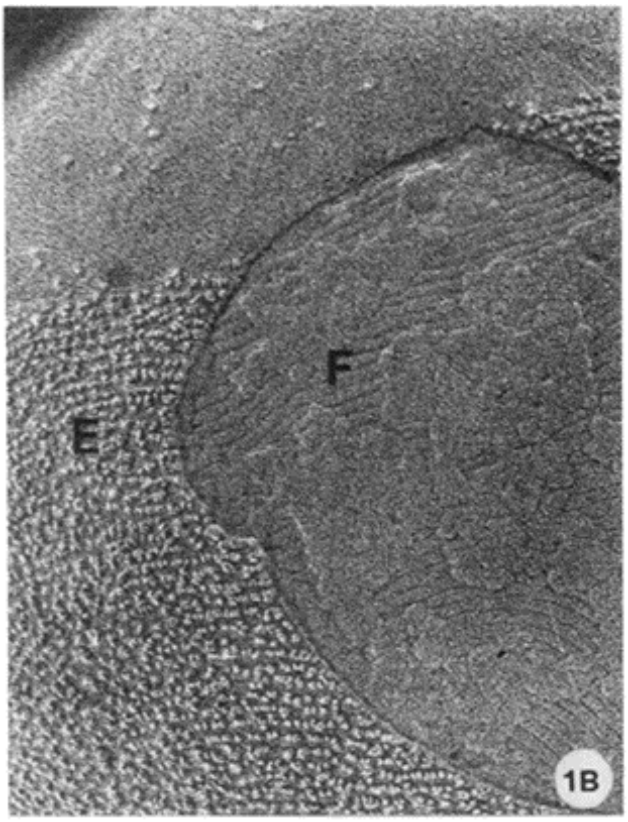


**Figure 1.3** – A freeze-etch micrograph of a liposome containing DEPC/DPPC (1:1) doped with 1.0 mol% GM1 and label with cholera toxin demonstrates that the GM1/cholera toxin partitions within gel phases (left, E) and exclude from liquid crystalline phase (right, F) within the film at a magnification of 130000x. Figure used with permission from Ref. [26].

Non-imaging techniques have also provided an important tool for probing membrane structure. As an example, x-ray diffraction measurements are often used to measure lipid tail in-plane ordering [29, 30]. Non-imaging methods are, however, somewhat limited by the inherent difficultly of monitoring the small structural perturbations of trace components within membranes. This limitation is due to the nature of the ensemble average approach of probing membrane structure. In the case of diffraction measurements, structural perturbations which do not induce changes in acyl-tail ordering within the film are not detected.

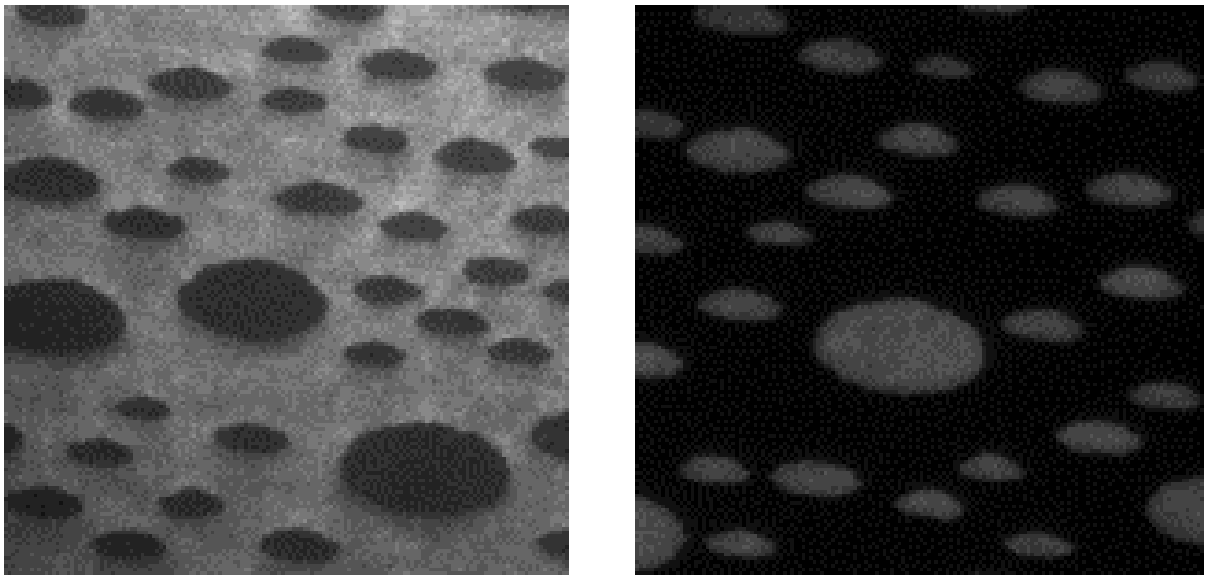

**Figure 1.4** – Fluorescence images of LB monolayers of DPPC / DOPC / cholesterol (1:1:0.1 mol%) containing a fluorescence lipid analog. The film on the left contains Texas Red – DHPE which marks the expanded (more fluid) phases within the monolayer. On the right, the film contains a BODIPY-linked cholesterol analog which partitions into and marks the condensed phases with the membrane. [Image collected by Brittney DeWitt, unpublished data]

Fluorescence microscopy, one of the most popular approaches for membrane studies, offers the ability to image live cells under biological conditions with a variety spectroscopic techniques. These studies have been particularly useful as numerous fluorescent lipid dyes have been identified which are known to partition preferentially into different membrane phase

[31]. Phase partitioning of lipid dyes within model membrane is demonstrated in **Fig. 1.4.** Several studies have been performed to identify how the microstructure within model membranes is influenced by membrane composition and environmental stress [32-34]. These studies typically monitor the evolution of phase structure within the membrane as the membrane is systematically perturbed. The role in membrane structure and function of various membrane components have been studied using this versatile technique.

As discussed, fluorescence microscopy has been tremendously useful for measuring structure and dynamics of microdomains within biological and model membranes. However, the major drawback associated with optical imaging approaches is limited resolution. The diffraction limit of light restricts the structural features which can be resolved to ~λ/2, or approximately 200 nm. While this resolution has been sufficient for several studies of membrane structure, it is highly restrictive when probing for nanometric domains, such as those associated with lipid rafts.

As such, several new imaging approaches with superior resolution capabilities have begun to be employed to further examine membrane heterogeneity. These include imaging techniques such as near field scanning optical microscopy (NSOM) which provides optical and topographical sub-diffraction limited resolution [35-38]. Additionally, super-resolution techniques such as stimulated emission depletion (STED) nanoscopy [39] and single molecule approaches including stochastic optical reconstruction microscopy (STORM) [40, 41] and photoactivated localization microscopy (PALM) [42] can provide 20-30nm spatial resolution of membrane components within the cellular membrane. Studies utilizing these methods have begun to provide further evidence which supports the lipid raft hypothesis. For instance, STED studies have shown that GPI-anchored proteins can become temporally trapped within ~20nm regions within cellular membranes, thereby providing substantial evidence for raft formation in biological systems [39].

Even before these new super resolution techniques became available numerous studies had been directed toward elucidating the function of lipid rafts within cellular membranes. Many of these studies suggested that lipid rafts sequester and traffic signaling proteins within the membrane giving them a significant biological role in intracellular communication [12-17]. For instance, there was early evidence which demonstrated that lipid rafts may play a role in T-cell receptor (TCR) signaling based on the findings that cross-linked GPI-anchored proteins, which do not span the entire membrane, could still simulate signaling [12]. Several further studies have supported these findings which suggest nanometric lipid heterogeneities are involved in TCR signaling [17, 43]. Furthermore, lipid raft formation is also implicated in protein trafficking and endocytosis. For example, these studies have found that transport vesicles were more selectively enriched in putative raft components, such as sterols and sphingolipids [44]. Additionally, certain membrane components which are associated with lipid rafts, such as ganglioside GM1, are well known receptors for toxins. Studies of these systems have suggested that a high density of receptors is required for multivalent toxins to bind and undergo endocytosis [45]. Therefore, as these studies and many others provide mounting evidence for lipid raft formation in biological systems, considerable interest remains as to how individual molecular species contribute to raft formation and stability within biological membranes.

### 1.5 - Motivation and Dissertation Overview

As previously discussed, there has been a longstanding and continued interest in the structural and functional role of individual membrane components and the biological membrane as a whole. These highly heterogeneous and dynamic structures have proven difficult to fully understand. While, numerous minor membrane components, such ganglioside GM1, have been implicated in raft formation, the findings regarding the full role of each component in raft

formation remain unresolved [32, 46, 47]. As single molecule approaches have proven to be a powerful tool for membrane structural investigations, this dissertation will present a molecular level imaging approach for measuring the orientation of lipid species within membranes which is capable of probing the structural effects of minor membrane components.

In addition to molecular level structural measurements of lipid films, this dissertation will also explore the utility of model membranes in biosensor applications. The ability to control composition and surface density provided by membrane deposition techniques permit the opportunity to functionalize biosensor surfaces in a measured manner. Applications of model membranes incorporating elements for analyte detection and membranes containing PEGylated lipids for limiting nonspecific absorption will be discussed. Furthermore, preliminary studies of single molecule orientations of antibodies will be explored for improving immobilization protocols for traditional immunoassays.

Chapter 2 will outline and discuss the instrumental methods used to perform the work presented in this dissertation and those relevant to membrane studies. In particular, the methods for creating model membranes, including Langmuir-Blodgett (LB) deposition, Langmuir-Schaffer (LS) deposition, and vesicle fusion, will be discussed. Traditional methods for membrane investigations will be reviewed, with a focus on bulk fluorescence microscopy. The approach for elucidating the three dimensional orientation of single fluorophores with defocused single molecule fluorescence imaging will be thoroughly addressed. Finally, the chapter will conclude with a brief overview of previous studies of single molecule orientations studies.

The use of acyl-linked fluorescent lipid analogs for studies of membrane structure will be the subject of Chapter 3. Specifically, this study will address the effect of fluorophore position along the acyl lipid tail of fluorescent lipid analogs in terms of their sensitivity to surrounding lipid

order. Through this study, an optimal probe of membrane order was identified for use in future studies. Additionally, this chapter will introduce the factors proposed to contribute to the insertion geometry of the fluorophore within the lipid matrix.

Chapter 3 and previous studies have demonstrated the utility of the single molecule approach for probing molecular level structure changes within model membranes [48-52]. These studies have validated the use of acyl-linked fluorescent lipid analogs for measuring structural perturbations within membranes due to surface pressure changes, membrane additives, and changes in ambient humidity [48-52]. Thus, Chapter 4 will utilize this method to evaluate the structural influence of a minor biological membrane component, ganglioside GM1 (GM1), within model membranes of DPPC. GM1 is a particularly interesting natural membrane component, typically comprising less than 0.1% of the total lipid content of a cellular membrane[53]. It is not only implicated in the formation lipid rafts, but it is also a known receptor for the bacterial toxin, cholera toxin [54]. Additionally, GM1 is known to have some unique physical properties within model membranes. For example, films comprised of only GM1 are completely fluid at all surface pressures [32]. However, in mixed membranes containing condensed phases, GM1 preferentially partitions within those phases which are more condensed at certain concentrations [32, 46, 47]. This obviously peculiar and interesting membrane component has been the subject of many membrane studies. Several of these have identified GM1 as being capable of significantly modulating microdomain structure within model films [32, 46, 47]. However, these studies observe this effect at unnaturally high GM1 concentrations. Therefore, the study discussed in Chapter 4 utilizes the single molecule approach to probe membrane order and determine the influence of GM1 at biologically relevant concentrations where bulk techniques are less informative.

Chapter 5 will introduce concepts for the application of synthetic membranes as functional coatings for label-free biosensors. In the past, there have been several examples for

utilizing self-assembled monolayers for various biosensing applications [55, 56]. These films offer the ability to incorporate antigen capture materials with the films for specific analyte detection. Langmuir films have been less popular, but are highly controllable in terms of composition and surface density and, thus, provide some potential advantages. The study presented in Chapter 5 utilizes bilayer membranes containing ganglioside GM1 to capture cholera toxin on the surface of a label-free biosensor platform. Within this section, the label-free, whispering gallery mode (WGM) biosensing platform will be briefly explained. The WGM platform was used to perform a GM1/cholera toxin binding study from which the binding constant was measured.

Chapter 6 will explore more advanced applications of model membranes in biosensing, as well as single molecule orientation measurement applications in biosensing. Traditionally, two of the primary issues plaguing label-free biosensors are loss of antibody activity and nonspecific binding. Antibody activity loss commonly occurs in immunoassays as a result of antibody immobilization [57-59]. One reason these antibodies become inactive is that they are immobilized with the active site of the antibody hidden from the sample matrix. To address this issue, Chapter 6 provides preliminary studies of single antibody orientations, which are intended to assist in correlating antibody orientation to binding efficiency. Additionally, a synthetic membrane approach for limiting nonspecific binding on label-free biosensors will be presented.

A summary of the findings from these studies along with future directions for these projects will conclude this dissertation in Chapter 7.

## 1.6 - References


1. Simons, K., and E. Ikonen. 1997. Functional rafts in cell membranes. Nature 387:569-572.

2. Field, K. A., D. Holowka, and B. Baird. 1995. Fc epsilon RI-mediated recruitment of p53/56lyn to detergent-resistant membrane domains accompanies cellular signaling. Proc. Nat. Acad. Sci. U.S.A. 92:9201-9205.

3. van Meer, G., D. R. Voelker, and G. W. Feigenson. 2008. Membrane lipids: where they are and how they behave. Nat. Rev. Mol.Cell Biol. 9:112-124.

4. Fadok, V. A., D. R. Voelker, P. A. Campbell, J. J. Cohen, D. L. Bratton, and P. M. Henson. 1992. Exposure of phosphatidylserine on the surface of apoptotic lymphocytes triggers specific recognition and removal by macrophages. J. Immunol. 148:2207-2216.

5. Yeagle, P. 1992. The Structrue of Biological Membranes. CRC Press, Inc., Boca Raton, FL.

6. Singer, S. J., and G. L. Nicolson. 1972. The fluid mosaic model of the structure of cell membranes. Science 175:720-731.

7. Brown, D. A., and E. London. 1998. Structure and Origin of Ordered Lipid Domains in Biological Membranes. J. Membrane Biol. 164:103-114.

8. Kaganer, V. M., H. Möhwald, and P. Dutta. 1999. Structure and phase transitions in Langmuir monolayers. Rev. Mod. Phys. 71:779-819.

9. McConnell, H. M. 1991. Structures and Transitions in Lipid Monolayers at the Air-Water Interface. Annu. Rev. Phys. Chem. 42:171-195.

10. Pike, L. J. 2006. Rafts defined: a report on the Keystone Symposium on Lipid Rafts and Cell Function. J. Lipid Res. 47:1597-1598.

11. Simons, K., and M. J. Gerl. 2010. Revitalizing membrane rafts: new tools and insights. Nature Reviews: Mol.Cell Biol. 11:688-699.

12. Štefanová, I., V. Hořejši, I. J. Ansotegui, W. Knapp, and H. Stockinger. 1991. GPI-Anchored Cell-Surface Molecules Complexed to Protein Tyrosine Kinases. Science 254:1016-1019.

13. Brown, D. A., and J. K. Rose. 1992. Sorting of GPI-anchored proteins to glycolipid-enriched membrane subdomains during transport to the apical cell surface. Cell 68:533-544.

14. Janes, P. W., S. C. Ley, A. I. Magee, and P. S. Kabouridis. 2000. The role of lipid rafts in T cell antigen receptor (TCR) signalling. Semin. Immunol. 12:23-34.

15. Langlet, C., A.-M. Bernard, P. Drevot, and H.-T. He. 2000. Membrane rafts and signaling by the multichain immune recognition receptors. Curr. Opin. Immunol. 12:250-255.

16. He, H.-T., and D. Marguet. 2008. T-cell antigen receptor triggering and lipid rafts: a matter of space and time scales. EMBO Rep. 9:525-530.

17. Sharma, P., R. Varma, R. C. Sarasij, Ira, K. Gousset, G. Krishnamoorthy, M. Rao, and S. Mayor. 2004. Nanoscale Organization of Multiple GPI-Anchored Proteins in Living Cell Membranes. Cell 116:577-589.

18. Shaw, A. S. 2006. Lipid rafts: now you see them, now you don't. Nat. Immunol. 7:1139-1142.

19. Lenne, P.-F., L. Wawrezinieck, F. Conchonaud, O. Wurtz, A. Boned, X.-J. Guo, H. Rigneault, H.-T. He, and D. Marguet. 2006. Dynamic molecular confinement in the plasma membrane by microdomains and the cytoskeleton meshwork. EMBO J. 25:3245-3256.

20. Dietrich, C., L. A. Bagatolli, Z. N. Volovyk, N. L. Thompson, M. Levi, K. Jacobson, and E. Gratton. 2001. Lipid rafts reconstituted in model membranes. Biophys. J. 80:1417-1428.

21. Munro, S. 2003. Lipid Rafts: Elusive or Illusive? Cell 115:377-388.

22. Lichtenberg, D., F. M. Goñi, and H. Heerklotz. 2005. Detergent-resistant membranes should not be identified with membrane rafts. Trends Biochem. Sci. 30:430-436.

23. Lingwood, D., and K. Simons. 2007. Detergent resistance as a tool in membrane research. Nat. Protoc. 2:2159+.

24. Kenworthy, A. K. 2008. Have we become overly reliant on lipid rafts? EMBO Rep. 9:531-535.

25. Shvartsman, D. E., O. Gutman, A. Tietz, and Y. I. Henis. 2006. Cyclodextrins but not compactin inhibit the lateral diffusion of membrane proteins independent of cholesterol. Traffic 7:917-926.

26. Rock, P., M. Allietta, W. W. Young, Jr., T. E. Thompson, and T. W. Tillack. 1991. Ganglioside GM1 and asialo-GM1 at low concentration are preferentially incorporated into the gel phase in two-component, two-phase phosphatidylcholine bilayers. Biochemistry 30:19-25.

27. Wagenknecht, T., R. Grassucci, J. Frank, A. Saito, M. Inui, and S. Fleischer. 1989. Three-dimensional architecture of the calcium channel/foot structure of sarcoplasmic reticulum. Nature 338:167-170.

28. Thompson, T. E., M. Aliietta, R. E. Brown, M. L. Johnson, and T. W. Tillack. 1985. Organization of ganglioside GM1 in phosphatidylcholine bilayers. Biochim. Biophys. Acta, Biomembr. 817:229-237.

29. Als-Nielsen, J., and K. Kjaer. 1989. X-ray reflectivity and diffraction studies of liquid surfaces and surfactant monolayers. NATO ASI Ser., Ser. B 211:113-138.

30. Jensen, T. R., and K. Kjaer. 2001. Structural properties and interactions of thin films at the air-liquid interface explored by synchrotron X-ray scattering. Stud. Interface Sci. 11:205-254.

31. Baumgart, T., G. Hunt, E. R. Farkas, W. W. Webb, and G. W. Feigenson. 2007. Fluorescence probe partitioning between Lo/Ld phases in lipid membranes. Biochim. Biophys. Acta, Biomembr. 1768:2182-2194.

32. Frey, S. L., E. Y. Chi, C. Arratia, J. Majewski, K. Kjaer, and K. Y. C. Lee. 2008. Condensing and fluidizing effects of ganglioside G(M1) on phospholipid films. Biophys. J. 94:3047-3064.

33. McConnell, H. M., L. K. Tamm, and R. M. Weis. 1984. Periodic structures in lipid monolayer phase transitions. Proc. Natl. Acad. Sci. U.S.A. 81:3249-3253.

34. Worthman, L. A., K. Nag, P. J. Davis, and K. M. Keough. 1997. Cholesterol in condensed and fluid phosphatidylcholine monolayers studied by epifluorescence microscopy. Biophys. J. 72:2569-2580.

35. Dickenson, N. E., K. P. Armendariz, H. A. Huckabay, P. W. Livanec, and R. C. Dunn. 2010. Near-field scanning optical microscopy: a tool for nanometric exploration of biological membranes. Anal. Bioanal. Chem. 396:31-43.

36. Dunn, R. C. 1999. Near-field scanning optical microscopy. Chem. Rev. 99:2891-2928.

37. Huckabay, H. A., K. P. Armendariz, W. H. Newhart, S. M. Wildgen, and R. C. Dunn. 2013. Near-field scanning optical microscopy for high-resolution membrane studies. Methods Mol. Biol. 950:373-394.

38. Burgos, P., C. Yuan, M.-L. Viriot, and L. J. Johnston. 2003. Two-Color Near-Field Fluorescence Microscopy Studies of Microdomains (“Rafts”) in Model Membranes. Langmuir 19:8002-8009.

39. Eggeling, C., C. Ringemann, R. Medda, G. Schwarzmann, K. Sandhoff, S. Polyakova, V. N. Belov, B. Hein, C. von Middendorff, A. Schonle, and S. W. Hell. 2009. Direct observation of the nanoscale dynamics of membrane lipids in a living cell. Nature 457:1159-1162.

40. Rust, M. J., M. Bates, and Z. Xiaowei. 2006. Sub-diffraction-limit imaging by stochastic optical reconstruction microscopy (STORM). Nat. Meth. 3:793-796.

41. Jones, S. A., S.-H. Shim, J. He, and X. Zhuang. 2011. Fast, three-dimensional super-resolution imaging of live cells. Nat. Meth. 8:499-505.

42. Shroff, H., C. G. Galbraith, J. A. Galbraith, and E. Betzig. 2008. Live-cell photoactivated localization microscopy of nanoscale adhesion dynamics. Nat. Meth. 5:417-423.

43. Nika, K., C. Soldani, M. Salek, W. Paster, A. Gray, R. Etzensperger, L. Fugger, P. Polzella, V. Cerundolo, O. Dushek, T. Höfer, A. Viola, and O. Acuto. 2010. Constitutively Active Lck Kinase in T Cells Drives Antigen Receptor Signal Transduction. Immunity 32:766-777.

44. Klemm, R. W., C. S. Ejsing, M. A. Surma, H.-J. Kaiser, M. J. Gerl, J. L. Sampaio, Q. de Robillard, C. Ferguson, T. J. Proszynski, A. Shevchenko, and K. Simons. 2009. Segregation of sphingolipids and sterols during formation of secretory vesicles at the trans-Golgi network. J. Cell Biol. 185:601-612.

45. Ewers, H., W. Romer, A. E. Smith, K. Bacia, S. Dmitrieff, W. Chai, R. Mancini, J. Kartenbeck, V. Chambon, L. Berland, A. Oppenheim, G. Schwarzmann, T. Feizi, P. Schwille, P. Sens, A. Helenius, and L. Johannes. 2010. GM1 structure determines SV40-induced membrane invagination and infection. Nat. Cell Biol. 12:11-18.

46. Burns, A. R. 2003. Domain structure in model membrane bilayers investigated by simultaneous atomic force microscopy and fluorescence imaging. Langmuir 19:8358-8363.

47. Vie, V., N. Van Mau, E. Lesniewska, J. P. Goudonnet, F. Heitz, and C. Le Grimellec. 1998. Distribution of ganglioside G(M1) between two-component, two-phase phosphatidylcholine monolayers. Langmuir 14:4574-4583.

48. Armendariz, K. P., H. A. Huckabay, P. W. Livanec, and R. C. Dunn. 2012. Single molecule probes of membrane structure: Orientation of BODIPY probes in DPPC as a function of probe structure. Analyst 137:1402-1408.

49. Huckabay, H. A., and R. C. Dunn. 2011. Hydration Effects on Membrane Structure Probed by Single Molecule Orientations. Langmuir 27:2658-2666.

50. Livanec, P. W., and R. C. Dunn. 2008. Single-molecule probes of lipid membrane structure. Langmuir 24:14066-14073.

51. Livanec, P. W., H. A. Huckabay, and R. C. Dunn. 2009. Exploring the effects of sterols in model lipid membranes using single-molecule orientations. J. Phys. Chem. B 113:10240-10248.

52. Song, K. C., P. W. Livanec, J. B. Klauda, K. Kuczera, R. C. Dunn, and W. Im. 2011. Orientation of fluorescent lipid analogue BODIPY-PC to probe lipid membrane properties: insights from molecular dynamics simulations. J. Phys. Chem. B 115:6157-6165.

53. Sonnino, S., L. Mauri, V. Chigorno, and A. Prinetti. 2007. Gangliosides as components of lipid membrane domains. Glycobiology 17:1R-13R.

54. Reed, R. A., J. Mattai, and G. G. Shipley. 1987. Interaction of cholera toxin with ganglioside GM1 receptors in supported lipid monolayers. Biochemistry 26:824-832.

55. Silin, V., H. Weetall, and D. J. Vanderah. 1997. SPR Studies of the Nonspecific Adsorption Kinetics of Human IgG and BSA on Gold Surfaces Modified by Self-Assembled Monolayers (SAMs). Journal of Colloid and Interface Science 185:94-103.

56. Senaratne, W., L. Andruzzi, and C. K. Ober. 2005. Self-Assembled Monolayers and Polymer Brushes in Biotechnology: Current Applications and Future Perspectives. Biomacromolecules 6:2427-2448.

57. Wild, D. 2001. The Immunoassay handbook. Nature Pub. Group, London.

58. Herron JN, W. H.-K., Janatová V, Durtschi JD, Caldwell KD, Christensen DA, Chang I-N, Huang S-C. 2003. Orientation and Activity of Immobilized Antibodies. In Biopolymers at Interfaces. M. M, editor. Marcel Dekker, New York. 115-163.

59. Jung, Y., J. Y. Jeong, and B. H. Chung. 2008. Recent advances in immobilization methods of antibodies on solid supports. Analyst 133:697-701.

# Chapter 2: Methods and Instrumentation for Membrane Investigations

## 2.1 - Introduction

This chapter will review the methods for the fabrication of model membranes and the instrumental methods utilized to perform the studies within this dissertation. First, methods for monolayer and bilayer membrane fabrication and transfer to solid substrates will be discussed. Second, an introduction to bulk fluorescence microscopy techniques for evaluating the microstructure within model membranes will be provided. While bulk fluorescent techniques have a proven track record of providing important findings regarding membrane structure and dynamics under biological conditions; these techniques are restricted in their information content due to limited spatial resolution. As discussed in Chapter 1, new microscopy techniques, such as STED, STORM, and PALM, provide promising alternative approaches to membrane investigation through superior resolution and by tracking individual molecules within the membrane. This has provided motivation for the development a single molecule approach allowing for orientation measurements of individual molecules within membranes.

## 2.2 – Membrane fabrication methods

The most fundamental structure of the cellular membrane is formed by a bilayer of lipid molecules. As such, there are several well-established methods which can be employed to reliably generate model lipid membranes for research purposes. The ability to form natural and model membranes is a result of the amphiphilic nature of lipid species in a surrounding aqueous environment.

Lipid molecules are amphipathic in structure, containing a hydrophilic headgroup and a hydrophobic tailgroup. Typically, the lipid headgroup is composed of a phosphate, an amine, or

an alcohol, while the tailgroup is composed of long hydrocarbon chain. The formation of a lipid bilayer is naturally driven by the hydrophobic effect mostly due to entropic contributions [1]. The insertion of a hydrophobic lipid tailgroup within surrounding water molecules has an associated free energy cost. In order to accommodate the hydrocarbon structure within water, the hydrogen bonding network within the water must be rebuilt around the hydrocarbon chain, essentially forming a cage. The formation of these cages limits the freedom of hydrogen bonding networks forming within the water, which is entropically unfavorable. Additionally, the polar headgroups of lipid molecules can contribute to the aqueous hydrogen bonding network, which is enthalpically favorable. Therefore, lipid molecules in an aqueous environment spontaneous orient the polar headgroups toward aqueous phases and tailgroups away from aqueous phases. Thus, it is the amphipathic nature of lipid molecules in an aqueous environment which induces the spontaneous formation of lipid monolayers, bilayers, liposomes, and vesicles.

Investigations of the controlled formation of model membranes can be traced back nearly 100 years to the work of Irving Langmuir. In 1917, Langmuir published findings of hydrophobic molecules effects on surface tension [2]. In this publication he utilized a device, now known as a Langmuir trough, which contained a water bath, a movable barrier, and pressure sensor. As others had previously shown, amphipathic molecules dispersed on the water bath become trapped at the air-water interface. With the trough, Langmuir was able to show that these trapped lipid molecules could be compressed with a movable barrier and that the surface tension of the liquid would decrease. He theorized that these films constituted a single layer of molecules which oriented hydrophobic tail groups of amphipathic molecules away from the water interface. In 1932, Dr. Langmuir was awarded the Noble Prize in chemistry for his contributions based on this work. In 1934, Katharine Blodgett demonstrated that these monolayer films could be controllably transferred onto a solid substrate by slowly moving the

substrate through the air-water interface [3, 4]. This process is illustrated in **Fig 2.1** as the lipid molecules trapped at an air-water interface are deposited onto a glass slide. This technique, now known as Langmuir-Blodgett transfer, continues to be used extensively to create monolayer and multilayer films that mimic biological membranes.

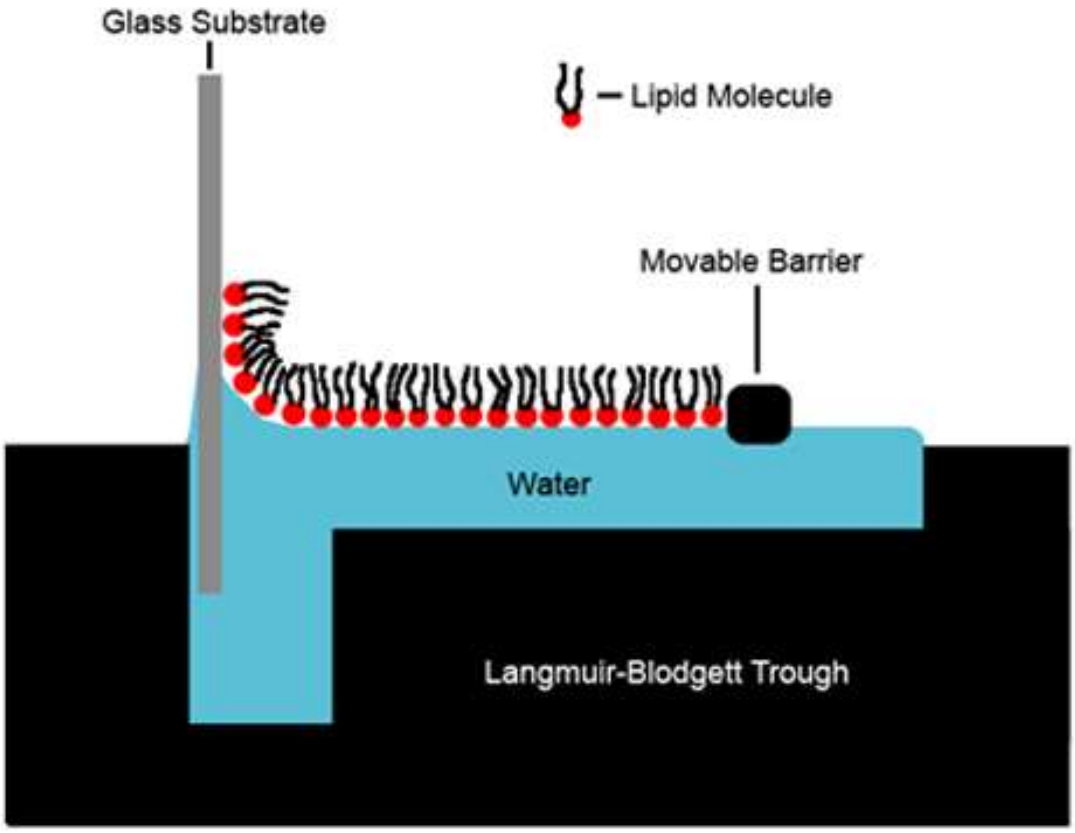


**Figure 2.1** – Langmuir-Blodgett deposition of lipid molecules on to a glass substrate is illustrated above. Lipid molecules trapped at the air-water interface on the trough are transferred to the substrate by pulling it slowly through the water sub-phase while maintaining a constant surface pressure with a movable barrier.

Over the years the instrumentation for creating Langmuir-Blodgett (LB) films has advanced, however the principle components from Langmuir's original device have remained unchanged. **Figure 2.2** illustrates a modern Langmuir-Blodgett trough for transferring lipids onto a solid substrate. The LB trough contains a water bath held in a polytetrafluoroethylene

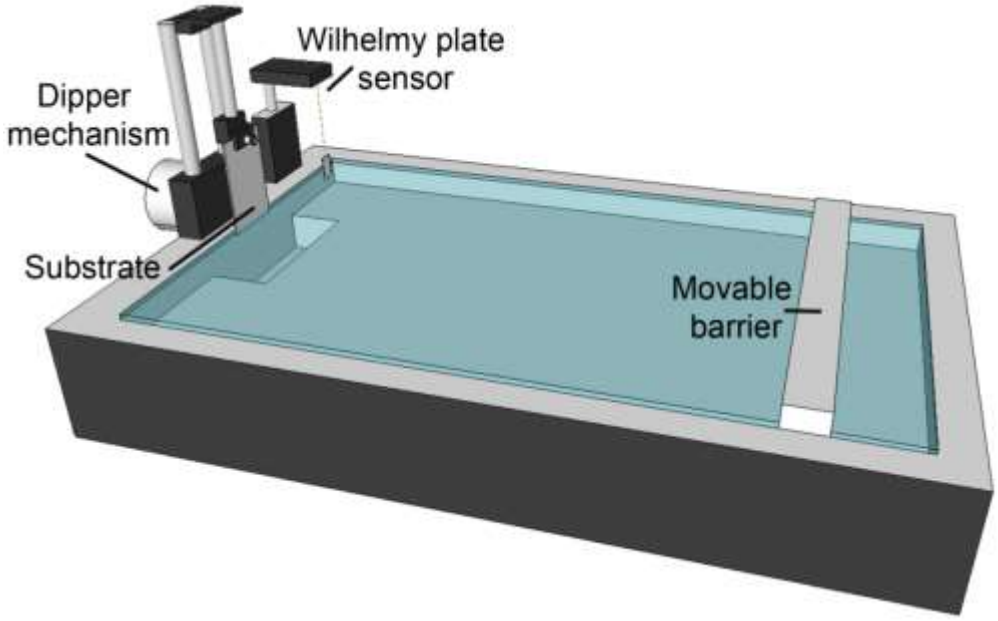


**Figure 2.2** – The Langmuir-Blodgett (LB) trough is commonly used to generate model lipid films. The key components include a PTFE lined exterior for holding a water bath, a movable barrier, a dipper mechanism, and a Wilhelmy plate pressure sensor. The barrier position is controlled by a computer which works in a feedback loop with the pressure sensor for maintaining surface pressure control.

(PTFE) container, a motorized movable barrier, Wilhelmy plate pressure sensor, and a dipping mechanism. For typical hydrophilic substrates, such as glass, the substrate should be lowered into the water prior to dispersing lipids onto the trough. Lipid molecules are dispersed on the water in a volatile solvent, which is allowed to evaporate. The lipid molecules trapped at the air-water interface can be compressed with the barrier to a desired surface pressure, which is measured by the Wilhelmy plate sensor. The monolayer formed on the air-water interface can then be deposited onto a solid substrate by slowly pulling it through the air-water interface while maintaining a constant surface pressure. Surface pressure is described by:

$$\Pi = \Upsilon_0 - \Upsilon \qquad \textbf{Eq. 2.1}$$

where surface pressure (Π) is the difference of the surface tension of the subphase ($Y_0$) in the absence of a monolayer and the surface tension of monolayer present (Y).

Prior to the deposition of a lipid film onto a substrate, it is routine to anneal the film by subjecting it an isotherm cycle, where the film is slowly compressed and expanded with the movable barrier. During these isotherm cycles, the surface pressure is monitored by a Wilhelmy plate pressure sensor. The measured change in surface pressure for a typical membrane lipid, DPPC, during an isotherm cycle is shown in **Fig. 2.3**. The isotherm shown in **Fig 2.3** demonstrates that DPPC undergoes phase transitions which can be observed by the plateau region in the pressure-area isotherm occurring at approximately 7 mN/m. At surface pressures below this region, each lipid molecule at the air-water interface experiences freedom of motion and orientation, in what is termed the liquid expanded (LE) phase. As the barrier is compressed the lipid molecules undergo several phase transitions as the area per molecule is decreased and freedom of motion and orientation of each lipid is restricted [5, 6]. At surface pressures above the plateau region, the lipid molecules are ordered with their acyl tail oriented away from the water interface. This ordered state is termed the liquid condensed (LC) phase. At intermediate surface pressures along the plateau region of the pressure-area isotherm these LE and LC phases coexist and can be measured by a variety of techniques. Additionally, there are other membrane phases accessible at very high surface pressures, which are not shown in **Fig. 2.3**. At these high surface pressures, lipid films transition to the solid condensed (SC) state. Eventually the membrane will collapse by folding and/or fracturing if enough pressure is applied and the membrane can no longer fit all of the membrane components within the compressed film [7, 8]. A monolayer can be transferred to a substrate at any of these measured surface pressures by maintaining a constant surface pressure through computer feedback control as the substrate is drawn through the air-water interface. Langmuir and Langmuir-Blodgett films have proven enormously useful for creating controllable lipid films for scientific studies. These films are simple to fabricate and film composition, temperature, and surface pressure can be easily controlled. Given these attributes, LB films have been widely employed to study membrane structure.

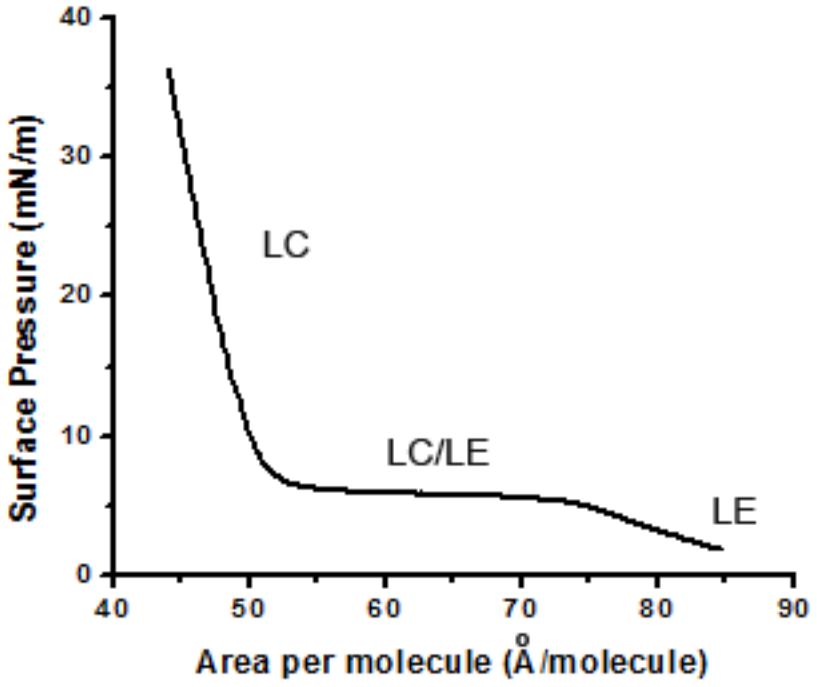


**Figure 2.3** – A pressure-area isotherm of DPPC monolayer. As the area per molecule is reduced the lipid molecules undergo a phase change from liquid expanded (LE) to liquid condensed (LC) with an intermediate region of phase coexistence (LC/LE) between the two extremes.

Methods have also been developed to fabricate bilayer membranes, which are a more accurate mimic of the cellular bilayer. One method for bilayer formation is Langmuir-Schaffer (LS) transfer, which is an extension of the LB technique [9, 10]. This method uses a hydrophobic substrate to transfer lipids from a Langmuir trough to a substrate in a tail-down geometry relative to the substrate. To create a lipid bilayer using the LS method, an LB monolayer is first formed on a substrate as discussed above. This deposited LB monolayer is oriented in a head-down geometry relative the substrate, as shown in **Fig. 2.2**. With the attached LB film, this surface is hydrophobic as the lipid tailgroups are oriented away from the substrate. The substrate is rotated such that the hydrophobic surface is directed toward the trough air-water interface. The hydrophobic surface is then lightly touched with another monolayer on the air-water interface, such that the tailgroups of each monolayer are in contact.

The substrate is gently lifted off the water surface transferring a second layer of lipids to the substrate and forming a bilayer.

Another method for transferring bilayers onto solid substrates uses the formation of lipid vesicles in solution. For the purposes of this work we will only be concerned with those methods for the formation of bilayers on solid substrates. Vesicle fusion is one method often used for bilayer formation on a substrate [11-13]. In this method, lipid multilamellar vesicles are first formed from dried lipids hydrated with an aqueous medium. These mutli-walled vesicles are then sonicated to form small unilamellar vesicles (SUVs), which can be fused to hydrophilic surfaces at elevated temperatures to form a lipid bilayer.

Each of these membrane fabrication methods have been employed in investigations of membrane structure utilizing the single molecule orientation approach [14-17]. In this dissertation, the single molecule studies presented in Chapters 3 and 4 utilize the LB method for monolayer generation. Previous studies of single molecule orientations have demonstrated that the packing density and structure within monolayer membranes deposited at the equivalent surface pressure measured in bilayers provide a more realistic mimic of model bilayer membrane structure [16]. Thus, the study of biological membrane components' effect on membrane structure presented in Chapter 4 are performed on monolayers deposited at 23 mN/m, the measured equivalent surface pressure in bilayers from previous single molecule studies. The LS method is used extensively in Chapters 5 and 6 to create controlled bilayers for biosensing applications.

### 2.3 – Fluorescence microscopy

Fluorescence microscopy is one of the most useful and versatile techniques for membrane investigations. This technique measures light emitted from fluorescent lipid analogs

within membranes. This technique is flexible as biological or model samples can be imaged under biological conditions on an air-water interface or when immobilized on a solid substrate. Furthermore, numerous fluorescence based techniques have been developed, which have proven useful for membrane studies. These techniques include fluorescent lifetime (FLIM) [18, 19], fluorescence recovery after photobleaching (FRAP) [20], fluorescence resonance energy transfer (FRET) [19, 21, 22], fluorescence polarization [23, 24], time-resolved fluorescence [25], and spectroscopy measurements [26].

Fluorescence microscopy is employed in several of the studies in the following chapters to elucidate the structure of model membranes given its broad utility and ease of use. However, the main disadvantage of optical techniques is limited resolution. As first theorized by Ernst Abbe in 1873, there is a limit to the spot size which light can focused through a lens[27]. For a particular wavelength of light, this spot size is limited by the numerical aperture of the lens, as described by:

$$d = \frac{\lambda}{2\, n\, sin\theta} \qquad \textbf{Eq - 2.1}$$

where the diameter of the spot size, *d*, is a function of the wavelength of light, *λ*, and the numerical aperture (NA) of the objective, which is described by the refractive index of the objective (n) and the half-angle of the maximum cone for light entering or exiting the objective (θ). At the spot which the light is focused, a diffraction pattern is generated, known as the Airy disk pattern, which is shown in **Fig. 2.4** [28]. Therefore, the resolution capability of an optical lens is limited by the inability to accurately identify two such spots in close proximately to one another. It is generally accepted that in order to resolve two spots they must be separated by a distance, known as the Rayleigh criterion, equal to or greater than the diameter of an individual spot or approximately λ/2 [29]. As shown in the center of **Fig**. **2.4**, overlapping spots in an image can be resolved when they are separated by a sufficient distance. When the distance

between these spots is less than λ/2, as shown on the right in **Fig. 2.4,** each spot cannot be individually resolved. So, even with a perfect lens, resolution for visible light microscopy is limited to approximately 200 nm. The example images shown in **Fig. 2.4** have an excellent signal-to-noise ratio, and thus the Rayleigh criterion approximation of ~λ/2 is valid. However, in images where signal-to-noise ratio is low the distance required to sufficiently resolves two spots in an images may be considerably greater than λ/2.

**Figure 2.4** – Above left is an illustration of the diffraction pattern formed from point source of light being focused onto an imaging plane. The resulting diffraction pattern, known as an Airy disc pattern, has a central maximum intensity distribution surrounded by concentric rings of successively decreasing intensity. Each spot must be separated by a distance equal or greater than the Rayleigh criterion, or ~λ/2, in order to resolve each spot, as shown in the middle. Spots separated by a distance less than the Rayleigh criterion cannot be resolved, as shown on the right.

While the fluorescence approach has been a popular tool for membrane investigations, several alternative imaging techniques with superior resolution capabilities have provided further insight into membrane structure. An example of ganglioside GM1/cholera toxin partitioning with a membrane as studied by EM was shown Chapter 1 [30]. However, EM techniques require that samples be examined under vacuum and often require staining, which detracts from the biological relevance of these studies. Other techniques, such as AFM, have shown that there are resolvable submicron domains within model membrane bilayers which are beyond the resolution of traditional optical techniques [31, 32]. However, these AFM studies typically rely upon topography measurements which lack chemical specificity. Super-resolution fluorescence techniques, including near field scanning optical microscopy (NSOM) [31, 33-35] and stimulated

emission depletion (STED) [36, 37] microscopy have also been employed in studies of membrane structure. NSOM and STED have allowed for optical measurements of membranes with optical resolution nearly an order of magnitude beyond the diffraction limit. However, these techniques are also not without their disadvantages. Similar to other fluorescence techniques, STED requires significant dye concentrations which can perturb the structure within membrane films. NSOM, like other scanning probe techniques, is limited in terms of time resolution and difficult to implement with biological samples. While each of these techniques has offered valuable insight in membrane studies, each technique, with the exception of NSOM, provides as ensemble-averaged view of membrane structure.

This has motivated the development of single molecule approaches for structural studies in membranes. By monitoring individual molecules the information content provided reveals molecular level detail, which can be hidden in bulk measurements. For example, single-particle tracking (SPT) techniques have provided access to information on the mobility of individual molecules within a membrane [38, 39]. This has allowed distinct components within the membranes to be measured individually and identified based on their unique diffusion constant within the film. Prior to these SPT techniques, fluorescence recovery after photobleaching (FRAP) was used to determine lateral mobility within membranes yielding an ensemble-averaged diffusion constant [40]. Other single molecule techniques such as PALM and STORM have further demonstrate the utility of single molecule approaches for tracking protein density, spatial organization, and the presence of protein clusters in membranes [41-43]. Clearly, these single molecule approaches allow molecular level heterogeneities to be probed more accurately than ensemble-averaged measurements. As such, this has motivated the development of advanced imaging methodologies which allow three-dimensional structural information from individual molecules to be extracted.

## 2.4 Defocused Fluorescence Imaging of Single Molecule Orientations

Single molecule fluorescence measurements require that light emitted from a single fluorophore be captured by a sensitive photodetector. This has been made possible with the advent of high numerical aperture (NA) objectives and modern optical detectors. High NA objectives are capable of accepting light entering the objective at higher angles and thus capture more light emitted from the sample. Additionally, sensitive photodetectors, such as EMCCDs, provide high quantum efficiency and low noise, which allow the fluorescence emission from single molecules to be detected and spatially resolved. The fluorescence emission for individual fluorescent lipid analogs doped into a model membrane is demonstrated in **Fig. 2.5**. The ability to measure single molecule emission has led to the advancement of imaging techniques for extracting the three-dimensional orientation of individual molecules through defocused imaging, which is discussed below.

In order to understand how the three-dimensional orientation of an individual molecule can be measured from a defocused image, first consider the emission dipole of a fluorophore. The emission dipole of a single fluorophore typically lies along the long axis of the conjugated bond system of the molecule as shown in **Fig. 2.6.** For example, the BODIPY fluorophore, which is employed in studies discussed in Chapters 3 and 4, has been shown to have a ~13º difference between absorption and emission dipoles [44]. In free space, the fluorescence emission from an individual fluorophore occurs in a $\sin^2$ pattern about the emission dipole[28]. This pattern becomes distorted if the emitting fluorophore is brought near an interface of higher refractive index [45-47], as shown in **Fig. 2.6**. The light entering this interface does so at various angles dependent upon the orientation of the emission dipole relative to the surface, as shown in **Fig. 2.7**. Therefore, the light coupled into the collection optics of a microscope from an individual fluorophore has an angle dependency based upon on its emission dipole orientation relative to

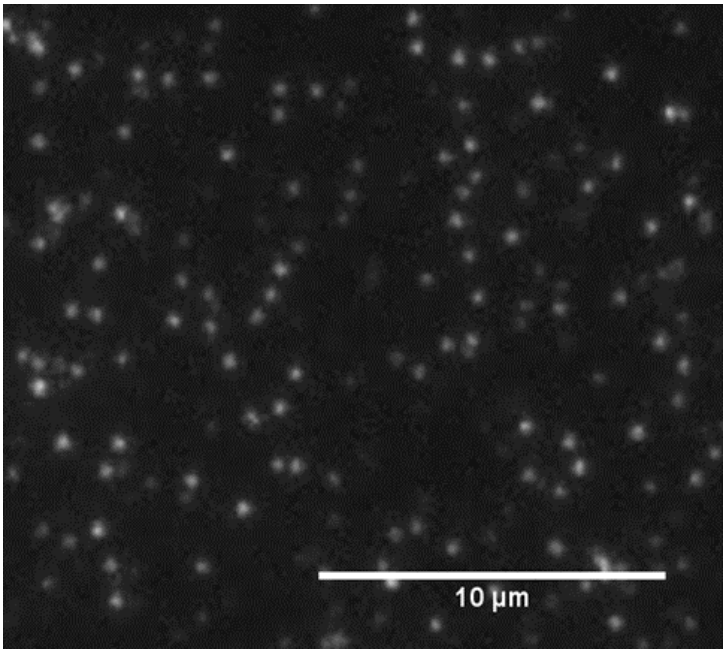


**Figure 2.5** – The fluorescence emission from individual molecules of a fluorescent lipid analog, BODIPY-PC, doped at trace levels into a monolayer of DPPC deposited at 30 mN/m can be clearly resolved with a sufficient signal-to-noise ratio.

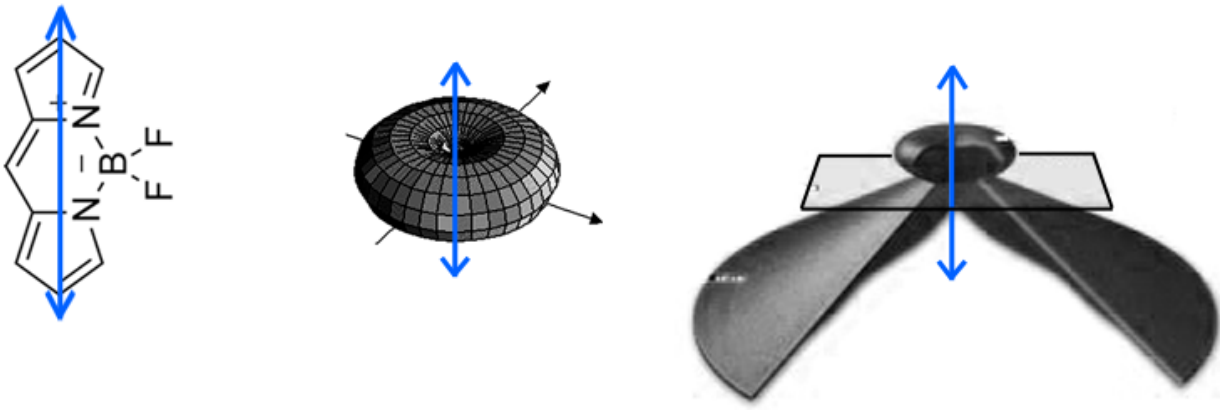


**Figure 2.6** – Above is a schematic representation of the fluorescence emission from a single molecule. As shown on the left, the emission dipole (blue line) lies approximately along the long axis of the fluorophore. In free space the emission pattern from a single fluorophore is in a $\sin^2$ pattern about the emission dipole, as shown in the center. When a fluorophore is near an interface of higher refractive index, the emission pattern of light passing through that interface becomes distorted, as shown on the right.

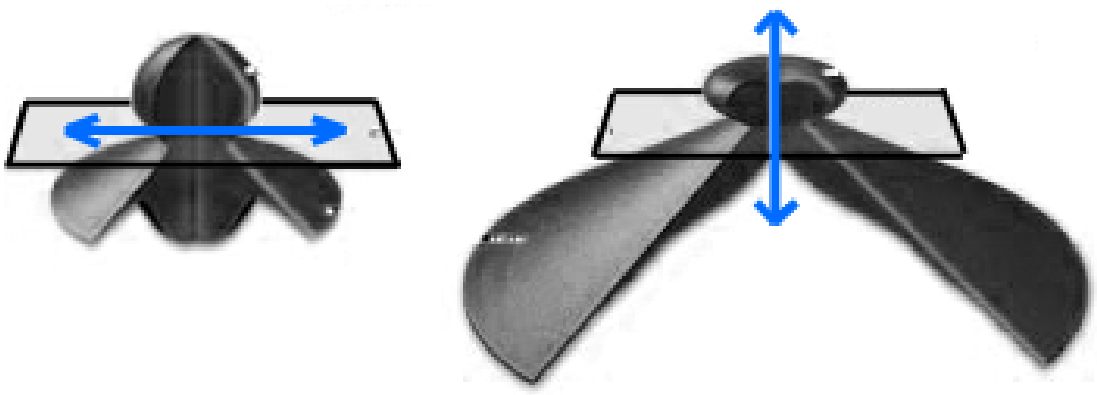

**Figure 2.7** – When near an interface of higher refractive index, light from an individual fluorophore is coupled into the interface a various angles dependent upon the orientation of the fluorophore relative to the interface. Examples of two extreme cases are illustrated above. When the emission dipole (blue line) is parallel to the interface, light couples into the interface at low angles, as shown on the left. When the emission dipole is perpendicular to the interface, light couples into the interface at high angles, as shown on the right.

the imaging surface. This phenomenon allows the orientation of individual molecules to be measured through an imaging method.

While this coupling angle phenomenon will be useful for imaging single molecule orientations, it is important to note that modern microscope objectives are corrected for problems caused by multiple coupling angles in traditional images. In typical microscopy optics, it is desirable that light emanating from a single point in the sample plane be focused to a single point on the imaging plane regardless of the angle with which it enters the microscope objective. When an objective is not corrected for this coupling angle issue, the objective is said to have spherical aberrations. An objective which has spherical aberrations does not effectively focus light entering the optics train at various angles from a point on the sample plane to a single point on the imaging plane, as shown in **Fig. 2.8** [27]. Traditional fluorescent samples imaged with an objective with spherical aberrations will appear blurry. Therefore, while it is obviously advantageous to correct for spherical aberrations in traditional imaging applications, spherical

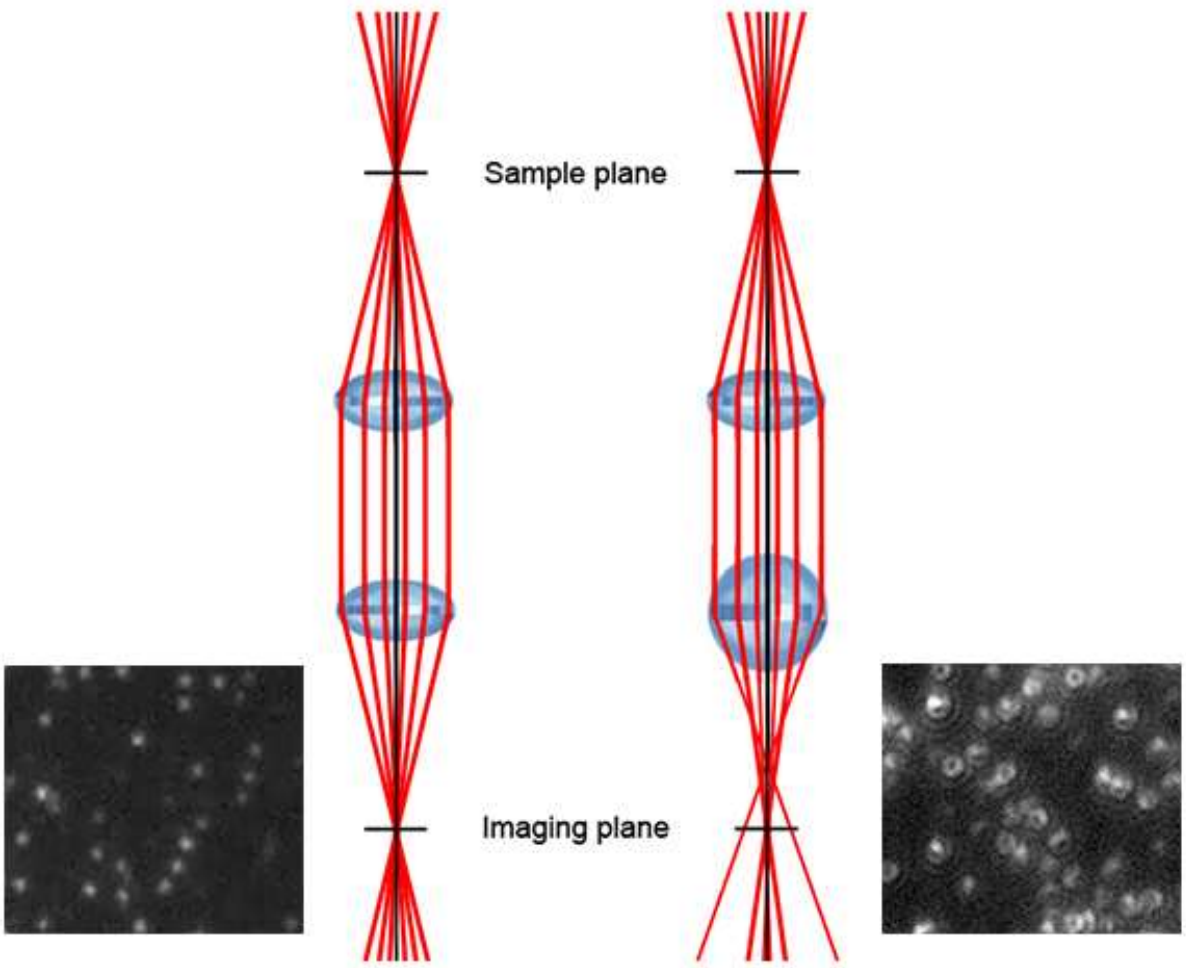


**Figure 2.8** – The ray diagram above illustrates how spherical aberrations can be utilized to create unique emission patterns for individual molecules imaged from the same sample plane. Shown on the left, an aberration-free lens focuses light coupled into the lens at various angles from the sample plane to a single point on the imaging plane. This results in each individual molecule appearing as a two-dimensional Gaussian bright spot, as shown in the left image. Shown on the right, a lens which has not been corrected for spherical aberrations focuses light coupled into the lens at various angles from the sample plane to multiple imaging planes. When capturing an image from a single imaging plane, as shown, light is focused dependent upon the angle at which it enters the objective. Imaging single molecules with these uncorrected optics results in a unique emission pattern at the selected imaging plane for each molecule within the sample, as shown in the right image.

aberrations can be exploited to allow for the imaging of single molecule orientation. Spherical aberrations can be introduced to the optics train of a microscope by slightly defocusing the

objective (~500nm) [15, 46]. Creating spherical aberrations in single molecule images causes the light entering the objective at various angles from each molecule to be focused to a unique imaging plane. This results in distinctive emission patterns at the selected imaging plane for each molecule. **Figure 2.8** demonstrates how spherical aberrations are utilized to generate unique emission patterns for single molecules.

The emission patterns generated by defocused imaging of single molecule fluorescence can be analyzed to determine the three-dimensional orientation of each fluorophore's emission dipole relative to the sample surface. Orientation analysis of single molecule emission patterns is achieved through comparison of measured emission patterns with a library of emission patterns created in a MATLAB simulation[48]. This simulation utilizes an equation which describes the diffraction of light through a lens in the presence of spherical aberrations, as shown in **Eq. 2.2**:

$$I(x,y,z) = \frac{I_0(\theta,\Phi)}{z^2}\left|\int_0^1 J_0\left(ka\rho\frac{\sqrt{x^2+y^2}}{z}\right)\exp\left(-ik\ opd(\rho)\right)\bullet\rho\bullet d\rho\right|^2 \qquad \textbf{Eq 2.2}$$

Where the intensity pattern is described in Cartesian coordinates by the intensity pattern of the dipole emission pattern in polar coordinates *I(θ,Φ)* using the polar angle *(Φ)* and azimuthal angle *(θ)* of the emission dipole relative to the surface, as shown in **Fig 2.9**, $J_0$ is the zeroth order Bessel function, *k* describes the wave vector magnitude, *a* is the limiting aperture of the optical system, *p* incorporates the non-ideality of optics, and opd(*p)* is the optical path length difference between light travelling through the center and outer edge of the objective described as a function of *p* [48, 49]. Within this equation and MATLAB simulation the optical parameters of the defocused imaging experiment of single molecule fluorescence emission can be defined. Parameters including objective magnification and numerical aperture are known and held constant while defocus distance and orientation parameters are adjusted to fit each measured emission pattern. An advantage of employing this technique in studies of supported

membranes is that each of the fluorophores within the film is confined to a single z-plane (or defocus distance). This not only allows each of the fluorophores within the film to be imaged simultaneously, but it allows the defocus depth to be accurately measured with a piezoelectric focusing collar attached to the objective. Thus, this eliminates one of the unknown variables used to simulate single molecule emission patterns and only adjustable parameters become the polar (Φ) and azimuthal (θ) angles, which are used to define to orientation of the emission dipole in three-dimensional space. **Figure 2.9** illustrates how these angles are used to define to orientation of the emission dipole in three-dimensional space relative the sample surface in the simulated images. With the orientation of each emission dipole being controlled within the simulation, a library of simulated emission patterns can be created. Each measured emission pattern is compared to this library in order to extract the orientation of the emission dipole for each fluorophore within the sample (±5°), as demonstrated in **Fig. 2.10**.

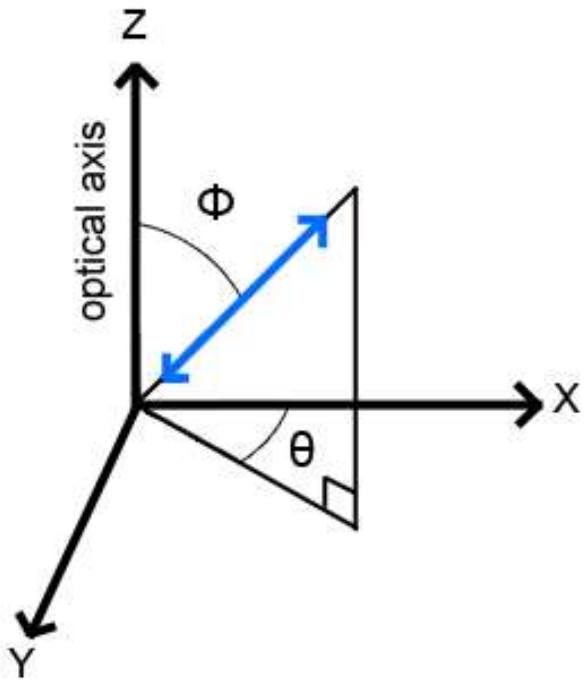


**Figure 2.9** – The three-dimensional orientation of each emission dipole is defined in relation to the imaging surface (the X-Y plane) by two angles, the polar angle (Φ) and the azimuthal angle (θ).

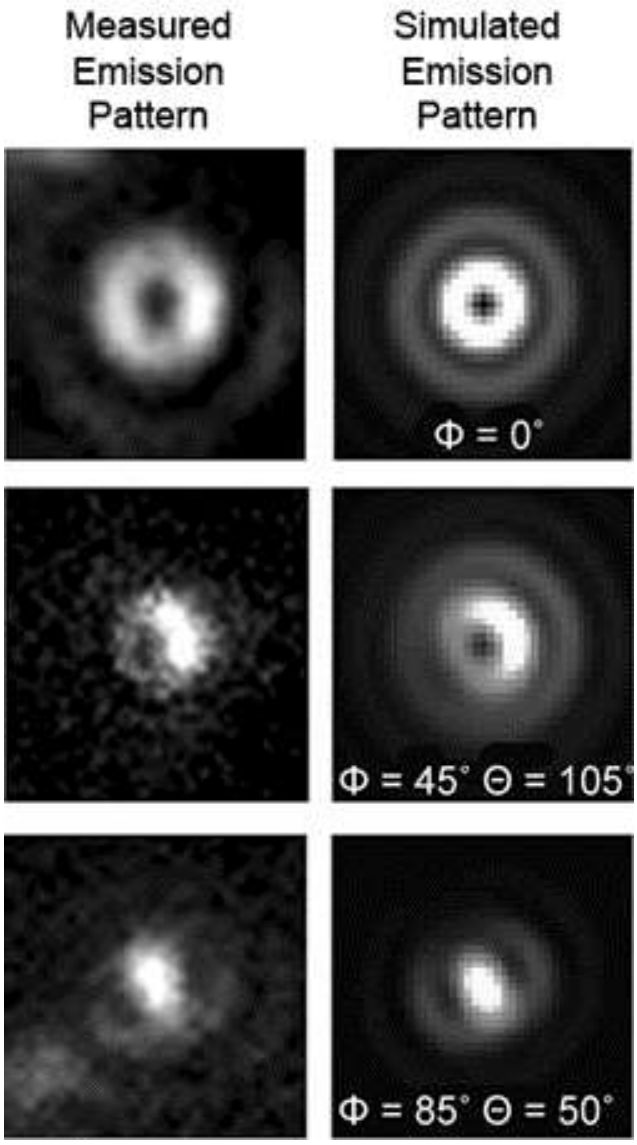


**Figure 2.10** – The three-dimensional orientation of single molecules is measured by comparison of measured emission pattern from defocused single molecule images with simulated emission patterns generated in MATLAB.

The defocused imaging method described above permits the measurement of molecular orientation for single molecules of all orientations within a sample. Therefore, it is imperative that the method of excitation chosen be capable of exciting all molecular orientations as well. An epi-fluorescence configuration is one of the most common methods of excitation for standard fluorescence measurements. However, this configuration is limited in terms of the capability to

excite molecules with their absorption dipoles oriented parallel to the direction of the propagating light. Therefore, an epi-fluorescence configuration is inadequate for single molecule orientation imaging. To address this issue, evanescent field excitation by total internal reflection (TIR) with p-polarized light can be utilized.

A non-propagating, exponentially decaying, evanescence wave is generated at an interface where light undergoes total internal reflection [28]. The optical phenomenon of refraction which occurs at the interface of two mediums of differing refractive indices is described by Snell's Law:

$$\frac{\sin\theta_1}{\sin\theta_2} = \frac{n_2}{n_1} \qquad \textbf{Eq. 2.3}$$

where $n$ is the refractive index of each medium and $\theta$ is the angle of light from the interface normal in each medium. As described by Snell's law and shown in **Fig. 2.11**, light traveling in a high refractive index medium ($n_1$) will be bent away from the normal as it crosses an interface into a lower refractive index medium ($n_2$). As shown **in Fig. 2.11**, at low angles of incidence the majority of light is refracted away from the normal in the incident medium ($n_2$), while a fraction of the light is reflected within the initial medium ($n_1$). If angle of incidence is increased beyond the critical angle, the light will be totally internally reflected within the high refractive index medium. Snell's law describes the critical angle:

$$\theta_{crit} = \arcsin\frac{n_2}{n_1} \qquad \textbf{Eq. 2.4}$$

where $n_1$ is greater than $n_2$. At the point on the interface where total internal reflection occurs, an evanescent wave is produced which penetrates into the lower refractive index medium. Not only is this evanescent field capable of exciting molecules near the interface in the lower refractive index medium, but it can excite all molecular orientations when p-polarized light is

used [45, 46]. P-polarized light has the electric field component of the electromagnetic wave oriented perpendicular to the interface. Upon total internal reflection, E-field component arcs through the interface into lower refractive index medium, which allows all molecular orientations to be excited.

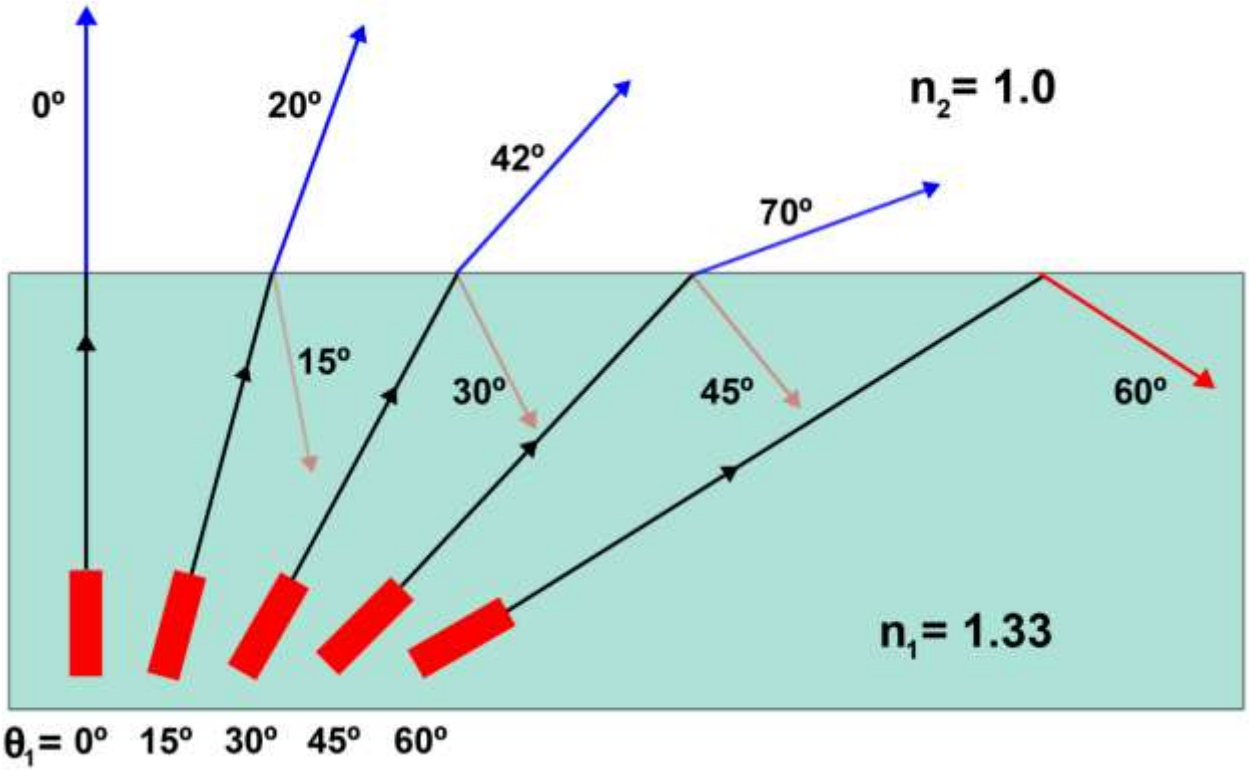


Figure 2.11 – The diagram above illustrates the phenomenon of optical refraction of light traveling in a water medium incident on an air interface. Light traveling in a high refractive index medium incident on an interface of lower refractive is bent away from the interface normal. At angles less than the critical angle, most of the light is refracted, while a small fraction of the light is reflected within the initial medium. At angles beyond the critical, the incident light experiences total internal refection.

The advent of single molecule detection and spectroscopy in solid phases began in 1989 with the work of Moerner and Kador [50]. Since this time, other groups have furthered single molecule measurements with a technique, termed polarized total internal reflection fluorescence microscopy (P-TRIFM), for measuring the single molecule orientation of fluorophores. Hellen

and Alexrod revealed using a fixed-power dipole model for fluorophore to calculate emission distortion through a dielectric interface resulted in an angle-dependent intensity at the imaging plane as a function of fluorophore orientation and distance from the interface [47]. Bartko and Dickson demonstrated this technique for measuring the orientation of individual fluorophores within polymer films [45, 46]. Further single molecule orientation studies, also called defocused orientation and position imaging (DOPI), demonstrated the orientation measurement of F-actin [51, 52] and a cellular motor protein, myosin V [53]. Together these studies provided evidence that the single molecule orientation technique could provide a valuable tool for molecular level structural measurements in biological systems. As such, several of the studies discussed in this dissertation utilize this molecular approach to study the structure of model membranes and immobilized antibodies.

Recently, the single molecule orientation approach has been applied to studies of lipid structure in model membranes[14-16]. This approach utilizes model membranes doped with a trace amount of a fluorescent lipid analog which can be imaged to report back molecular level structure within the membrane. The approach for defocused imaging of single molecules is particularly apt for probing these systems as the thin lipid films deposited onto glass substrates confine the fluorescent lipids analogs being measured to a single z-dimension in the imaging plane. By limiting the molecules being measured to a single z-plane not only can each molecule be imaged simultaneously, but defocus distance is consistent for each molecule. Therefore, analysis of the imaged emission dipole pattern is simplified considerably as defocus distance is known, and the distance is the same for each molecule in the sample. This has made model membranes an excellent model system to explore the utility of single molecule orientations for structural studies of biological systems.

Initial single molecule orientation studies of membrane structure have provided several interesting findings. These studies have demonstrated the utility of acyl-label fluorescent lipid

analogs over headgroup labeled probes for structural measurements in membranes [15]. These findings affirmed that the acyl-label probe orientation was augmented by lipid packing density while headgroup-label probes with fluorophores external to the hydrophobic membrane region were insensitive to lipid tail packing[15]. Additionally, these studies have proven that orientation measurements of acyl-labeled probes in monolayer and bilayer membranes are capable of reporting molecular level structure perturbations induced by changes in surface pressure, sterol concentration, and relative humidity[14-16]. Through these studies the equivalent surface pressure in bilayers was determined, which is a valuable tool for monolayer studies as bilayers exists in a tension-free state [16]. Furthermore, time-lapsed studies of single molecule orientations have demonstrated that the dynamic nature of lipids within membranes can also be measured with this technique [14]. Clearly, these studies have provided a foundation for further single molecule structural measurements in membranes.

## 2.5 - Conclusion

Several of the studies described in the following chapters build upon the previous single molecule work in membranes. The study described in Chapter 3 tests the sensitivity of a series of acyl-labeled fluorescent lipid analogs to determine the optimal probe structure for orientation measurements in membranes. In Chapter 4, this optimal single molecule probe is utilized to elucidate the structural influence of a minor membrane component, ganglioside GM1, within LB monolayers. Through this study, single molecule structural measurements proved to be a valuable tool as structural perturbations within the membrane, typically not observed by bulk techniques, were able to be probed. Moreover, the single molecule approach is expanded upon in Chapter 6 to explore the orientation of immobilized proteins. These studies report the preliminary findings from immobilized antibody orientation measurements for improving antibody binding efficiency in immunoassay applications.

## 2.6 - References


1. Yeagle, P. 1993. The membranes of cells. Academic Press, San Diego.

2. Langmuir, I. 1917. The constitution and fundamental properties of solids and liquids. II. Liquids. J. Am. Chem. Soc. 39:1848-1906.

3. Blodgett, K. B. 1934. Monomolecular films of fatty acids on glass. J. Am. Chem. Soc. 56:495-495.

4. Blodgett, K. B. 1935. Films built by depositing successive monomolecular layers on a solid surface. J. Am. Chem. Soc. 57:1007-1022.

5. McConnell, H. M. 1991. Structures and Transitions in Lipid Monolayers at the Air-Water Interface. Annu. Rev. Phys. Chem. 42:171-195.

6. Kaganer, V. M., H. Möhwald, and P. Dutta. 1999. Structure and phase transitions in Langmuir monolayers. Rev. Mod. Phys. 71:779-819.

7. Ries, H. E., and H. Swift. 1987. Twisted double-layer ribbons and the mechanism for monolayer collapse. Langmuir 3:853-855.

8. Lipp, M. M., K. Y. C. Lee, D. Y. Takamoto, J. A. Zasadzinski, and A. J. Waring. 1998. Coexistence of Buckled and Flat Monolayers. Phys. Rev. Lett. 81:1650-1653.

9. Langmuir, I., and V. J. Schaefer. 1937. Built-up films of proteins and their properties. Science 85:78-82.

10. Langmuir, I., V. J. Schaefer, and H. Sobotka. 1937. Multilayers of sterols and the adsorption of digitonin by deposited monolayers. J. Am. Chem. Soc. 59:1751-1759.

11. Cheng, Y. L., N. Boden, R. J. Bushby, S. Clarkson, S. D. Evans, P. F. Knowles, A. Marsh, and R. E. Miles. 1998. Attenuated total reflection Fourier transform infrared spectroscopic characterization of fluid lipid bilayers tethered to solid supports. Langmuir 14:839-844.

12. Kalb, E., S. Frey, and L. K. Tamm. 1992. Formation of Supported Planar Bilayers by Fusion of Vesicles to Supported Phospholipid Monolayers. Biochim. Biophys. Acta 1103:307-316.

13. Reviakine, I., and A. Brisson. 2000. Formation of supported phospholipid bilayers from unilamellar vesicles investigated by atomic force microscopy. Langmuir 16:1806-1815.

14. Huckabay, H. A., and R. C. Dunn. 2011. Hydration Effects on Membrane Structure Probed by Single Molecule Orientations. Langmuir 27:2658-2666.

15. Livanec, P. W., and R. C. Dunn. 2008. Single-molecule probes of lipid membrane structure. Langmuir 24:14066-14073.

16. Livanec, P. W., H. A. Huckabay, and R. C. Dunn. 2009. Exploring the effects of sterols in model lipid membranes using single-molecule orientations. J. Phys. Chem. B 113:10240-10248.

17. Livanec, P. W., H. A. Huckabay, and R. C. Dunn. 2012. Reduced single molecule photobleaching in fumed Langmuir–Blodgett films. Thin Solid Films 520:6233-6237.

18. Ho, C., S. J. Slater, and C. D. Stubbs. 1995. Hydration and Order in Lipid Bilayers. Biochemistry 34:6188-6195.

19. Verveer, P. J., F. S. Wouters, A. R. Reynolds, and P. I. H. Bastiaens. 2000. Quantitative Imaging of Lateral ErbB1 Receptor Signal Propagation in the Plasma Membrane. Science 290:1567-1570.

20. Goodwin, J. S., and A. K. Kenworthy. 2005. Photobleaching approaches to investigate diffusional mobility and trafficking of Ras in living cells. Methods 37:154-164.

21. Kenworthy, A. K., N. Petranova, and M. Edidin. 2000. High-Resolution FRET Microscopy of Cholera Toxin B-Subunit and GPI-anchored Proteins in Cell Plasma Membranes. Mol. Biol. Cell 11:1645-1655.

22. Rao, M., and S. Mayor. 2005. Use of Forster's resonance energy transfer microscopy to study lipid rafts. Biochim. Biophys. Acta (BBA) - Molecular Cell Research 1746:221-233.

23. Jacobson, K., and D. Papahadjopoulos. 1975. Phase transitions and phase separations in phospholipid membranes induced by changes in temperature, pH, and concentration of bivalent cations. Biochemistry 14:152-161.

24. Van Blitterswijk, W. J., R. P. Van Hoeven, and B. W. Van der Meer. 1981. Lipid structural order parameters (reciprocal of fluidity) in biomembranes derived from steady-state fluorescence polarization measurements. Biochim. Biophys. Acta 644:323-332.

25. de Almeida, R. F. M., J. Borst, A. Fedorov, M. Prieto, and A. J. W. G. Visser. 2007. Complexity of Lipid Domains and Rafts in Giant Unilamellar Vesicles Revealed by Combining Imaging and Microscopic and Macroscopic Time-Resolved Fluorescence. Biophys. J. 93:539-553.

26. Bacia, K., D. Scherfeld, N. Kahya, and P. Schwille. 2004. Fluorescence Correlation Spectroscopy Relates Rafts in Model and Native Membranes. Biophys. J. 87:1034-1043.

27. Meyer-Arendt, J. R. 1995. Introduction to classical and modern optics. Prentice Hall, Englewood Cliffs, N.J.

28. Chartier, G. 2005. Introduction to optics. Springer, New York.

29. Banerjee, P. P., and T.-C. Poon. 1991. Principles of applied optics. Aksen Associates, Pacific Palisades, CA.

30. Rock, P., M. Allietta, W. W. Young, Jr., T. E. Thompson, and T. W. Tillack. 1991. Ganglioside GM1 and asialo-GM1 at low concentration are preferentially incorporated into the gel phase in two-component, two-phase phosphatidylcholine bilayers. Biochemistry 30:19-25.

31. Hollars, C. W., and R. C. Dunn. 1998. Submicron structure in L-alpha-dipalmitoylphosphatidylcholine monolayers and bilayers probed with confocal, atomic force, and near-field microscopy. Biophys. J. 75:342-353.

32. Richter, R. P., and A. R. Brisson. 2005. Following the Formation of Supported Lipid Bilayers on Mica: A Study Combining AFM, QCM-D, and Ellipsometry. Biophys. J. 88:3422-3433.

33. Dickenson, N. E., K. P. Armendariz, H. A. Huckabay, P. W. Livanec, and R. C. Dunn. 2010. Near-field scanning optical microscopy: a tool for nanometric exploration of biological membranes. Anal. Bioanal. Chem. 396:31-43.

34. Dunn, R. C. 1999. Near-field scanning optical microscopy. Chem. Rev. 99:2891-2928.

35. Burgos, P., C. Yuan, M.-L. Viriot, and L. J. Johnston. 2003. Two-Color Near-Field Fluorescence Microscopy Studies of Microdomains (“Rafts”) in Model Membranes. Langmuir 19:8002-8009.

36. Sezgin, E., I. Levental, M. Grzybek, G. Schwarzmann, V. Mueller, A. Honigmann, V. N. Belov, C. Eggeling, Ü. Coskun, K. Simons, and P. Schwille. 2012. Partitioning, diffusion, and ligand binding of raft lipid analogs in model and cellular plasma membranes. Biochim.Biophys. Acta (BBA) - Biomembranes 1818:1777-1784.

37. Eggeling, C., C. Ringemann, R. Medda, G. Schwarzmann, K. Sandhoff, S. Polyakova, V. N. Belov, B. Hein, C. von Middendorff, A. Schonle, and S. W. Hell. 2009. Direct observation of the nanoscale dynamics of membrane lipids in a living cell. Nature 457:1159-1162.

38. Schütz, G. J., H. Schindler, and T. Schmidt. 1997. Single-molecule microscopy on model membranes reveals anomalous diffusion. Biophys. J.73:1073-1080.

39. Kiessling, V., J. M. Crane, and L. K. Tamm. 2006. Transbilayer Effects of Raft-Like Lipid Domains in Asymmetric Planar Bilayers Measured by Single Molecule Tracking. Biophys. J. 91:3313-3326.

40. Chen, Y., B. C. Lagerholm, B. Yang, and K. Jacobson. 2006. Methods to measure the lateral diffusion of membrane lipids and proteins. Methods 39:147-153.

41. Manley, S., J. M. Gillette, G. H. Patterson, H. Shroff, H. F. Hess, E. Betzig, and J. Lippincott-Schwartz. 2008. High-density mapping of single-molecule trajectories with photoactivated localization microscopy. Nat.Meth. 5:155-157.

42. Sengupta, P., T. Jovanovic-Talisman, D. Skoko, M. Renz, S. L. Veatch, and J. Lippincott-Schwartz. 2011. Probing protein heterogeneity in the plasma membrane using PALM and pair correlation analysis. Nat. Meth. 8:969-975.

43. van de Linde, S., M. Sauer, and M. Heilemann. 2008. Subdiffraction-resolution fluorescence imaging of proteins in the mitochondrial inner membrane with photoswitchable fluorophores. J. Struct. Biol.164:250-254.

44. Karolin, J., L. B. A. Johansson, L. Strandberg, and T. Ny. 1994. Fluorescence and Absorption Spectroscopic Properties of Dipyrromethene boron Difluoride (Bodipy) Derivatives in Liquids, Lipid-Membranes, and Proteins. J. Am. Chem. Soc. 116:7801-7806.

45. Bartko, A. P., and R. M. Dickson. 1999. Three-dimensional orientations of polymer-bound single molecules. J. Phys. Chem. B 103:3053-3056.

46. Bartko, A. P., and R. M. Dickson. 1999. Imaging three-dimensional single molecule orientations. J. Phys. Chem. B 103:11237-11241.

47. Hellen, E. H., and D. Axelrod. 1987. Fluorescence Emission at Dielectric and Metal-Film Interfaces. Journal of the Optical Society of America B: Opt. Phys. 4:337-350.

48. Patra, D., I. Gregor, and J. Enderlein. 2004. Image analysis of defocused single-molecule images for three-dimensional molecule orientation studies. J. Phys. Chem. A 108:6836-6841.

49. Frisken Gibson, S., and F. Lanni. 1991. Experimental test of an analytical model of aberration in an oil-immersion objective lens used in three-dimensional light microscopy. J. Opt. Soc. Am. A 8:1601-1613.

50. Moerner, W. E., and L. Kador. 1989. Optical detection and spectroscopy of single molecules in a solid. Phys. Rev. Lett. 62:2535-2538.

51. Forkey, J. N., M. E. Quinlan, M. A. Shaw, J. E. T. Corrie, and Y. E. Goldman. 2003. Three-dimensional structural dynamics of myosin V by single-molecule fluorescence polarization. Nature 422:399-404.

52. Forkey, J. N., M. E. Quinlan, and Y. E. Goldman. 2005. Measurement of single macromolecule orientation by total internal reflection fluorescence polarization microscopy. Biophys. J. 89:1261-1271.

53. Toprak, E., J. Enderlein, S. Syed, S. A. McKinney, R. G. Petschek, T. Ha, Y. E. Goldman, and P. R. Selvin. 2006. Defocused orientation and position imaging (DOPI) of myosin V. Proc. Natl. Acad. Sci. 103:6495-6499.

# Chapter 3: Sensitivity of Single Molecule Probes to Membrane Structure

## 3.1 - Introduction

The view of biological membranes and their functional role in cellular processes continues to evolve as new approaches are developed to probe these intricate structures. Biomembranes are composed of a complex mixture of lipids, proteins, sterols, and other species which combine to create highly heterogeneous and dynamic systems [1-5]. This often makes it difficult to directly link structural changes with membrane constituents, which has motivated the long historical development of model systems that mimic the natural cellular barrier. These simplified systems offer a high degree of control over important thermodynamic and compositional parameters and have been essential in understanding natural membranes and developing and validating new tools for examining biological systems.

Fluorescence microscopy is one of the most widely used approaches for probing structural and dynamic attributes of both model and natural membranes. A wide variety of fluorescent lipid analogs have been developed that readily insert into the macroscopic lipid assembly and often partition into particular domains, thus enabling heterogeneous structural features to be delineated. This approach has been used extensively to probe specific environments within lipid monolayers and bilayers, characterize phase structure, probe models of lipid rafts, and study the dynamics and fluidity of lipid membranes [6-9]. While fluorescence based analysis of membranes has been extensively developed and utilized, interpretation of the results and comparisons between studies is often complicated by the lack of detailed knowledge of probe/lipid interactions. For example, measured diffusion constants of the same dye within the same lipid system can vary by orders of magnitude, the assignment of dye partitioning within localized domains is often contradictory, and even the same fluorescent probe can alter its

domain partitioning preference as a function of the lipid system composition [9-14]. This has renewed interest in understanding and controlling how probes insert into their target system.

There has been a considerable effort to design fluorescent probes capable of sensing the hydrophobic regions of membranes by positioning the fluorophore within the lipid acyl tails. For example, 1,6-diphenyl-1,3,5-hexatriene (DPH) has an elongated structure which is expected to insert along lipid acyl tails and has been widely used to probe order in the lipid tail region [15, 16]. However, anisotropy measurements by Levine *et al.* have shown that DPH does not consistently insert as expected along lipid acyl tails but also inserts parallel to the membrane plane [17].

Similar efforts have led to the development of lipid analogs incorporating the BODIPY fluorophore [18, 19]. BODIPY probes are conceptually attractive for investigating the hydrophobic region of lipid membranes since they are less hydrophilic than other probes and have no net charge. BODIPY probes also exhibit excellent fluorescent properties with high extinction coefficients, near unity quantum yields, and favorable photostability properties [20, 21]. In order to examine the incorporation of this fluorophore within the structure of lipid membranes, several studies have examined insertion properties of BODIPY lipid analogs located at incrementally longer regions of the acyl tail [22-25].

Utilizing parallax analysis of fluorescence quenching, Kaiser and London have shown that while the average depth of the BODIPY fluorophore within the membrane is dependent on its position along the acyl tail, the BODIPY fluorophore also exhibits a broad distribution of locations within the membrane [24]. These results suggest that while the location of the BODIPY marker within the membrane generally tracks its location along the acyl chain of the probe, a significant population of fluorophores wrap back towards the headgroups and interact with the hydrophilic region of the membrane. Quenching studies in giant vesicles, moreover,

found that essentially all of the BODIPY probes in the tailgroup looped back around to interact with the headgroups of the membrane, regardless of their location along the tailgroup [25].

Clearly, the insertion geometry of BODIPY fluorescent membrane probes into lipid systems is complicated and requires further exploration using complementary techniques. Recently, we have shown that single molecule fluorescence measurements can characterize the orientation of individual fluorescent lipid probes doped into lipid membranes [26-31]. Using polarized total internal fluorescence microscopy (P-TIRFM), the three-dimensional orientation of fluorescent lipid analogs doped into films at trace levels can be characterized by emission pattern mapping. Using an acyl chain linked BODIPY-$C_4C_9$-PC probe, we have shown that these measurements are sensitive to membrane structure at the single molecule level. Variations in membrane structure induced by surface pressure changes, relative humidity, or additives such as cholesterol can all be tracked through changes in single molecule probe orientation [26-28, 32]. Moreover, these studies revealed a distinctive bimodal insertion geometry for the BODIPY-$C_4C_9$-PC probe, consistent with previous bulk studies of probe orientations in membranes.

Here we extend those studies to characterize the insertion geometry for a range of BODIPY lipid analogs in lipid films. In this study, the single molecule orientation distributions of six BODIPY fluorescent probes in DPPC Langmuir-Blodgett (LB) monolayers are examined [33]. The BODIPY location in the acyl tail group is varied and analogs containing both phosphocholine (PC) and fatty acid (FA) headgroups are compared. These measurements are used to characterize how these probes insert and orient within DPPC monolayers and how their orientation changes with surface pressure. These studies reveal a general trend towards bimodal insertion geometries for BODIPY containing analogs. All six analogs reorient in response to changes in membrane surface pressure. The sensitivity to membrane surface pressure, however, is probe dependent and subject to the specific location of the BODIPY probe

in the acyl tail and identity of the headgroup. These results, therefore, provide new insights into BODIPY containing probe insertion within membranes at the molecular level, which is important for interpreting results from bulk studies using these probes. The trends also provide guidance for the development of probes with increased sensitivity to changes in their surrounding lipid matrix. Together, these measurements illustrate the utility of single molecule fluorescence measurements for understanding the complicated and highly heterogeneous interactions that are indicative of membrane systems.

### 3.2 - Materials and Methods

Dipalmitoylphosphatidylcholine (DPPC) (Avanti Polar Lipids, Alabaster, AL) was obtained at >99% purity and used without further purification. Fluorescent lipid analogs 2-(4,4-difluoro-5,7-dimethyl-4-bora-3a,4a-diaza-*s*-indacene-3-dodecanoyl)-1-hexadecanoyl-*sn*-glycero-3-phosphocholine (BODIPY-$C_5$-PC) (D-3803), 2-(5-butyl-4,4-difluoro-4-bora-3a,4a-diaza-*s*-indacene-3-nonanoyl)-1-hexadecanoyl-*sn*-glycero-3-phosphocholine (BODIPY-$C_4$,$C_9$-PC) (B-3794), 2-(4,4-difluoro-5,7-methyl-4-bora-3a,4a-diaza-*s*-indacene-3-dodecanoyl)-1-hexadecanoyl-*sn*-glycero-3-phosphocholine (BODIPY-$C_{12}$-PC) (D-3792), 4,4-difluoro-5,7-dimethyl-4-bora-3a,4a-diaza-*s*-indacene-3-pentanoic acid (BODIPY-$C_5$-FA) (D-3834), 5-butyl-4,4-difluoro-4-bora-3a,4a-diaza-*s*-indacene-3-nonanoic acid (BODIPY-$C_4$,$C_9$-FA) (B-3824), 4,4-difluoro-5,7-dimethyl-4-bora-3a,4a-diaza-*s*-indacene-3-dodecanoic acid (BODIPY-$C_{12}$-FA) (D-3822) (Invitrogen Corporation, Carlsbad, CA) were used as received.

Lipid monolayers were prepared from 1 mg/ml stock solutions of DPPC dissolved in chloroform and doped with ~$10^{-8}$ mol % of the appropriate reporter dye. The solutions were dispersed on a subphase of 18 MΩ water in a Langmuir–Blodgett trough (Type 611, Nima Technology, Coventry, England). The chloroform was allowed to evaporate for 15 minutes prior

to beginning compression cycles. Each monolayer was subjected to two compression and expansion cycles up to a surface pressure of 40 mN/m. Compression and expansion rates were 100 $cm^2$/min and 80 $cm^2$/min, respectively. Each monolayer was then compressed to a particular target pressure and held at that pressure for 10 minutes. The monolayer was then transferred to a Piranha-cleaned glass coverslip in a headgroup down geometry at a dipping speed of 5 mm/min. All monolayers were transferred and studied at 22 $^oC$.

Monolayer films were imaged using a total internal reflection fluorescence microscope (TIRF-M) (Olympus IX71, Center Valley, PA) equipped with a 100x, 1.45 NA objective (Achromat, Olympus). The 514nm line form an argon ion laser (Coherent Innova 90, Santa Clara, CA) was directed through half-wave and quarter-wave plates (Newport, Irvine , CA) to select for p-polarized excitation before being coupled into the microscope. Excitation was directed through the objective with the optics defocused ~500nm and fluorescence was collected, filtered, and imaged on a cooled CCD camera (Cascade 650, Roper Scientific, Tuscon, AZ). Image collection was controlled with Slidebook software (Version 4.2.0.3, Intelligent Imaging Innovations, Denver, CO) and analyzed with MATLAB (Natick, MA).

### 3.3 - Results and Discussion

To expand the capabilities of the single molecule orientation approach and explore how probe orientations reflect membrane properties, here we analyze the single molecule orientations of a series of BODIPY-linked fluorescent lipid analogs doped into DPPC monolayers. The structures of DPPC and each of the fluorescent lipid analogs studied are displayed in **Fig. 3.1**. Each probe incorporates a BODIPY fluorescent marker within the acyl tail region of the lipid analog and is unique in terms of its fluorophore position along the acyl chain

or headgroup type. These studies, therefore, will help establish the role of probe position and headgroup identity on insertion geometry in model membranes.

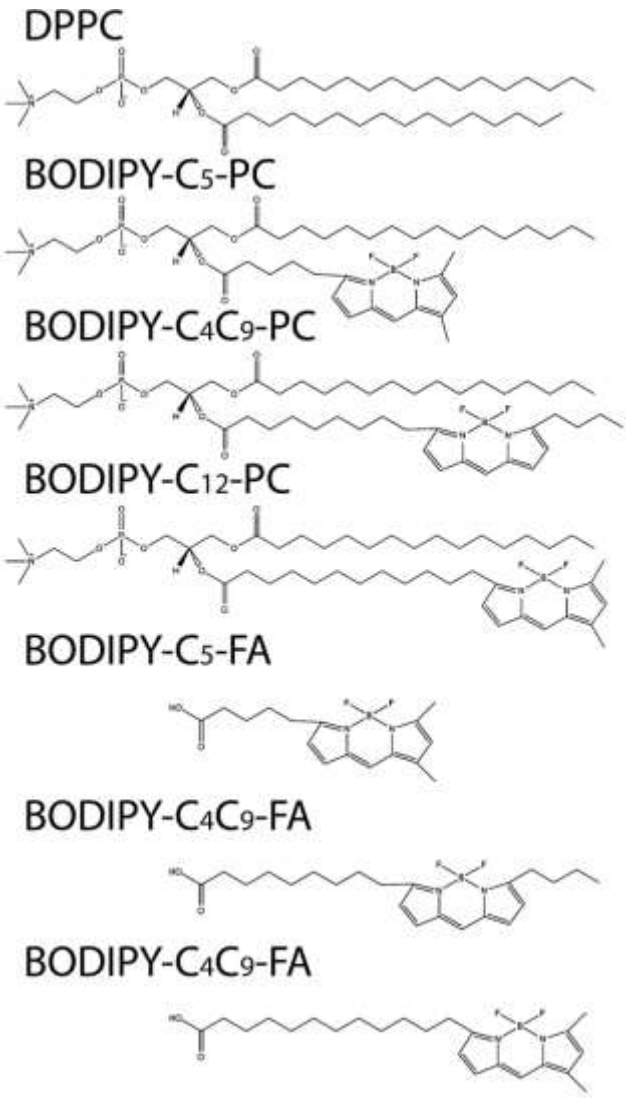


**Figure 3.1:** Chemical structures for DPPC and the six BODIPY fluorescent lipid analogs studied. As shown by the structures, the BODIPY probe location in the acyl tail group is systematically varied and analogs containing both phosphocholine (PC) and fatty acid (FA) headgroups are compared in this study.

The emission dipole of the BODIPY marker lies approximately along the long axis of the fluorophore [20]. As discussed in Chapter 2, defocused P-TIRFM measurements enable characterization of the three-dimensional orientation of the emission dipoles from individual

fluorescent lipid analogs doped into lipid membranes. These measurements, therefore, provide a direct visualization into the probe insertion geometry and can be used to track changes in the surrounding lipid matrix.

Each fluorescent marker was doped into DPPC monolayers at trace levels, compressed to the desired surface pressure on a Langmuir-Blodgett (LB) trough, and transferred to a glass coverslip for analysis. Deposition surface pressures ranged from 3 to 40 mN/m; which span DPPC phase transitions from the predominantly liquid expanded (LE) phase, through the liquid expanded (LE)/liquid condensed (LC) coexistence region, to the predominantly liquid condensed (LC) phase. At low surface pressures, the DPPC monolayer is predominantly in the LE state which is characterized by a large area per lipid (> 80 $Å^2$ / molecule at 20$^oC$), randomly oriented tailgroups, and reduced packing between the headgroups. As the available area per molecule is reduced by compressing the membrane, the LC phase appears with tighter lipid packing (< 60 $Å^2$ / molecule at 20$^oC$), ordered acyl tails oriented away from the interface, and close packing of the lipid headgroups.

To demonstrate the utility of defocused fluorescence imaging for determining single molecule orientations, emission pattern mapping of the BODIPY fluorophore is illustrated in **Fig. 3.2**. The figure displays examples of experimentally measured emission patterns observed for a range of BODIPY orientations. Each example is compared with simulated emission patterns using the approach described in Chapter 2, where the only adjustable parameters in the simulation are the polar (φ) and azimuthal (θ) angles of the BODIPY emission dipole and defocus distance [26]. The extracted emission dipole orientations are shown schematically in **Fig. 3.2.**

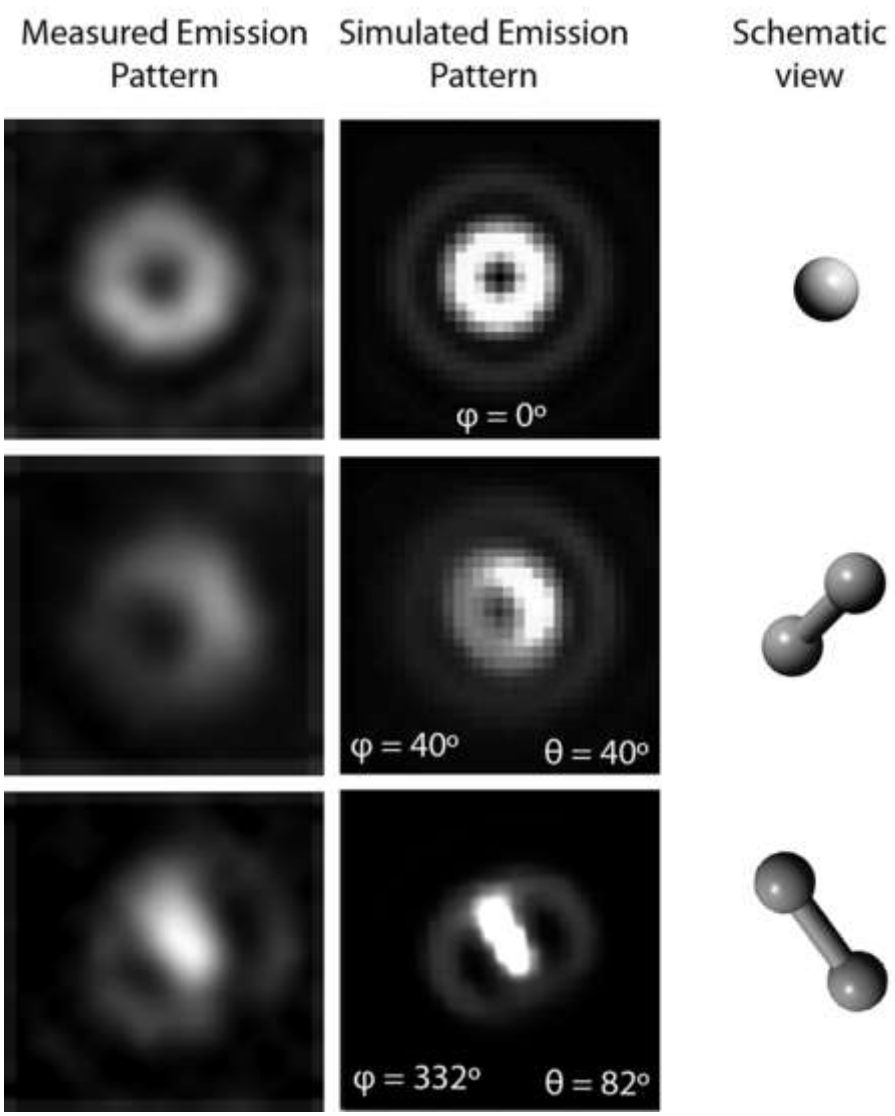


**Figure 3.2:** **(Left)** Representative single molecule emission patterns measured using defocused polarized total internal fluorescence microscopy. **(Center)** Simulated emission patterns used to characterize the polar (φ) and azimuthal (θ) angles of the BODIPY probe emission dipole. **(Right)** Schematic representations of the emission dipole orientations determined from the simulated emission patterns.

By comparing measured single molecule emission patterns with simulated results, orientation histograms are constructed to characterize the insertion geometry for each fluorescent marker shown in **Fig. 3.1**. In particular, the polar (φ) angle or tilt angle defines the

extent of BODIPY tilt away from the surface normal and is used to describe the effective ordering of the BODIPY probe within the acyl tails of the DPPC monolayer as a function of surface pressure.

**Figure 3.3** shows representative defocused single molecule fluorescence images of BODIPY-$C_4C_9$-PC doped at ~$10^{-8}$ mol % into DPPC monolayers deposited at increasing surface pressures. Analysis of the single molecule emission patterns enables quantification of each individual orientation which is shown schematically in the center panels of **Fig. 3.3**. The polar (φ) or tilt angle of each emission feature is compiled to create tilt angle population histograms for each surface pressure as shown in the bottom panel of **Fig. 3.3**.

As previous single molecule studies have shown, molecular orientations of BODIPY-$C_4$,$C_9$-PC doped into DPPC films track changes in membrane ordering. Interestingly, consistent with the results shown in **Fig. 3.3**, these measurements reveal a bimodal distribution of orientations for BODIPY-$C_4$,$C_9$-PC doped into DPPC at all surface pressures studied. Significant populations of BODIPY-$C_4$,$C_9$-PC molecules were found to orient either normal (φ ≤ 10º) or parallel (φ ≥ 81º) to the membrane plane, with little population observed in the intermediate orientations. As shown in **Fig. 3.3**, as the surface pressure is increased, the population shifts towards the surface normal orientation with a concomitant decrease in the parallel orientation.

The bimodal distribution seen in **Fig. 3.3** is consistent with a mechanism in which the lipid analog can insert into the DPPC membrane in an extended configuration with the BODIPY probe aligned along the lipid tails and a conformation in which the fluorophore wraps back to interact with the lipid headgroups. These configurations would lead to the normal oriented and parallel oriented populations, respectively. This is consistent with fluorescence quenching

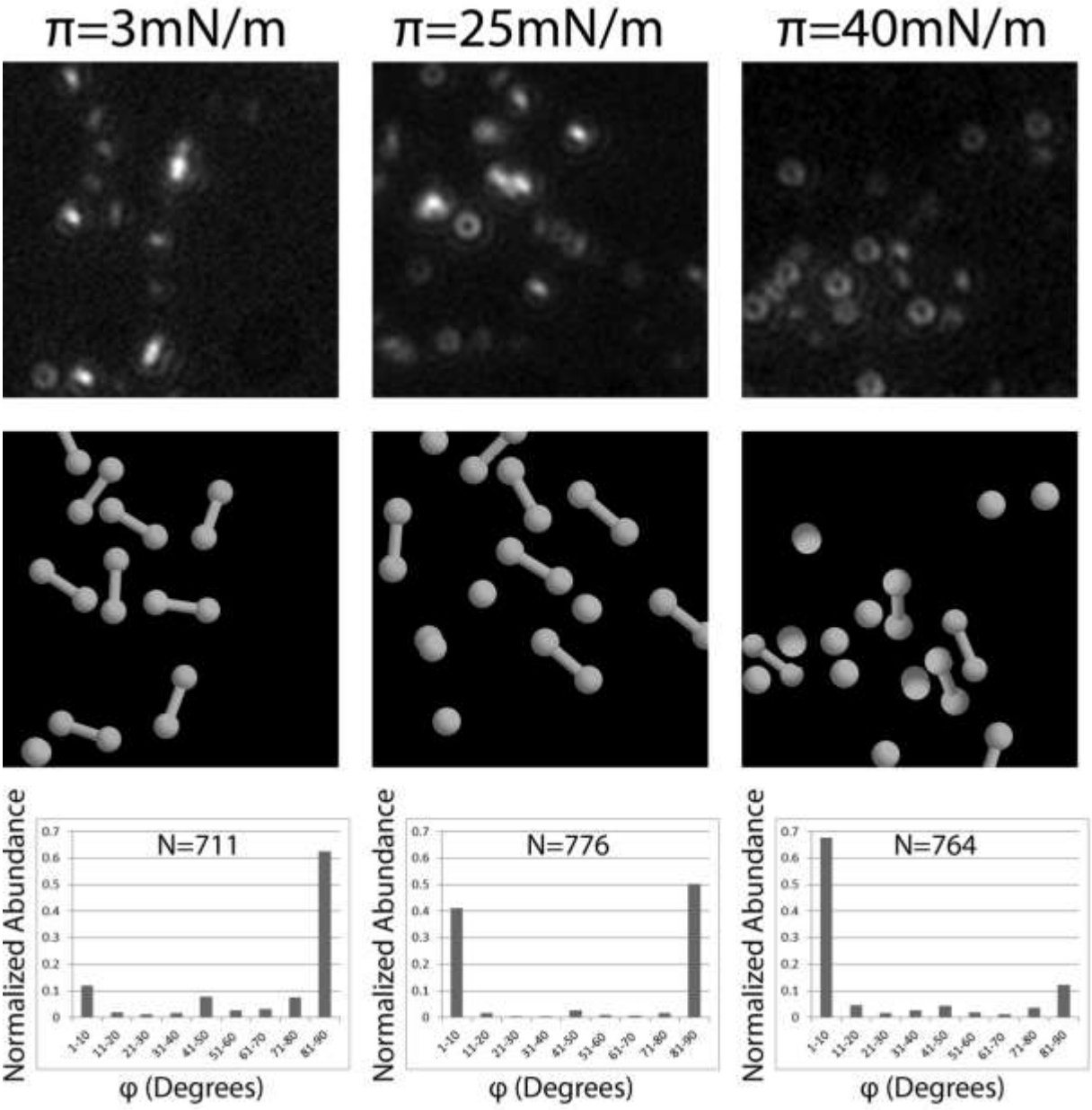


**Figure 3.3: (Top panels)** Representative defocused single molecule fluorescence images of BODIPY-$C_4C_9$-PC doped at ~$10^{-8}$ mol % into DPPC monolayers deposited at 3, 25, and 40mN/m. **(Center panels)** Schematics showing the single molecule orientations determined from simulating the single molecule fluorescence features measured in the top images. **(Bottom panels)** Polar (φ) or tilt angle histograms for BODIPY probes in DPPC monoalyers transferred at the surface pressure indicated. Each histogram summarizes hundreds of individual tilt angles measured using the single molecule emission patterns collected at each film condition. The bimodal tilt distributions reveal large populations of BODIPY probes oriented normal ($\varphi \leq 10^{o}$) and parallel ($\varphi \geq 81^{o}$) to the membrane plane which shifts toward normal oriented probes as surface pressure increases.

studies which found that the BODIPY probes tend to associate with the lipid headgroups even in condensed membranes [18, 24]. While BODIPY is often described as a hydrophobic marker, distributed charge density within the ring system and charged resonance structures contribute to the observed hydrophilic nature of the BODIPY probe and its tendency to associate with membrane headgroups.

As shown in **Fig. 3.3**, the proportion of BODIPY-$C_4C_9$-PC probes oriented normal to the membrane plane ($\varphi \leq 10^o$) increases with increasing surface pressure. The bimodal orientation distribution and trend towards increased ordered abundance at higher surface pressure is observed for all the BODIPY probes studied. **Figure 3.4** summarizes the single molecule orientation measurements for $C_5$, $C_4C_9$, and $C_{12}$ BODIPY-PC and -FA probes in DPPC monolayers deposited at 3, 25, and 40 mN/m. For clarity, only the fraction of probes oriented normal to the membrane plane are plotted as a function of monolayer surface pressure in **Fig. 3.4**. Each point in **Fig. 3.4** is extracted from single molecule population histograms such as that shown in **Fig. 3.3**, containing at least 450 molecules characterized from 3 different films. These plots clearly show that as the molecular area is reduced by compressing the monolayer to higher surface pressures, the ordered abundance for each probe studied increases linearly.

As shown in **Fig. 3.4**, the sensitivity with which each probe responds to increasing surface pressure, however, is dependent on head group type and BODIPY position along the acyl tail. Interestingly, the trends observed between BODIPY position and corresponding sensitivity to increasing surface pressure are not the same for PC and FA probes. The BODIPY-$C_4C_9$-PC probe exhibits the greatest sensitivity to changes in surface pressure compared to the other BODIPY-PC probes, while BODIPY-$C_{12}$-FA shows the greatest sensitivity among the fatty acid probes examined. In addition, similar length PC and FA probes show statistically different sensitivities to surface pressure. The $C_5$ and $C_4C_9$ FA analogs, for example, exhibit lower sensitivities to surface pressure compared with their PC counterparts,

while only the $C_{12}$ FA analog exhibits higher sensitivity to surface pressure than its PC equivalent.

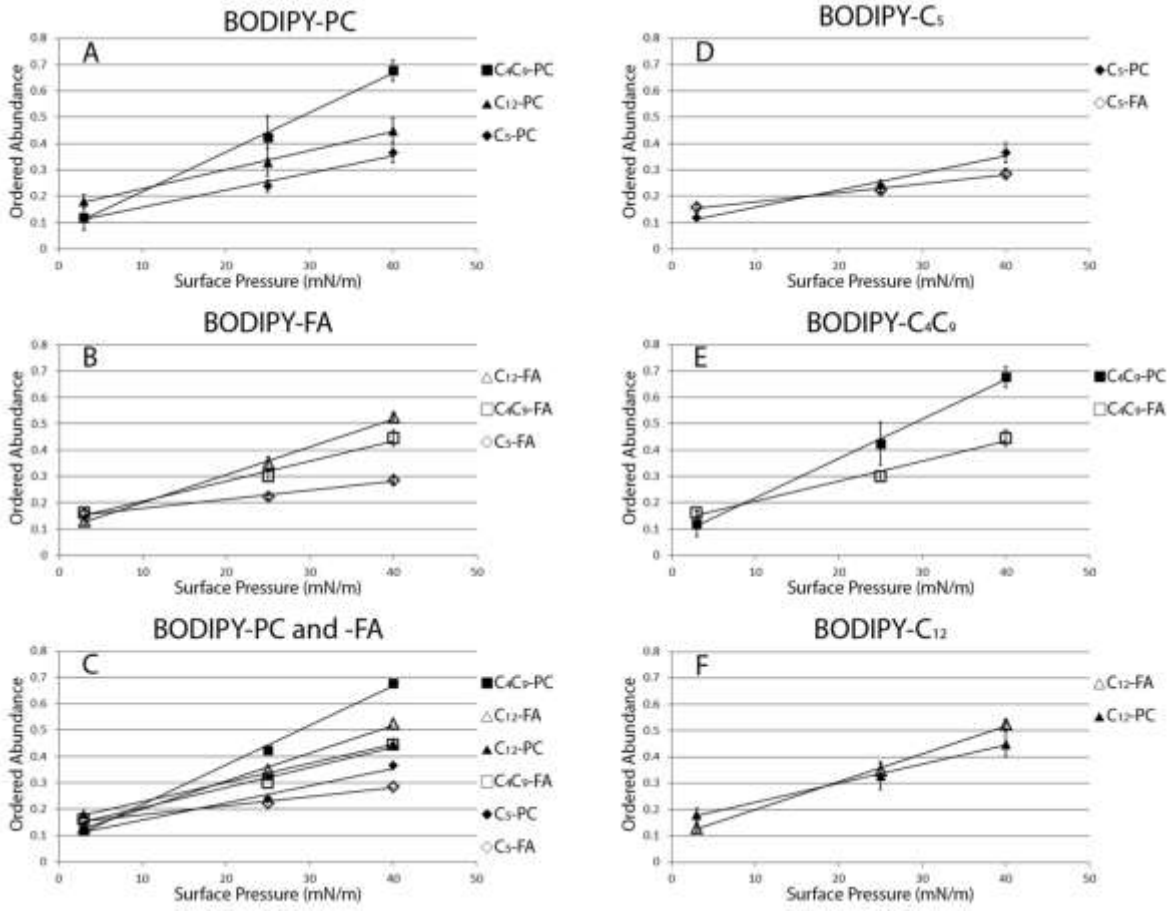


**Figure 3.4:** Comparisons of the normalized population of normal oriented probes ($\varphi \leq 10^{o}$) as a function of DPPC surface pressure for the BODIPY probes shown in **Fig. 3.1**. Trends in the normal oriented BODIPY probes with **(A)** PC headgroups, **(B)** FA headgroups, and **(C)** all the probes studied are plotted as a function of surface pressure. **(D-F)** The populations of normal oriented probes versus surface pressure are plotted for lipid analogs that differ in headgroup but place the BODIPY probe in comparable positions along the acyl chain.

Several contributing factors may influence how the BODIPY probes insert into the membrane and thus influence their sensitivity to the changing lipid environment as the surface pressure is increased. The bimodal orientation distributions observed for all the BODIPY probes studied here is consistent with a general insertion model in which BODIPY probes aligned along the acyl chains lead to the normal oriented population ($\varphi \leq 10^{o}$) while probes

wrapped back towards the lipid headgroups give rise to the parallel oriented group (φ ≥ 81º). In general, as surface pressure is increased and the area per lipid is reduced, the rise in normal oriented probes is consistent with an increasing population of BODIPY probes aligned along the acyl chains. Two primary factors, therefore, contribute to the probe insertion geometry; the order of the surrounding DPPC acyl tails and the probe proximity to the polar headgroups.

Before discussing the trends observed in **Fig. 3.4**, it is instructive to consider how the different headgroups affect the BODIPY location for similar length probes. Previous studies have shown that the position of fatty acid probes within membranes is strongly linked to pH [24, 34]. Upon protonation and deprotonation, fatty acids can change depths within the membrane of up ~3 Å. Given this, the fatty acid BODIPY analogs shown in **Fig. 3.1** are expected to sit deeper within the DPPC headgroups, or closer to glass substrate, than their PC counterparts, pulling the acyl attached BODIPY probe several angstroms closer to the surrounding lipid headgroups. As a first approximation, therefore, one would expect the relative probe depth of the BODIPY probes in the membrane to follow the general trend BODIPY-$C_5$-FA < BODIPY-$C_5$-PC < BODIPY-$C_4C_9$-FA < BODIPY-$C_4C_9$-PC < BODIPY-$C_{12}$-FA < BODIPY-$C_{12}$-PC.

Order within the surrounding DPPC acyl tails is necessary to induce order in the BODIPY probe and thus increase the abundance of φ ≤ 10º emission patterns. Evidence for this mechanism is provided by the trend that all PC and FA probes generally show an increase in ordered abundance with increasing surface pressure. NMR and molecular dynamics simulations show that the orientational freedom at each carbon along the acyl chain in a DPPC membrane is dependent on its distance from the headgroup [35, 36]. These methods suggest that toward the end of the acyl tail (at approximately carbon 12) order begins to decrease rapidly with increasing distance from the headgroup, even at high surface pressures. Therefore, a lipid analog which places the fluorescent marker towards the end of the acyl tails in the monolayer will exhibit a decrease in ordered abundance compared to shorter probes due to a lack of

rigidity from the surrounding acyl chains. In **Fig. 3.4**, for example, the BODIPY-$C_{12}$-PC probe is much less sensitive to changes in membrane surface pressure than the shorter BODIPY-$C_4C_9$-PC probe. For the FA probes, however, the trend is complicated. The trends in **Fig. 3.4** reveal that the BODIPY-$C_{12}$-FA probe is marginally more sensitive to surface pressure than the shorter BODIPY-$C_4C_9$-FA probe which is the reverse from that observed with the PC probes. However, because FA probes sit deeper in the headgroups and pull the BODIPY probes several Ångstroms closer to the headgroups, these probes in practice place the BODIPY group in ordered regions of the acyl tails as discussed below.

The second factor considered to influence BODIPY insertion geometry is probe-headgroup electrostatic attraction given the charged resonance structures of the BODIPY probe. Probes located closer to the phosphocholine headgroups are more affected by this attraction and will have a greater resistance to orient along the acyl tails. Thus, probes linked with shorter acyl tails, such as the $C_5$ probes, are expected to exhibit lower sensitivity to acyl tail ordering with surface pressure since the BODIPY probe experiences stronger headgroup association. In **Fig. 3.4**, both the BODIPY-$C_5$-PC and BODIPY-$C_5$-FA probes exhibit the least sensitivity to changes in membrane surface pressure, consistent with this mechanism.

In general, the trends observed in **Fig. 3.4** suggest that fluorescent lipid analogs with probes located closer to the headgroups exhibit progressively lower sensitivities due to increased electrostatic attraction to the headgroup region, while probes located near the terminal end of the acyl chains show reduced sensitivities due to the of lack acyl chain order in this region. Thus, these effects suggest that lipid analogs can be optimally tuned by judicious placement of the BODIPY probe along the acyl tail to maximize its orientation sensitivity to the surrounding membrane structure. Clearly, the data in **Fig. 3.4** shows that the BODIPY-$C_4C_9$-PC probe experiences the greatest sensitivity to changes in the membrane surface pressure. This suggests that its BODIPY probe is positioned such that it minimizes the electrostatic interactions

with the lipid headgroups while keeping it in the ordered region of the acyl tails. Because the FA probes sit deeper in the headgroups, the trends observed in **Fig. 3.4** suggest that probe lengths between BODIPY-$C_4C_9$-FA and BODIPY-$C_{12}$-FA would maximize their sensitivity to the surrounding lipid matrix. The slight difference in sensitivities observed for comparable PC and FA probes in **Fig. 3.4** is consistent with trends expected given the different depths at which the headgroups reside in the membrane. This also indicates that the extra acyl chain of the PC probes has little effect on probe insertion or reorientation with surface pressure. The studies presented here, therefore, suggest that bimodal insertion geometries for BODIPY lipid analogs are a general feature of this probe and the BODIPY position can be tuned to maximize their sensitivity to the surrounding lipid matrix.

The findings from this study and previous studies of acyl-linked BODIPY probe location in membranes reveal a bimodal distribution of BODIPY probe orientations/locations have implications on several studies of diffusion within membranes. Fluorescence recovery after photobleaching (FRAP) [37], single-particle tracking (SPT) [38, 39], and stimulated emission depletion (STED) [40] studies have often attributed anomalous diffusion of the same dye within membrane systems to the dye diffusing through more or less condensed regions within the membrane. However, one must now consider whether differences in diffusion rates are not the effect of differently oriented fluorescent probes. Therefore, single molecule orientation studies may be able to provide a method for elucidating the relationship between single molecule structure and diffusion rate within membranes.

### 3.4 - Conclusions

Defocused polarized TIRF-M measurements were used to characterize the tilt angles of BODIPY containing fluorescent lipid analogs doped into DPPC monolayers. A total of six

analogs are studied where the location of the BODIPY probe is varied along the acyl chain. Analogs with PC and FA headgroups are also compared with BODIPY probes located at comparable locations in the acyl tail. Each probe was doped into LB films of DPPC at ~$10^{-8}$ mol % and their single molecule orientations characterized over a range of surface pressures. For all probes studied, the single molecule tilt angle histograms reveal a predominately bimodal population distribution with probes oriented normal and parallel to the membrane plane. The bimodal tilt distribution is consistent with other studies that have shown BODIPY probes interact with both the acyl tails and lipid headgroups. The single molecule measurements reported here for a range of BODIPY probes suggest this is a general feature of membrane insertion for these lipid analogs. As the surface pressure of the film is increased, the population shifts from parallel to normal oriented probes for all the BODIPY analogs studied. The sensitivity to surface pressure, however, is shown to strongly depend on BODIPY location within the acyl tails and identity of the headgroup. The single molecule measurements suggest that analog structures which minimize BODIPY/lipid headgroup interactions while placing the BODIPY probe within structured regions of the acyl chains provides the optimal sensitivity to membrane surface pressure. Of the fluorescent lipid analogs studied here, the BODIPY-$C_4C_9$-PC probe demonstrated the highest sensitivity to membrane surface pressure changes. These results show that single molecule orientation measurements can help unravel the complicated interactions between fluorescent lipid probes and their surrounding membrane environments and provides a new tool for studying membrane structure and heterogeneity at the molecular level.

*This chapter has been adapted in part from previously published work: Armendariz, K. P., H. A. Huckabay, P. W. Livanec, and R. C. Dunn. 2012. Single molecule probes of membrane structure: Orientation of BODIPY probes in DPPC as a function of probe structure. Analyst 137:1402-1408.*

### 3.5 - References


1. Simons, K., and E. Ikonen. 1997. Functional rafts in cell membranes. Nature 387:569-572.

2. Brown, D. A., and E. London. 1998. Structure and Origin of Ordered Lipid Domains in Biological Membranes. J. Membrane Biol. 164:103-114.

3. Shaw, A. S. 2006. Lipid rafts: now you see them, now you don't. Nat. Immunol. 7:1139-1142.

4. Singer, S. J., and G. L. Nicolson. 1972. The Fluid Mosaic Model of the Structure of Cell Membranes. Science 175:720-731.

5. Silvius, J. R. 2003. Role of cholesterol in lipid raft formation: lessons from lipid model systems. Biochim. Biophys. Acta (BBA) - Biomembranes 1610:174-183.

6. Burns, A. R., D. J. Frankel, and T. Buranda. 2005. Local mobility in lipid domains of supported bilayers characterized by atomic force microscopy and fluorescence correlation spectroscopy. Biophys. J. 89:1081-1093.

7. Frey, S. L., E. Y. Chi, C. Arratia, J. Majewski, K. Kjaer, and K. Y. C. Lee. 2008. Condensing and fluidizing effects of ganglioside GM1 on phospholipid films. Biophys. J. 94:3047-3064.

8. Dietrich, C., L. A. Bagatolli, Z. N. Volovyk, N. L. Thompson, M. Levi, K. Jacobson, and E. Gratton. 2001. Lipid rafts reconstituted in model membranes. Biophys. J. 80:1417-1428.

9. Gudmand, M., M. Fidorra, T. Bjørnholm, and T. Heimburg. 2009. Diffusion and Partitioning of Fluorescent Lipid Probes in Phospholipid Monolayers. Biophys. J. 96:4598-4609.

10. Schneider, M. B., W. K. Chan, and W. W. Webb. 1983. Fast diffusion along defects and corrugations in phospholipid P beta, liquid crystals. Biophys. J. 43:157-165.

11. Juhasz, J., J. H. Davis, and F. J. Sharom. 2010. Fluorescent probe partitioning in giant unilamellar vesicles of ‘lipid raft’ mixtures. Biochem. J.430:415-423.

12. Baumgart, T., G. Hunt, E. R. Farkas, W. W. Webb, and G. W. Feigenson. 2007. Fluorescence probe partitioning between Lo/Ld phases in lipid membranes. Biochim. Biophys. Acta (BBA) - Biomembranes 1768:2182-2194.

13. Kahya, N., D. Scherfeld, K. Bacia, B. Poolman, and P. Schwille. 2003. Probing Lipid Mobility of Raft-exhibiting Model Membranes by Fluorescence Correlation Spectroscopy. J. Biol. Chem. 278:28109-28115.

14. Kahya, N., D. Scherfeld, and P. Schwille. 2005. Differential lipid packing abilities and dynamics in giant unilamellar vesicles composed of short-chain saturated glycerol-phospholipids, sphingomyelin and cholesterol. Chem. Phys. Lipids 135:169-180.

15. Parasassi, T., F. Conti, M. Glaser, and E. Gratton. 1984. Detection of phospholipid phase separation. A multifrequency phase fluorimetry study of 1,6-diphenyl-1,3,5-hexatriene fluorescence. Journ. Biol. Chem. 259:14011-14017.

16. Zannoni, C., A. Arcioni, and P. Cavatorta. 1983. Fluorescence depolarization in liquid crystals and membrane bilayers. Chem. Phys.Lipids 32:179-250.

17. van der Heide, U. A., G. van Ginkel, and Y. K. Levine. 1996. DPH is localised in two distinct populations in lipid vesicles. Chem. Phys. Lett. 253:118-122.

18. Boldyrev, I. A., X. Zhai, M. M. Momsen, H. L. Brockman, R. E. Brown, and J. G. Molotkovsky. 2007. New BODIPY lipid probes for fluorescence studies of membranes. J Lipid Res. 48:1518-1532.

19. Boldyrev, I. A., and I. G. Molotkovsky. 2006. [A synthesis and properties of new 4,4-difluoro-3a,4a-diaza-s-indacene (BODIPY))-labeled lipids]. Bioorg. Khim. 32:87-92.

20. Karolin, J., L. B. A. Johansson, L. Strandberg, and T. Ny. 1994. Fluorescence and Absorption Spectroscopic Properties of Dipyrrometheneboron Difluoride (BODIPY) Derivatives in Liquids, Lipid Membranes, and Proteins. J. Am. Chem. Soc. 116:7801-7806.

21. Johnson, I. D., H. C. Kang, and R. P. Haugland. 1991. Fluorescent membrane probes incorporating dipyrrometheneboron difluoride fluorophores. Anal. Biochem. 198:228-237.

22. Omel'kov, A. V., Y. B. Pavlova, I. A. Boldyrev, and J. G. Molotkovsky. 2007. Depth-dependent investigation of the apolar zone of lipid membranes using a series of fluorescent probes, Me-4-BODIPY-8-labeled phosphatidylcholines. Russ. J. Bioorg. Chem. 33:505-510.

23. Sachl, R., I. Boldyrev, and L. B. A. Johansson. 2010. Localisation of BODIPY-labelled phosphatidylcholines in lipid bilayers. Phys. Chem. Chem. Phys. 12:6027-6034.

24. Kaiser, R. D., and E. London. 1998. Determination of the depth of BODIPY probes in model membranes by parallax analysis of fluorescence quenching. Biochim. Biophys. Acta (BBA) - Biomembranes 1375:13-22.

25. Menger, F. M., J. S. Keiper, and K. L. Caran. 2002. Depth-profiling with giant vesicle membranes. J. Am. Chem. Soc. 124:11842-11843.

26. Livanec, P. W., and R. C. Dunn. 2008. Single-molecule probes of lipid membrane structure. Langmuir 24:14066-14073.

27. Livanec, P. W., H. A. Huckabay, and R. C. Dunn. 2009. Exploring the effects of sterols in model lipid membranes using single-molecule orientations. J. Phys. Chem. B 113:10240-10248.

28. Huckabay, H. A., and R. C. Dunn. 2011. Hydration Effects on Membrane Structure Probed by Single Molecule Orientations. Langmuir 27:2658-2666.

29. Toprak, E., J. Enderlein, S. A. Mckinney, S. Syed, R. G. Petschek, T. Ha, Y. E. Goldman, and P. R. Selvin. 2005. Simultaneous position and orientation analysis using focused and defocused image analysis: Application to quantum dots and myosin V. Biophys. J. 88:664a.

30. Toprak, E., J. Enderlein, S. Syed, S. A. McKinney, R. G. Petschek, T. Ha, Y. E. Goldman, and P. R. Selvin. 2006. Defocused orientation and position imaging (DOPI) of myosin V. Proc. Natl. Acad. Sci. 103:6495-6499.

31. Patra, D., I. Gregor, and J. Enderlein. 2004. Image analysis of defocused single-molecule images for three-dimensional molecule orientation studies. J. Phys. Chem. A 108:6836-6841.

32. Song, K. C., P. W. Livanec, J. B. Klauda, K. Kuczera, R. C. Dunn, and W. Im. 2011. Orientation of fluorescent lipid analogue BODIPY-PC to probe lipid membrane properties: insights from molecular dynamics simulations. J. Phys. Chem. B 115:6157-6165.

33. Armendariz, K. P., H. A. Huckabay, P. W. Livanec, and R. C. Dunn. 2012. Single molecule probes of membrane structure: Orientation of BODIPY probes in DPPC as a function of probe structure. Analyst 137:1402-1408.

34. Abrams, F. S., A. Chattopadhyay, and E. London. 1992. Determination of the location of fluorescent probes attached to fatty acids using parallax analysis of fluorescence quenching: effect of carboxyl ionization state and environment on depth. Biochemistry 31:5322-5327.

35. Seelig, A., and J. Seelig. 1977. Effect of a single cis double bond on the structure of a phospholipid bilayer. Biochemistry 16:45-50.

36. Song, K. C., P. W. Livanec, J. B. Klauda, K. Kuczera, R. C. Dunn, and W. Im. 2011. Orientation of Fluorescent Lipid Analogue BODIPY-PC to Probe Lipid Membrane Properties: Insights from Molecular Dynamics Simulations. J. Phys. Chem. B 115:6157-6165.

37. Chen, Y., B. C. Lagerholm, B. Yang, and K. Jacobson. 2006. Methods to measure the lateral diffusion of membrane lipids and proteins. Methods 39:147-153.

38. Schütz, G. J., H. Schindler, and T. Schmidt. 1997. Single-molecule microscopy on model membranes reveals anomalous diffusion. Biophys. J. 73:1073-1080.

39. Kiessling, V., J. M. Crane, and L. K. Tamm. 2006. Transbilayer Effects of Raft-Like Lipid Domains in Asymmetric Planar Bilayers Measured by Single Molecule Tracking. Biophys. J. 91:3313-3326.

40. Eggeling, C., C. Ringemann, R. Medda, G. Schwarzmann, K. Sandhoff, S. Polyakova, V. N. Belov, B. Hein, C. von Middendorff, A. Schonle, and S. W. Hell. 2009. Direct observation of the nanoscale dynamics of membrane lipids in a living cell. Nature 457:1159-1162.

# Chapter 4: Ganglioside Influence on Phospholipid Films Investigated with Single Molecule Fluorescence Measurements

## 4.1 - Introduction

Understanding the functional roles of lipids in biological membranes has continued to evolve since the introduction of the fluid mosaic model in 1972 [1]. Far from being passive matrices that simply support membrane constituents, lipids now appear to provide active roles in organizing and modulating events at the cellular membrane. One of the more intriguing and enigmatic roles that has emerged from these studies involves the formation of nanometric lipid domains termed lipid rafts [2, 3]. These small, dynamic domains represent compositional heterogeneities in the membrane that are thought to be important in signaling and organizational processes [4, 5].

The formation of domains in complex mixtures, such as those found in biomembranes, is neither surprising nor unexpected. Characterizing their physical, chemical, and biological properties, however, has proven daunting in natural membranes given the complexity of the system and often lack of clear controls. Moreover, the small size and dynamic nature of lipid rafts makes them difficult to probe directly in intact membranes, which has led to some controversy in the literature [5-7]. These challenges have led to the widespread use of model membranes where specific interactions can be probed in highly controlled environments [8, 9]. These studies have proven invaluable for understanding how putative raft components interact in various lipid environments and in identifying key interactions that modify membrane structure. For example, these studies have characterized the formation of domains in lipid membranes [10, 11], elucidated the effect of cholesterol on membrane fluidity [12], and characterized the complex partitioning of lipid raft components [13]. For the latter, studies involving ganglioside

GM1, a putative raft component, illustrates the complexity that can be encountered even in simple membrane mixtures [14-21].

GM1 is part of a larger class of glycolipids found predominantly in the outer leaflet of animal cell membranes. GM1 is a member of the ganglioside family whose members contain oligosaccharides with one or more sialic acid residues, giving them a net negative charge. Over 100 gangliosides have been identified in vertebrate cells and their incorporation into membranes appears ubiquitous [22]. While they represent only a minor component in most cells, they are enriched in neuronal membranes where they can comprise ~2 to 10% of the total lipid content [23, 24]. Among other functions, they appear to play roles in cell recognition, signal transduction, and as receptors for viruses and toxins [25-28]. Ganglioside GM1, for example, is a cell-surface receptor for cholera toxin, the bacterial toxin which leads to the incapacitating diarrhea of cholera.

GM1 is anchored in the external leaflet of cellular bilayers through its hydrophobic ceramide group while its bulky oligosaccharide region is exposed to the extracellular milieu. Structural diversity within the ceramide group has recently been shown to influence how GM1 traffics cholera toxin from the plasma membrane to the endoplasmic reticulum, illustrating the complex structure/function relationships associated with GM1 [29]. This complexity is also manifest in model membrane studies which have revealed complex partitioning of GM1 between lipid phases [14-21].

Atomic force microscopy (AFM) studies of model membranes have shown that GM1 partitions into condensed domains at low GM1 concentrations [14-19]. In Langmuir-Blodgett (LB) mixed monolayers of DOPC and DPPC, for example, the addition of GM1 (0.2 mol% to 1 mol%) leads to the formation of nanometric domains within condensed regions of the film [18]. As the GM1 concentration is increased to 4 mol%, the number of these domains increases

accompanied by the formation of elongated domains along the condensed phase boundaries. These studies also identified small domains in the expanded membrane regions at higher GM1 concentrations.

Studies on more complicated mixtures have found essentially the same trends. AFM studies on supported membranes of sphingomyelin, DOPC, and cholesterol found evidence for GM1 partitioning into condensed domains rich in cholesterol and sphingomyelin [15]. As GM1 was increased to 5 mol%, additional GM1 rich condensed microdomains were observed in the expanded regions of the films. These and related studies largely agree that GM1 segregates into condensed domains at low mole percentages and experiences expanded phase partitioning at higher concentrations.

Isotherm and X-ray diffraction studies have shown that pure GM1 monolayers remain fluid at all surface pressures, which is attributed to the bulky charged headgroup of GM1 [14, 30]. Even when the GM1 headgroups are tightly packed at high surface pressures, there remains sufficient freedom for the acyl tails to adopt disordered configurations. These observations raise intriguing questions regarding the mechanism that drives GM1 to partition within condensed domains in mixed membranes. In mixed monolayers with the zwitterionic lipid DPPC, for example, GM1 has a condensing effect on the monolayer at low mole percentages [14]. Fluorescence studies of phase partitioning have found a gradual growth in the liquid condensed (LC) domains with increasing [GM1] from 10 mol% to 25 mol%. Interestingly, as the GM1 component is increased above 25 mol%, the fluorescence measurements revealed a reversal in the trend. At the higher GM1 levels, the LC domains gradually diminish as the film becomes expanded, eventually becoming purely liquid expanded (LE) at high GM1 concentration. The transition from condensing to expanding effect observed at 25 mol% was interpreted as reflecting a stoichiometric interaction between GM1 and DPPC that leads to an

optimal packing in the membrane. Once the GM1 component exceeds this stoichiometric limit, additional GM1 expands the membrane.

These measurements reveal the complicated influence that GM1 can have on membrane structure. Due to experimental constraints, however, most studies have focused on relatively high GM1 concentrations, which are not reflective of the typically low levels found in most natural membranes. The phase structure observed in fluorescence measurements at low GM1 levels, for instance, is ill-defined which limits the amount of useful information that can be extracted from these measurements. This places a practical limit of ~5 mol% GM1 in these studies. Recently, we have shown that single molecule fluorescence measurements can provide a complementary view into membrane structure [31-36]. These studies characterize the orientation of acyl-linked-BODIPY fluorescent lipid analogs doped into membranes at trace levels which have been shown to be sensitive to the surrounding lipid matrix. These measurements have been used to characterize changes in membrane structure due to surface pressure, the addition of additives such as cholesterol, and ambient humidity levels [31-34]. Here we use this approach to probe changes in DPPC structure at the molecular level with the addition of GM1. Within this study the optimal BODIPY probe in terms of sensitivity, BODIPY-PC (or BODIPY-$C_4C_9$-PC from Chapter 3), is employed.

Single molecule fluorescence measurements on Langmuir-Blodgett (LB) mixed monolayers of DPPC and GM1 are studied over the GM1 concentration range of 0.05 mol% to 100 mol%. The low concentration range is several orders of magnitude lower than previous fluorescence studies of GM1 influence and reveals significant changes occur in the monolayers even at these low levels. At the higher concentration range, the single molecule measurements of membrane structure reveal complicated trends with GM1 that are consistent with previous bulk studies in model systems [14, 15, 18]. The trends observed from 0.05 mol% to 0.10 mol% GM1 in DPPC suggest that GM1 partitions into the expanded phase at low concentrations and

only above 0.10 mol% begins to partition into the condensed regions as observed previously. Thus, the single molecule orientation measurements presented here offer new insight into the complex phase partitioning of GM1 at the low concentrations typically observed in most biological cell types.

### 4.2 - Materials and Methods

Dipalmitoylphosphatidylcholine (DPPC), dipalmitoylphosphatidylserine (DPPS), and ganglioside GM1 (GM1) (Avanti Polar Lipids, Alabaster, AL) were obtained at >99% purity and used without further purification. Lipid stock solutions of DPPC were prepared at 1 mg/mL in chloroform. Stock solutions containing DPPS or GM1 were prepared at 1 mg/mL in a 65:35 volume mixture of chloroform and methanol. The fluorescent lipid analog 2-(5-butyl-4,4-difluoro-4-bora-3a,4a-diaza-s-indacene-3-nonanoyl)-1-hexadecanoyl-sn-glycero-3-phosphocholine (BODIPY-PC) (Invitrogen Corporation, Carlsbad, CA) was diluted in methanol to obtain appropriate working concentrations. The chemical structures for the lipids employed in this study are shown in **Fig. 4.1**.

Lipid monolayers prepared for bulk fluorescence studies were doped with 0.5 mol% BODIPY-PC dye, while monolayers prepared for single molecule measurements were doped with ~$10^{-8}$ mol% of the reporter dye. Approximately 50 µL of the appropriate lipid solution was dispersed on an 18MΩ water subphase in a Langmuir-Blodgett trough (Type 611, Nima Technology, Coventry, England). The solvent was allowed to evaporate for at least 15 min prior to initiating compression/expansion cycles to anneal the film. Each monolayer was subjected to two compression/expansion cycles between surface pressures of 40 mN/m and 10 mN/m. The barrier rate during these cycles was held at 100 $cm^2$/min. Following the last expansion, the monolayers were compressed to the desired target pressure and held for ~10 min prior to transfer onto a solid substrate. Monolayers were transferred on to Piranha-cleaned glass

coverslips in a headgroup down arrangement using a dipping velocity of 5 mm/min. All monolayers were transferred and imaged at 22°C.

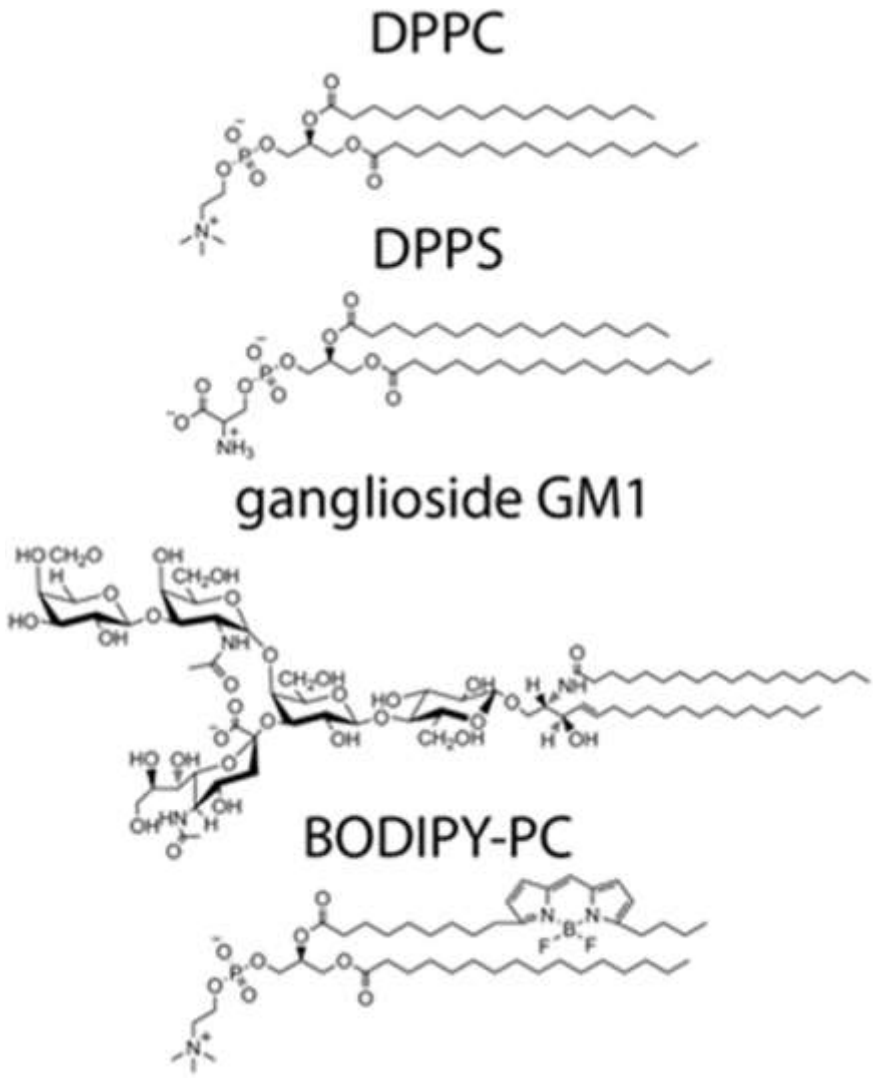


**Figure 4.1** - Chemical structures for DPPC, DPPS, ganglioside GM1, and the fluorescent lipid analog, BODIPY-PC.

Monolayers were imaged with a total internal reflection microscope (TIRF-M) (Olympus IX71, Olympus, Center Valley, PA) equipped with a 100x, 1.45 NA objective (Achromat, Olympus, Center Valley, PA) for single molecule imaging, and a 60x, 1.45 NA (Achromat, Olympus) objective for bulk fluorescence imaging. P-polarized excitation was generated at the

sample by directing the 514nm line from an argon ion laser (Coherent Innova 90, Coherent Inc., Santa Clara, CA) through half-wave and quarter-wave plates (Newport, Irvine, CA). Bulk and single molecule fluorescence images were collected in an epi-illumination configuration with a cooled CCD camera (Retiga 1300, Q Imaging, Surrey, BC, Canada). Single molecule orientation measurements were collected with the optics defocused ~500 nm using a piezo focusing collar (Mad City Labs Inc., Madison, WI) on the objective. The defocus distance was consistent with single molecule emission pattern simulations using MATLAB (Mathworks, Natick, MA). The TIRF angle was controlled by positioning the excitation light in the back aperture of the objective to achieve an incident angle just greater than the critical angle of 41.4°. Image collection was controlled using Slidebook software (Intelligent Imaging Innovations, Denver, CO) with 500 ms integrations and no binning used in the single molecule captures. Bulk fluorescence and single molecule images were analyzed in ImageJ (U.S. National Institutes of Health, Bethesda, MD) and MATLAB (Mathworks, Natick, MA), respectively, as discussed elsewhere.[31]

In this work, we report the measured tilt angles of the individual BODIPY-PC molecules doped into supported monolayers containing DPPC, GM1, and/or DPPS. Each monolayer condition was studied at multiple areas of at least 3 separate films, and N represents the total number of single molecule orientations measured at each monolayer condition. The following monolayer conditions are included in this study: pure DPPC monolayers deposited at 7 mN/m (N= 324), 23 mN/m (N= 363), and 40 mN/m (N= 418); pure GM1 monolayers deposited at 7 mN/m (N= 258), 23 mN/m (N= 375), and 40 mN/m (N= 328); mixed monolayers of DPPC/GM1 deposited at 23 mN/m containing 0 (N= 363), 0.05 (N= 594), 0.1 (N= 865), 0.5 (N= 1013), 1 (N= 512), 5 (N= 980), 10 (N= 1312), 15 (N= 960), 20 (N= 653), 33 (N= 926), 50 (N= 605) and 100 (N= 375) mol % GM1; and mixed monolayers of DPPC/DPPS deposited at 23 mN/m containing 0 (N= 363), 0.05 (N= 603), 0.1 (N= 623), 1 (N= 638), 5 (N= 386), 20 (N= 764) mol % DPPS.

## 4.3 - Results and Discussion

The macroscopic membrane structure of DPPC monolayers doped with increasing amounts of GM1 was characterized using fluorescence microscopy with the results shown in **Fig. 4.2**. The DPPC/GM1 monolayers were doped with 0.5 mol% of the fluorescent lipid analog BODIPY-PC and transferred onto glass substrates at a surface pressure of 23 mN/m using the LB technique. This surface pressure has previously been found to mimic the effective surface pressure of bilayers, although higher surface pressures have also been reported [32]. The bright areas of the monolayers shown in **Fig. 4.2** denote liquid expanded (LE) phase regions of the membrane that incorporate the BODIPY-PC probe while the dark areas reflect liquid condensed (LC) domains. In agreement with previous studies, the series of images shown in **Fig. 4.2** reveal a striking evolution in monolayer structure as the GM1 concentration is increased from 0 to 60 mol% [14].

At low GM1 levels (<5 mol%), the dark LC domains are relatively irregular in shape and lack boundary definition. At approximately 5 mol% GM1, the LC domains take on a distinctive shape and the LC and LE phases become clearly defined, with sharp borders marking the transitions between the phases. As seen previously, as the mol% of GM1 is increased the percent LC area of the monolayer steadily increases up to approximately 20 mol% GM1. Above this concentration, additional GM1 leads to the steady reduction in LC domain size and increase in the expanded regions of the membrane. The trends observed in **Fig. 4.2** are quantified in **Fig. 4.3** which plots the percent area of the LC phase as a function of GM1 concentration.

As shown in **Fig. 4.3**, the percent area coverage of LC phase in the DPPC/GM1 mixture increases up to ~20 mol% GM1, after which the percent area steadily decreases as more GM1 is added. Previous studies have found similar trends and suggest that GM1 initially partitions

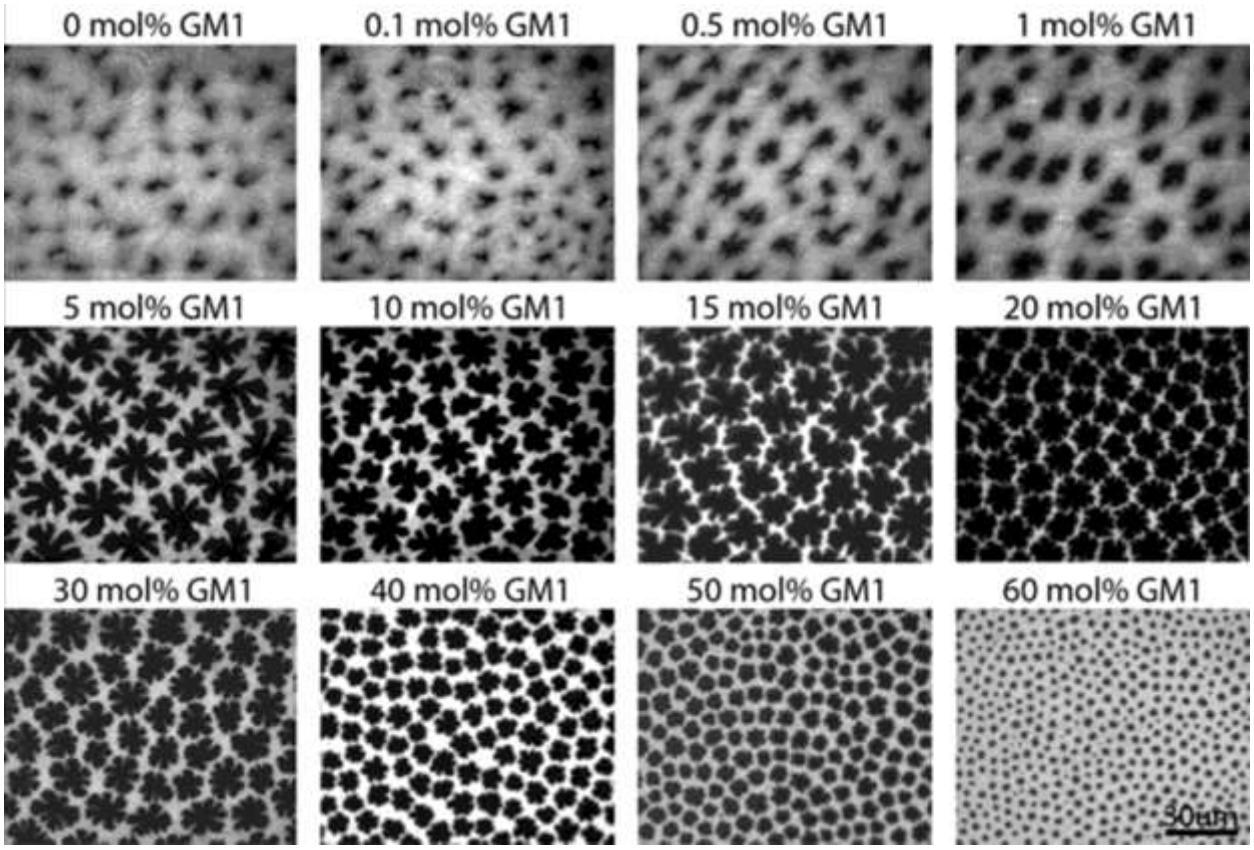


**Figure 4.2** - Fluorescence images of DPPC monolayers containing the indicated concentration of GM1. Monolayers were doped with 0.5 mol% of the fluorescent lipid analog BODIPY-PC and transferred onto a glass substrate at a surface pressure of 23 mN/m using the Langmuir-Blodgett technique. The liquid condensed (LC) phases exclude the BODIPY-PC probe and appear dark, while the liquid expanded (LE) phases incorporate the dye and appear bright. The scale bar is 30 μm.

into the condensed regions of membranes at low mole percentages [18]. Molecular area measurements suggest DPPC and GM1 mix stoichiometrically in these condensed domains, forming complexes with reduced area compared to the sum of the individual components [14]. Increasing GM1 concentration beyond the optimal packing ratio leads to GM1 appearing in the LE phase leading to increasingly expanded films above ~20 mol% GM1. The results shown in **Figs. 4.2** and **4.3**, therefore, are consistent with previously observed trends.

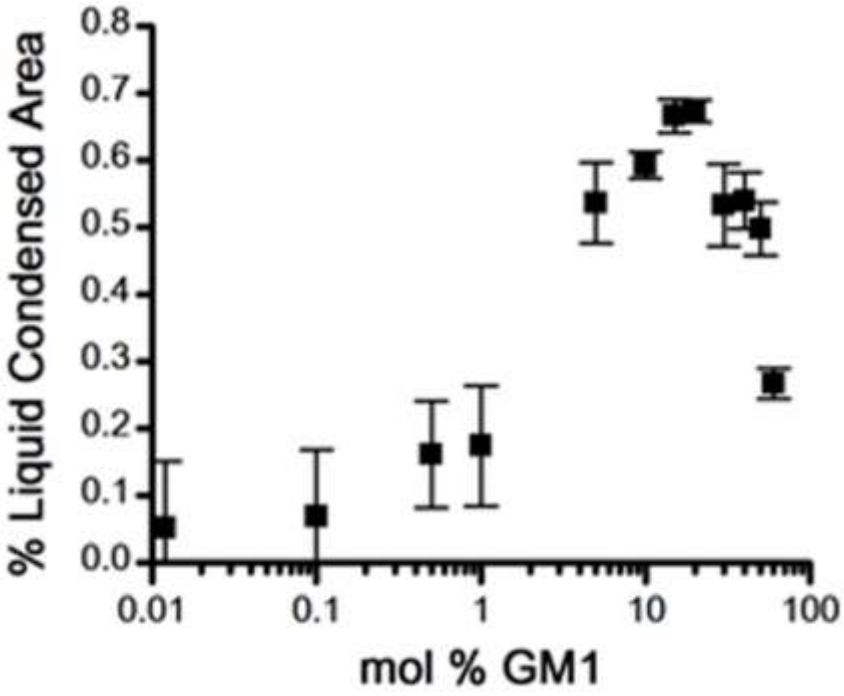


**Figure 4.3** - Plot of the percent coverage of liquid condensed (LC) phase as a function of [GM1], extracted from the fluorescence images shown in **Fig. 4.2**. The data points represent 0, 0.1, 0.5, 1, 5, 10, 15, 20, 30, 40, 50, and 60 mol% GM1 in DPPC.

As illustrated in **Fig. 4.2**, fluorescence microscopy is useful in visualizing and characterizing macroscopic phase separation in supported lipid monolayers of DPPC and GM1 when GM1 concentrations are above ~5 mol%. These approaches, therefore, can add insight into the role of GM1 in biological systems such as neuronal membranes where the GM1 component is highly enriched and can reach levels as high as ~2 to 10 mol% [23]. For the majority of biological membranes, however, gangliosides represent only a minor fraction of the membrane composition which raises intriguing questions about their role in modifying membrane structure at low abundance [24]. As shown in **Fig. 4.2**, fluorescence microscopy measurements become less informative at GM1 concentrations less than ~5 mol% as the macroscopic phase structure and effects of GM1 on film properties become less well defined.

Previously, we have shown that single molecule fluorescence measurements can provide new insight into membrane properties [31-34]. These measurements track changes in the orientation of fluorescent lipid analogs doped into films at trace levels and have been shown to be sensitive to changes in film surface pressure and the presence of additives [31-34]. These single molecule fluorescence measurements use defocused polarized total internal fluorescence microscopy (PTIRF-M) to excite and image fluorescent probes doped into lipid membranes at $\sim 10^{-8}$ mol%. As an example, **Fig. 4.4** compares defocused single molecule PTIRF-M images of BODIPY-PC doped into pure monolayers of DPPC and GM1. Monolayers transferred onto glass substrates at low ($\pi$ = 7 mN/m) and high ($\pi$ = 40 mN/m) surface pressures using the LB technique are compared.

As discussed elsewhere, the single molecule emission patterns observed in the defocused PTIRF-M images reflect the three-dimensional orientation of the probe emission dipole in the lipid matrix [31]. Emission dipoles oriented normal to the membrane plane, for example, lead to donut-like emission features while dipoles oriented in the membrane plane appear as elliptical features with wings. In **Fig. 4.4**, for instance, an evolution in the single molecule emission patterns from predominantly elliptical with wings to doughnut-like is observed for DPPC in going from low to high pressure, respectively. The BOPIDY-PC probe shown in **Fig. 4.1** has an acyl-linked fluorophore and anisotropy studies have shown that the emission dipole lies approximately along the long axis of the conjugated ring system [37]. The location of the fluorophore in the tail region makes its orientation sensitive to the structure of the surrounding lipid matrix. As the surface pressure of DPPC is increased, therefore, more doughnut-like emission features are observed as BODIPY-PC tails adopt an elongated conformation.

The results for DPPC can be contrasted with single molecule orientation measurements of BODIPY-PC doped into monolayers of GM1. The fluorescence images shown in **Fig. 4.4**

reveal little change in the single molecule emission patterns with surface pressure for BODIPY-PC doped into GM1 monolayers. Qualitatively, the lack of donut-like emission features

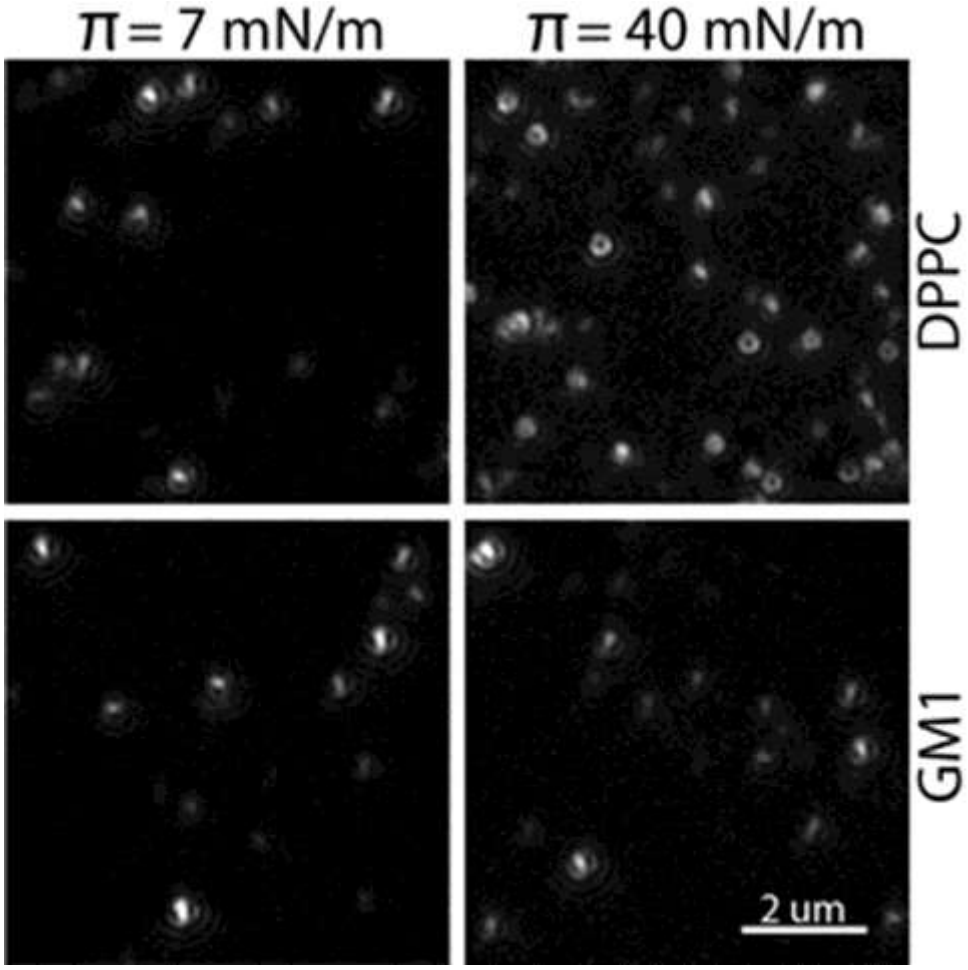


**Figure 4.4** - Representative defocused TIRF-M single molecule fluorescence images of pure DPPC and GM1 LB monolayers doped with ~$10^{-8}$ mol% BODIPY-PC and transferred at 7 mN/m and 40 mN/m. Each bright feature represents the fluorescence from a single BODIPY-PC dye molecule and has a distinctive emission pattern reflective of its orientation within the film. Fluorescent probes with emission dipoles lying in the plane of the film appear as elliptical structures with wings while those oriented perpendicular to the membrane plane exhibit doughnut like structures. For DPPC, a significant change in BODIPY-PC orientation with surface pressure is observed while orientations within GM1 films remain qualitatively the same with surface pressure. The scale bar is 2 μm.

suggests that most emission dipoles lie in the membrane plane. The similarity between the images collected at low and high surface pressure indicates that surface pressure has little effect on the BODIPY-PC probe orientation in GM1 films. This is consistent with previous measurements showing GM1 films remain expanded over the surface pressures studied.

The emission patterns, such as those shown in **Fig. 4.4**, can be analyzed to extract both the polar ($\varphi$) and azimuthal (θ) angles for each emission dipole in the image. This orientation information is used to populate histograms of the polar ($\varphi$) or tilt angle of the emission dipole with respect to the membrane normal. Previous studies have shown that the tilt angle of BODIPY-PC within supported lipid monolayers is a sensitive probe of the surrounding membrane environment. Tilt angle histograms for BODIPY-PC in monolayers of pure DPPC and pure GM1 at the surface pressures studied in **Fig. 4.4** are compared in **Fig. 4.5**.

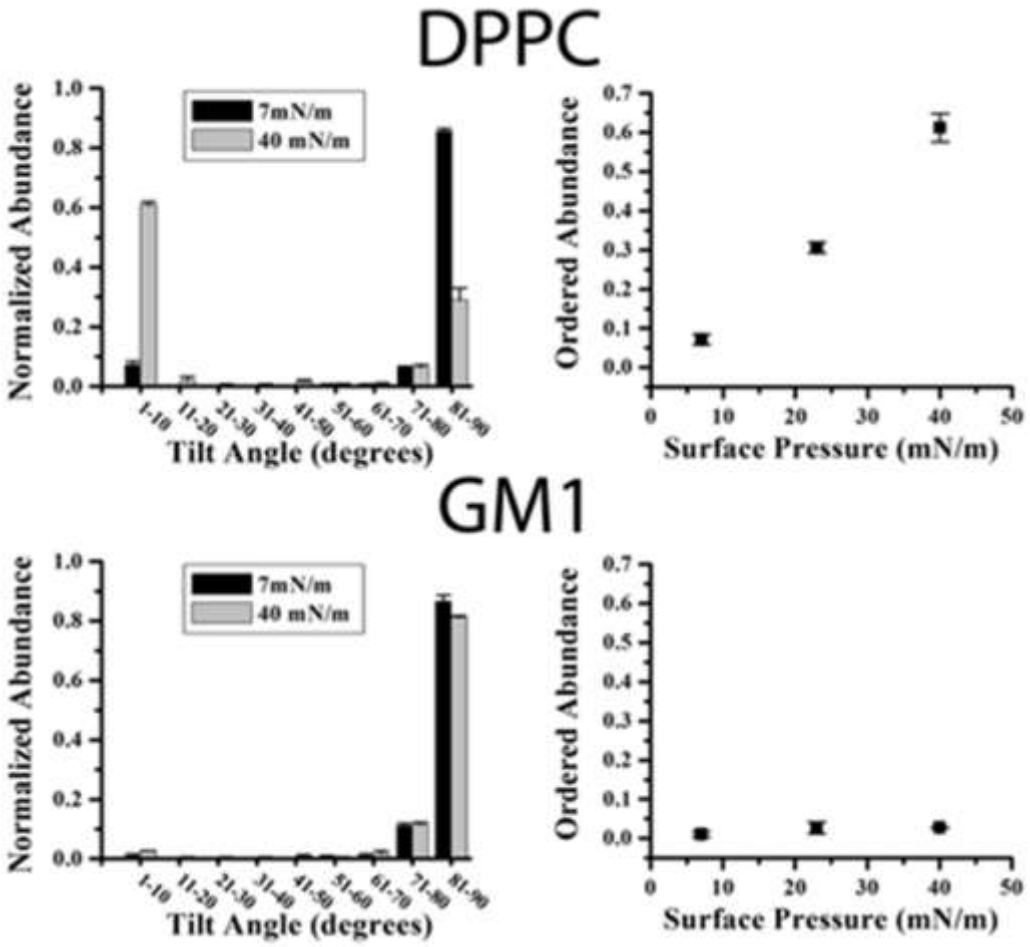


**Figure 4.5** – Tilt angle histograms for BODIPY-PC doped into monolayers of DPPC and GM1 transferred at 7 mN/m and 40 mN/m. Single molecule emission patterns, such as those shown in **Fig. 4.4**, are modeled to extract the BODIPY-PC emission dipole tilt angle with respect to the membrane normal to populate each histogram. At each surface pressure studied, more than 250 individual molecules were measured from at least 3 separate monolayers. The ordered abundance or population oriented normal to the surface normal ($\varphi \leq 10°$) at each surface pressure is extracted and plotted as a function of surface pressure. The ordered abundance in DPPC increases with surface pressure while ordered abundance in GM1 remains low at all surface pressures, reflecting its expanded state.

For BODIPY-PC in DPPC, **Fig. 4.5** reveals a bimodal distribution of probes predominantly oriented either normal ($\varphi \leq 10°$) or parallel ($\varphi \geq 81°$) to the membrane plane, with only a small fraction occupying intermediate tilt angles. Increasing the surface pressure leads to a shift in population from parallel to normal oriented probes, with little change in the intermediate tilt population. The reduced area per lipid at higher surface pressures in DPPC favors an elongated acyl chain configuration leading to normal oriented emission features. By tracking the proportion of BODIPY-PC probes oriented normal ($\varphi \leq 10°$) to the membrane plane, known henceforth as the *ordered abundance*, changes in the molecular level structure of the monolayer can be characterized for DPPC. The ordered abundance plotted in **Fig. 4.5** shows an increasing trend with surface pressure. This approach has been used previously to probe DPPC membranes as a function of relative humidity, the addition of additives such as cholesterol, and membrane surface pressure [31-34].

The results for GM1 show markedly different results. The tilt angle histograms show that the vast majority of the BODIPY-PC probes are oriented with their emission dipole lying in the plane of the film. Moreover, the tilt angle histograms measured at the surface pressures for GM1 are statistically indistinguishable, indicating that changes in monolayer surface pressure have little effect on BODIPY-PC orientation. As mentioned earlier, these measurements are consistent with bulk studies that have shown that GM1 films remain expanded at all surface pressures [30].

The results summarized in **Figs. 4.4** and **4.5** show that single molecule measurements of membrane order lead to dramatically different trends for films of DPPC and GM1 as a function of surface pressure. To probe the effects of GM1 on DPPC, similar measurements were carried out in mixed monolayers doped with ~$10^{-8}$ mol% BODIPY-PC. Single molecule defocused P-TIRFM studies of DPPC/GM1 monolayers as a function of [GM1] were measured on monolayers transferred at 23 mN/m. At each GM1 concentration, single molecule emission

patterns were measured and modeled to extract the tilt angles of the BODIPY-PC probe. As shown in **Fig. 4.4**, the ordered abundance or proportion of probes oriented normal ($\varphi \leq 10°$) to the membrane plane provides a useful metric for tracking changes in film structure. Therefore, **Fig. 4.6** plots the ordered abundance extracted from tilt angle histograms of BODIPY-PC in DPPC/GM1 monolayers as a function of GM1 concentration. Each point in **Fig. 4.6** represents the ordered abundance extracted from the measured tilt angle of at least 350 individual molecules from least 3 separate films.

**Figure 4.6** reveals a complicated trend in BODIPY-PC orientation with increasing GM1 levels. A sharp decrease in the single molecule ordered abundance is observed immediately upon the addition of GM1 to DPPC. The ordered abundance drops from ~30% in pure DPPC to just over 10% with the addition of 0.1 mol% GM1. As GM1 levels increase, however, this trend reverses. As shown in **Fig. 4.6**, the ordered abundance increases to 24% with the addition of 0.5 mol% GM1 and continues to rise back to ~30% at 15 mol% GM1. This value is approximately the same as that measured in pure DPPC containing no GM1 at this surface pressure. As GM1 levels increase above 15 mol%, however, the single molecule ordered abundance again decreases towards a final value of 3% observed in pure GM1 monolayers transferred at 23 mN/m.

Comparing the trends observed in **Figs. 4.3** and **4.6** reveals close agreement between the single molecule orientation measurements and bulk fluorescence measurements of film structure when GM1 levels are greater than 5 mol%. Both trends reflect increasing film order as GM1 levels rise from 5 to 15 mol% GM1. The single molecule measurements and ensemble fluorescence studies also sense the reversal in film order above approximately 20 mol% GM1, as increasingly more GM1 levels expand the film. At low GM1 levels, however, the single molecule orientation measurements reflect changes in film structure that are not apparent in the

bulk fluorescence measurements. This distinction is significant since GM1 is usually present at low levels in most biological membranes.

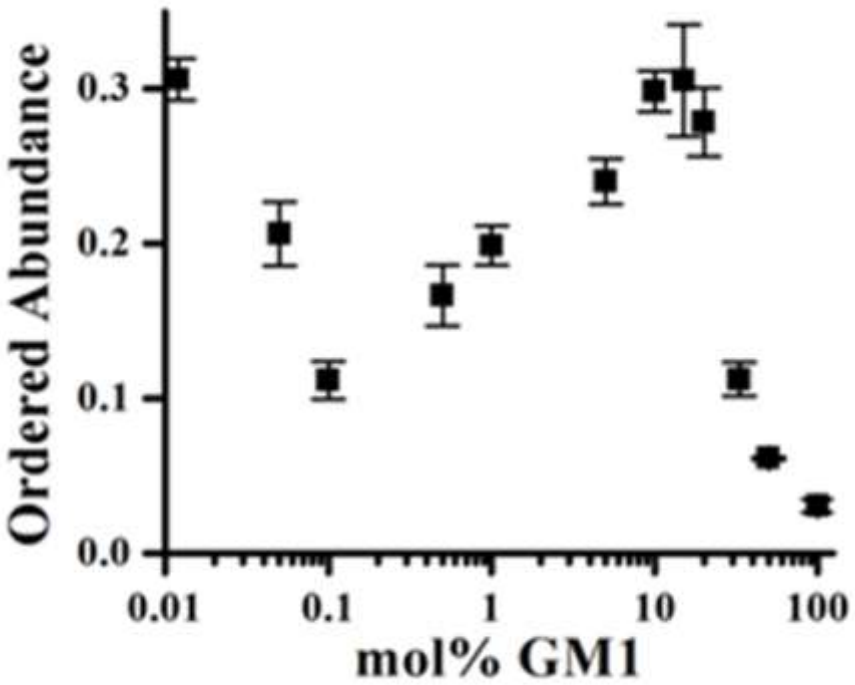


**Figure 4.6** – Plot of the BODIPY-PC single molecule ordered abundance versus mol% GM1 in DPPC monolayers transferred at 23 mN/m. The ordered abundance was quantified using the procedure outlined in **Figs. 4.4** and **4.5**. The data points represent 0, 0.05, 0.1, 0.5, 1, 5, 10, 15, 20, 33, 50, and 100 mol% GM1 in DPPC and are plotted on a log scale for clarity in the low mole percent region. Each point was extracted from tilt angle histograms including at least 350 individual molecules, measured from multiple areas of at least 3 films to ensure representative measurements.

**Figure 4.6** reveals the profound effect the addition of GM1 has on the molecular orientation of BODIPY-PC in DPPC films even when added at trace amounts. While bulk fluorescence measurements reveal no significant change in macroscopic membrane structure at low mol% GM1, single molecule orientation measurements reveal substantial changes occur in the molecular level structure of the film upon the addition of trace amounts of GM1. As shown

in **Fig. 4.6**, the addition of just 0.05 mol% GM1 causes a 10% drop in the single molecule ordered abundance. This drops another 10% as the GM1 content is increased to 0.1 mol%. These results suggest that even small additions of GM1 to DPPC can lead to significant structural changes in the film which are reflected in the single molecule orientation measurements, but hidden in bulk fluorescence measurements.

Previous single orientation studies have shown that BODIPY-PC orientation in lipid monolayers is influenced by the surrounding lipid acyl chain ordering and electrostatic interactions between the fluorophore and the lipid headgroups [34]. GM1 is a glycosphingolipid, containing neutral sugars and a single negatively charged sialic acid residue in the headgroup. This charge contributes to the electrostatic potential of the membrane and can influence the orientation of nearby BODIPY-PC probe molecules through electrostatic interaction [38]. To confirm that nearby charged headgroups can alter BODIPY-PC orientation, studies in mixed monolayers of DPPC and negatively charged DPPS were conducted. As shown in **Fig. 4.1**, DPPS contains a negatively charged serine group but is otherwise structurally similar to DPPC.

Single molecule orientation measurements of mixed monolayers of DPPC and DPPS were carried out as a function of DPPS. As in the GM1 studies, the monolayers were doped with $10^{-8}$ mol% BODIPY-PC and transferred at 23 mN/m. As before, the single molecule emission patterns were imaged and analyzed to create tilt angle histograms, from which the ordered abundance was extracted and plotted as shown in **Fig. 4.7**. As seen in **Fig. 4.7**, the single molecule ordered abundance immediately drops upon the addition of small mole percentages of DPPS to the DPPC film. The ordered abundance drops from ~30% in pure DPPC to ~10% upon the addition of just 0.1 mol% DPPS, similar to trends observed with the addition of GM1. Unlike the GM1 results, however, the ordered abundance levels off and remains roughly constant as the concentration of DPPS is increased further.

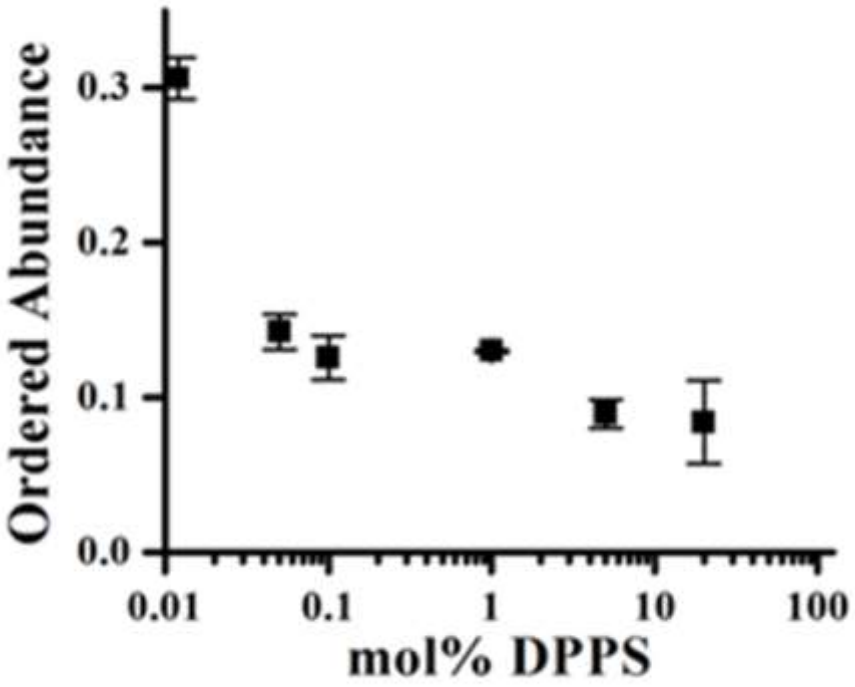


**Figure 4.7** – Plot of the BODIPY-PC single molecule ordered abundance versus mol% DPPS in DPPC monolayers. All monolayers were transferred at 23 mN/m and the data points represent 0, 0.05, 0.1, 1, 5, and 20 mol% DPPS in DPPC. Each point was extracted from tilt angle histograms including at least 350 individual molecules, measured from multiple areas of at least 3 films to ensure representative measurements.

The results shown in **Fig. 4.7** suggest that the negatively charged headgroups of DPPS can influence the orientation of nearby BODIPY-PC probes in the mixed monolayer, leading to decreased abundance of normal oriented probes. The addition of either DPPS or GM1 to DPPC causes a similarly sharp decrease in ordered abundance at low concentrations, suggesting a general mechanism based on favorable electrostatic interactions between the BODIPY-PC fluorophore and the negatively charged headgroups. The sharp decrease may also reflect a disruption in acyl chain packing. However, given the similarity in response to the addition of DPPS and GM1 at low concentrations, an electrostatic mechanism is favored. Given the propensity of BODIPY-PC to partition into the expanded phase and proximity required for

GM1 to influence BODIPY-PC orientation, these results further suggest that GM1 partitions into expanded membrane regions at low concentrations.

At higher concentrations, a significant divergence is observed when comparing the effects that GM1 and DPPS have on the BODIPY-PC probe. **Figure 4.7** shows that the ordered abundance reaches a minimum at ~0.1 mol% DPPS and remains level as more DPPS is added to DPPC. Previous reports have shown that DPPC and DPPS are miscible in the absence of calcium ions [39]. The leveling of ordered abundance with increasing DPPS concentration reflects a saturation of its effect on the BODIPY-PC probe. The results for GM1 shown in **Fig. 4.5**, however, reveal a more complicated evolution in probe orientation.

As GM1 concentration is increased from ~0.1 to ~15 mol%, the single molecule ordered abundance increases to a maximum value equal to pure DPPC films at this surface pressure. This is consistent with a mechanism where GM1 moves from the expanded phase to condensed domains where it packs tightly with condensed phase DPPC. This segregates GM1 from the expanded phase where the BODIPY-PC probe resides, thus leading to the recovery in normal oriented probes. As GM1 concentration is increased above ~20 mol%, the single molecule ordered abundance again decreases as GM1 begins partitioning back into the expanded regions of the film, where it can interact with the BODIPY-PC probe. This is consistent with previous fluorescence studies and results such as those shown in **Figs. 4.2** and **4.3** [14].

The single molecule measurements presented here add new insight into the influence that GM1 has on membrane structure at the low GM1 concentrations found in most biological membranes. The significant influence that GM1 has on the BODIPY-PC probe orientation at low GM1 concentration suggests there is a close proximity between the two, placing GM1 in the expanded regions of the membrane. Given previous observations of stoichiometric interactions between GM1 and DPPC, this may reflect the formation of small GM1/DPPC condensed

domains in the expanded membrane regions of the film [14]. It is interesting to note that AFM studies have also found evidence for GM1 rich domains in the expanded domains of model membranes [15, 18]. While not conforming to the working definition of a lipid raft due to the lack of cholesterol, these structures may nonetheless provide organizational or signaling platforms in cellular membranes. These measurements also help illustrate the utility of single molecule orientation measurements for providing new complementary views into membrane structure.

### 4.4 - Conclusion

Single molecule fluorescence measurements of the fluorescent lipid analog BODIPY-PC are used to probe the effects of GM1 in monolayers of DPPC. Defocused TIRF-M measurements lead to distinct single molecule fluorescence emission patterns which reflect the three-dimensional orientation of each BODIPY-PC probe molecule doped into the film. As shown previously, extracting the tilt angle of the emission dipole with respect to the membrane normal provides a sensitive marker for structural changes taking place in the lipid film. Using this approach, we track the effects of GM1 on LB monolayers of DPPC from 0.05 mol% to 100 mol% GM1. Above 5 mol% GM1, the single molecule measurements closely track trends seen in bulk measurements of membrane structure. At low GM1 levels, however, the single molecule measurements reveal dramatic changes in film properties that are hidden in bulk fluorescence measurements. Large changes are observed in the single molecule tilt histograms with the addition of just 0.05 mol% GM1 to the DPPC monolayer. Control studies using DPPS suggest that electrostatic interactions between the charged headgroup of GM1 and BODIPY-PC probe play an important role in influencing the measured tilt of the emission dipole. These measurements suggest that GM1 initially partitions into the expanded phase, in close proximity to the BODIPY-PC probe where it influences the tilt angle distribution. As GM1 levels increase, GM1 partitions into condensed domains leading to a recovery in the BODIPY-PC tilt angle

distribution as GM1 is segregated away from the probe in the membrane. Finally at high GM1 levels, GM1 appears in the expanded phase again and eventually leads to homogenously fluid membranes. The significant influence that GM1 exerts at low levels is interesting since it is only a minor component in most biological membranes. The formation of small, GM1 rich domains in the expanded phase is also intriguing given the evolving view of the importance of small membrane domains in cellular organization and signaling. Single molecule orientation measurements, therefore, provide a promising new tool for probing these enigmatic structures.

*This chapter has been adapted in part from previously published work: Armendariz, K. P., and R. C. Dunn. 2013. Ganglioside influence on phospholipid films investigated with single molecule fluorescence measurements. J. Phys. Chem. B 117:7959-7966.*

**4.5 - References**


1. Singer, S. J., and G. L. Nicolson. 1972. The fluid mosaic model of the structure of cell membranes. Science 175:720-731.

2. Simons, K., and E. Ikonen. 1997. Functional rafts in cell membranes. Nature 387:569-572.

3. Dietrich, C., L. A. Bagatolli, Z. N. Volovyk, N. L. Thompson, M. Levi, K. Jacobson, and E. Gratton. 2001. Lipid rafts reconstituted in model membranes. Biophys. J. 80:1417-1428.

4. Pike, L. J. 2006. Rafts defined: a report on the Keystone Symposium on Lipid Rafts and Cell Function. J. Lipid Res. 47:1597-1598.

5. Simons, K., and M. J. Gerl. 2010. Revitalizing membrane rafts: new tools and insights. Nat. Rev. Mol. Cell Biol. 11:688-699.

6. Shaw, A. S. 2006. Lipid rafts: now you see them, now you don't. Nat. Immunol. 7:1139-1142.

7. Munro, S. 2003. Lipid rafts: Elusive or illusive? Cell 115:377-388.

8. Janes, P. W., S. C. Ley, A. I. Magee, and P. S. Kabouridis. 2000. The role of lipid rafts in T cell antigen receptor (TCR) signalling. Semin. Immunol. 12:23-34.

9. Langlet, C., A.-M. Bernard, P. Drevot, and H.-T. He. 2000. Membrane rafts and signaling by the multichain immune recognition receptors. Curr. Opin. Immunol. 12:250-255.

10. Silvius, J. R. 2003. Role of cholesterol in lipid raft formation: lessons from lipid model systems. BBA-Biomembranes 1610:174-183.

11. Brown, D. A., and E. London. 1998. Structure and Origin of Ordered Lipid Domains in Biological Membranes. J. Membrane Biol.164:103-114.

12. Simons, K., and E. Ikonen. 2000. Cell biology - How cells handle cholesterol. Science 290:1721-1726.

13. Samsonov, A. V., I. Mihalyov, and F. S. Cohen. 2001. Characterization of cholesterol-sphingomyelin domains and their dynamics in bilayer membranes. Biophys. J. 81:1486-1500.

14. Frey, S. L., E. Y. Chi, C. Arratia, J. Majewski, K. Kjaer, and K. Y. C. Lee. 2008. Condensing and fluidizing effects of ganglioside G(M1) on phospholipid films. Biophys. J.94:3047-3064.

15. Bao, R., L. Li, F. Qiu, and Y. L. Yang. 2011. Atomic Force Microscopy Study of Ganglioside GM1 Concentration Effect on Lateral Phase Separation of

Sphingomyelin/Dioleoylphosphatidylcholine/Cholesterol Bilayers. J. Phys. Chem. B 115:5923-5929.

16. Burns, A. R. 2003. Domain structure in model membrane bilayers investigated by simultaneous atomic force microscopy and fluorescence imaging. Langmuir 19:8358-8363.

17. Burns, A. R., D. J. Frankel, and T. Buranda. 2005. Local mobility in lipid domains of supported bilayers characterized by atomic force microscopy and fluorescence correlation spectroscopy. Biophys. J. 89:1081-1093.

18. Vie, V., N. Van Mau, E. Lesniewska, J. P. Goudonnet, F. Heitz, and C. Le Grimellec. 1998. Distribution of ganglioside G(M1) between two-component, two-phase phosphatidylcholine monolayers. Langmuir 14:4574-4583.

19. Field, K. A., D. Holowka, and B. Baird. 1995. Fc epsilon RI-mediated recruitment of p53/56lyn to detergent-resistant membrane domains accompanies cellular signaling. Proc. Nat. Acad. Sci. 92:9201-9205.

20. Ohta, Y., S. Yokoyama, H. Sakai, and M. Abe. 2004. Membrane properties of binary and ternary systems of ganglioside GM1/ dipalmitoylphosphatidylcholine/ dioleoylphosphatidylcholine. Colloids Surf. B Biointerfaces 34:147-153.

21. Worthman, L. A., K. Nag, P. J. Davis, and K. M. Keough. 1997. Cholesterol in condensed and fluid phosphatidylcholine monolayers studied by epifluorescence microscopy. Biophys. J. 72:2569-2580.

22. Yu, R. K., Y. T. Tsai, T. Ariga, and M. Yanagisawa. 2011. Structures, biosynthesis, and functions of gangliosides--an overview. J. Oleo. Sci. 60:537-544.

23. Derry, D. M., and L. S. Wolfe. 1967. Gangliosides in isolated neurons and glial cells. Science 158:1450-1452.

24. Sonnino, S., L. Mauri, V. Chigorno, and A. Prinetti. 2007. Gangliosides as components of lipid membrane domains. Glycobiology 17:1R-13R.

25. Cheresh, D. A., J. R. Harper, G. Schulz, and R. A. Reisfeld. 1984. Localization of the gangliosides GD2 and GD3 in adhesion plaques and on the surface of human melanoma cells. Proc. Natl. Acad. Sci. U.S.A. 81:5767-5771.

26. Burns, G. F., C. M. Lucas, G. W. Krissansen, J. A. Werkmeister, D. B. Scanlon, R. J. Simpson, and M. A. Vadas. 1988. Synergism between membrane gangliosides and Arg-Gly-Asp-directed glycoprotein receptors in attachment to matrix proteins by melanoma cells. J. Cell Biol. 107:1225-1230.

27. Hakomori, S. 1993. Structure and function of sphingoglycolipids in transmembrane signalling and cell-cell interactions. Biochem. Soc. Trans. 21 ( Pt 3):583-595.

28. Reed, R. A., J. Mattai, and G. G. Shipley. 1987. Interaction of cholera toxin with ganglioside GM1 receptors in supported lipid monolayers. Biochemistry 26:824-832.

29. Chinnapen, D. J., W. T. Hsieh, Y. M. te Welscher, D. E. Saslowsky, L. Kaoutzani, E. Brandsma, L. D'Auria, H. Park, J. S. Wagner, K. R. Drake, M. Kang, T. Benjamin, M. D. Ullman, C. E. Costello, A. K. Kenworthy, T. Baumgart, R. H. Massol, and W. I. Lencer. 2012. Lipid sorting by ceramide structure from plasma membrane to ER for the cholera toxin receptor ganglioside GM1. Dev. Cell 23:573-586.

30. Maggio, B. 1994. The Surface Behavior of Glycosphingolipids in Biomembranes - a New Frontier of Molecular Ecology. Prog. Biophys. Mo.l Bio. 62:55-117.

31. Livanec, P. W., and R. C. Dunn. 2008. Single-molecule probes of lipid membrane structure. Langmuir 24:14066-14073.

32. Livanec, P. W., H. A. Huckabay, and R. C. Dunn. 2009. Exploring the effects of sterols in model lipid membranes using single-molecule orientations. J Phys Chem B 113:10240-10248.

33. Huckabay, H. A., and R. C. Dunn. 2011. Hydration Effects on Membrane Structure Probed by Single Molecule Orientations. Langmuir 27:2658-2666.

34. Armendariz, K. P., H. A. Huckabay, P. W. Livanec, and R. C. Dunn. 2012. Single molecule probes of membrane structure: Orientation of BODIPY probes in DPPC as a function of probe structure. Analyst 137:1402-1408.

35. Patra, D., I. Gregor, and J. Enderlein. 2004. Image analysis of defocused single-molecule images for three-dimensional molecule orientation studies. J. Phys. Chem. A 108:6836-6841.

36. Toprak, E., J. Enderlein, S. Syed, S. A. McKinney, R. G. Petschek, T. Ha, Y. E. Goldman, and P. R. Selvin. 2006. Defocused orientation and position imaging (DOPI) of myosin V. Proc. Natl. Acad. Sci. 103:6495-6499.

37. Karolin, J., L. B. A. Johansson, L. Strandberg, and T. Ny. 1994. Fluorescence and Absorption Spectroscopic Properties of Dipyrrometheneboron Difluoride (Bodipy) Derivatives in Liquids, Lipid-Membranes, and Proteins. J. Am. Chem. Soc. 116:7801-7806.

38. Patel, R. Y., and P. V. Balaji. 2007. Characterization of the conformational and orientational dynamics of ganglioside GM1 in a dipalmitoylphosphatidylcholine bilayer by molecular dynamics simulations. Biochim. Biophys. Acta 1768:1628-1640.

39. Ross, M., C. Steinem, H. J. Galla, and A. Janshoff. 2001. Visualization of chemical and physical properties of calcium-induced domains in DPPC/DPPS Langmuir-Blodgett layers. Langmuir 17:2437-2445.

# Chapter 5 – Integrating Model Membranes in Applications for Label-free Whispering Gallery Mode Biosensors

## 5.1 - Introduction

As discussed in previous chapters, biological membranes form the selective barrier which separate cells from their surroundings. Several of the components which are integrated within these membranes interact with the extracellular environment to allow for cellular signaling, molecular transport, and cell adhesion. In fact, a large percentage of modern medicines are targeted to interact with membrane bound proteins [1]. The role of these membrane components to bind specific extracellular targets has motivated the use of membrane coatings in biosensor applications.

While Chapters 3 and 4 were focused on elucidating the structure of model membranes in order to understand the function of membranes components in biological systems, this chapter will utilize membranes and the components bound within them for biosensing applications. Not only are model membranes capable of incorporating specific components which can be used for antigen capture, but the composition of each coating can be highly controlled, as discussed in Chapter 2. Several groups have already demonstrated the utility of membrane coatings in surface plasmon resonance (SPR) biosenors [2, 3]. These studies typically employ self-assembled monolayers (SAMs), which are easily formed on the gold sensing surface in SPR [3]. These SAMs have proven useful by demonstrating that membrane films can be used to incorporate capture materials for specific analyte detection [2, 4]. Furthermore, SPR studies have shown that SAMs can also be utilized to reduce nonspecific adsorption on the sensor surface [3]. While these findings have been important and SAMs can be attached to several types of surfaces, they are, however, limited in terms of control of

packing density within the film. While Langmuir films allow facile control of lipid surface density through control of surface pressure at the time of film deposition, there are many factors, some of which that are not easy controlled, which influence the formation and packing density of films made using the SAM technique. These factors include solvent type, adsorbate structure, concentration, and purity, and substrate surface charge and cleanliness [5]. Thus, the number of factors which influence SAM structure make controlled studies of packing density within these films a daunting task relative to the LB/LS technique. In this chapter we will address the use of LB/LS bilayers as a selective coating for hydrophilic biosensor surfaces. The importance of controlled packing density within the membrane afforded by LB/LS techniques will be more important in the biosensor study presented in Chapter 6.

Recently, whispering gallery mode (WGM) resonators have become a popular new tool within the biosensing community. These devices resonantly confine light at unique wavelengths within circular glass cavities through continuous total internal reflection. Similar to SPR, the resonant wavelength of a WGM cavity is dependent upon refractive index of the surrounding medium. Changes to the surrounding refractive index caused by binding events on the resonator surface can be detected through changes in the observed resonant wavelength. Using this phenomenon WGM resonators have begun to be employed as label-free detection method for biomolecule detection. The study presented below demonstrates the use of a selective membrane bilayer deposited using the LB/LS method to detect a bacterial toxin. However, we will first begin with a more thorough discussion of WGM biosensor properties, performance metrics, and challenges facing employment of these sensors as routine screening device for biomolecules.

### 5.2 - Whispering Gallery Mode Biosensors

Whispering gallery mode resonators are small dielectric structures that confine light via continuous total internal reflection. Light evanescently coupled into WGM resonators can be efficiently trapped when the wavelength of light is an integer multiple of the distance circumnavigated around the resonator [6-9]. Under these conditions, constructive interference leads to WGM resonances given by:

$$\lambda_r = \frac{2\pi r n_{eff}}{m} \qquad \textbf{Eq. 5.1}$$

where $\lambda_r$ is the resonant wavelength, r is the radius of the resonator, $n_{eff}$ is the effective refractive index, and m is an integer that indexes the mode number [7, 8].

The small size and high quality factors (Q-factors) of WGM resonators have led to widespread studies in both fundamental and applied applications. These attributes seem especially well-suited for sensing applications where their small footprint and large Q-factor naturally lend themselves to the developments taking place in miniaturized detection platforms [6, 9, 10]. Sensing applications with whispering gallery mode resonators take advantage of the link between effective refractive index and resonant wavelength as shown in **Eq. 5.1** [9-12]. Binding of target analytes to recognition elements on the resonator surface can alter the effective refractive index, leading to a shift in the WGM resonant wavelength [12-14]. This provides a sensitive, label-free approach for sensing which has been used to detect and quantify protein and nucleic acid biomarkers of disease [12-16].

Whispering gallery mode biosensing platforms are predominantly built around either high index glass microsphere resonators or microfabricated planar ring resonators [17-20]. The former uses commercially available or easily fabricated microspheres while the latter is produced on-chip using standard microfabrication techniques [17, 18]. Microfabricated planar

ring resonators have demonstrated multiplexing capabilities and are easily incorporated with the fluidics necessary for sample handling and delivery [21]. Microsphere resonators, on the other hand, have historically suffered by comparison in these metrics but offer superior optical characteristics [22]. Microspheres are formed from melts which yield exquisitely smooth surfaces, leading to Q-factors which can be orders of magnitude larger than other resonator designs [7, 19, 23]. Large Q-factors translate into long effective path lengths which improves both the sensitivity and limits of detection, both of which are obviously desirable in sensing applications [9, 24]. Moreover, microspheres are inexpensive, commercially available, and are offered in a range of sizes and materials.

For sensing, therefore, it is highly desirable to combine the multiplexing and fluidics capabilities of microring resonators with the optical properties of microsphere resonators. Recently, a fluorescence imaging approach has been reported that enables the WGM resonances from each microsphere in a field of resonators to be simultaneously measured [12, 16]. This enables large scale multiplexing which removes one of the barriers listed above when using microspheres in sensing applications.

In this approach, light is coupled into a large number of microspheres using the evanescent field created from total internal reflectance in a Dove prism. Each microsphere is labeled with the same fluorescent dye, which acts as marker signaling when a particular resonator comes into resonance. As the excitation wavelength from a tunable diode laser is scanned, a ring of enhanced fluorescence is observed around a microsphere when a WGM resonance is reached. This enables the WGM resonance from each sphere in a large field of view to be simultaneously measured using fluorescence imaging [12, 16].

A potential issue, when using fluorescence readout for the detection with WGM resonances, is the potential adverse effect of the fluorophores on Q-factor. The optimal Q-

factor attainable for an individual sphere is limited by a number of factors which results in light losses from the resonator cavity. As shown in **Eq. 5.2**, these factors include light loses due bending losses ($Q_{rad}$), scattering losses ($Q_{s.s}$), and losses due to the absorption of surface contaminates ($Q_{cont}$) and the resonator cavity itself ($Q_{rad}$). Therefore, adding fluorescent material to the resonator surface which absorbs light from the resonator can effectively limit the potential Q and lower the sensitivity of the sensor. While the fluorescent readout scheme has been advantageous for increasing the multiplex capabilities of the WGM approach, it is important to measure and potentially limit the adverse effect of fluorophore absorbace on the resonator surface. Therefore, within this study we test the performance of resonators coated in membranes of known dye concentration to assess effect of fluorophore absorbance on Q-factor.

$$Q^{-1} = Q_{rad}^{-1} + Q_{s.s}^{-1} + Q_{cont}^{-1} + Q_{mat}^{-1} \qquad \textbf{Eq. 5.2}$$

The fluorescence readout approach enables easily multiplexed WGM detection; however, developing sensing platforms remains problematic due to challenges associated with immobilizing microspheres. Typical biosensing assays require multiple fluid exchanges or mixing steps which can perturb spheres resting on a substrate through gravity alone. This creates problems since the resonant wavelength of a resonator is linked to the axis around which the WGM resonates [8, 10, 25]. Any change in the WGM path around the sphere due to reorientations on the substrate, therefore, can shift the resonant wavelength and nullify an assay.

Immobilizing microsphere resonators on a substrate, however, presents challenges for WGM sensing since the circumference of the sphere supporting the resonance must remain pristine. The fluorescence imaging scheme enabling large scale multiplexing mentioned above requires that light be launched into spheres from a common substrate. This precludes embedding the spheres in adhesives or other films that would disrupt the coupling of light

around the sphere. As shown in **Fig. 5.1,** we have demonstrated that spheres can be loaded into microfabricated arrays of wells to hold them in place. However, this methodology turns out to be problematic in practice. First, the poor monodispersity of spheres complicates matching well size with sphere dimensions for stable immobilization. Additionally, each of these of these spheres should be manually loaded into each well to ensure sphere immobilization, which detracts from the ease of use of this method. Finally, the most problematic issue arises from complications associated with efficiently coupling light into the immobilized spheres. It is very difficult to load arrays with spheres such that they are both tightly held and in good contact with the substrate, which is necessary for efficient coupling of light into the resonator through evanescent field excitation.

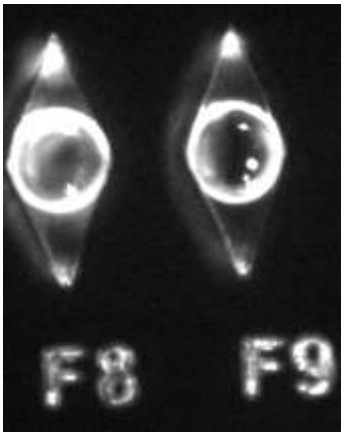


**Figure 5.1** – Microfabricated PDMS wells are used to immobilize and label 53 $\mu$m glass microspheres.

Here we report a method for immobilizing microsphere resonators on glass substrates adapted from a calcium-assisted glass-to-glass bonding method developed for microfluidic glass chip fabrication [26]. The method creates a stable contact between the high index glass microsphere resonators and a glass substrate, enabling efficient coupling of light into the immobilized microspheres. Measurement of resonator Q-factors confirms that the immobilization method does not degrade the WGM resonance or greatly perturb the interface

between the sphere and the substrate. With these microresonators sufficiently immobilized, lipid bilayers were transferred onto the substrate bound microspheres using a combination of the Langmuir-Blodgett (LB) and Langmuir Schaeffer (LS) techniques. Lipid bilayers of DOPC were doped with 5 mol% ganglioside GM1 (GM1) transferred to the substrate using a sequential transfer method where each leaflet was deposited at 25 mN/m. As discussed in Chapter 4, GM1 binds cholera toxin, the oligomeric protein secreted by *Vibrio cholera* which causes the dehabilitating diarrhea associated with cholera [27]. Here we demonstrate the sensing capabilities of the bilayer draped over immobilized microspheres by tracking changes in their WGM resonant wavelength upon the addition of cholera toxin. Analysis of the resulting binding curves yields a measured $K_d$ of $1.5 \times 10^{-11}$, consistent with literature values, and a detection limit of 3.3 pM [28, 29]. In addition to establishing the analyte binding capabilities of this approach, we utilize the compositional control afforded by membrane deposition techniques to analyze to effect of fluorophore absorption on Q-factor. Through these studies the reported bonding scheme and subsequent bilayer application are shown not to perturb the optical properties of the resonators while immobilizing them sufficiently onto the substrate for assay development and implementation. Additionally, reducing the fluorophore concentration on the resonator surface is shown to improve resonator Q-factors by nearly five-fold.

## 5.3 - Methods and Materials

### 5.3.1 - Microsphere Immobilization

High refractive index (n = 1.9), barium titanate ($BaTiO_3$) glass microspheres (45 μm diameter, Mo-Sci, Rolla, MO) were cleaned in a 5% Contrad solution. The spheres were rinsed in an ethanol/water (30/70 v/v) solution and stored in absolute ethanol. Spheres were exchanged into an aqueous PBS solution prior to use. A glass bonding solution was prepared

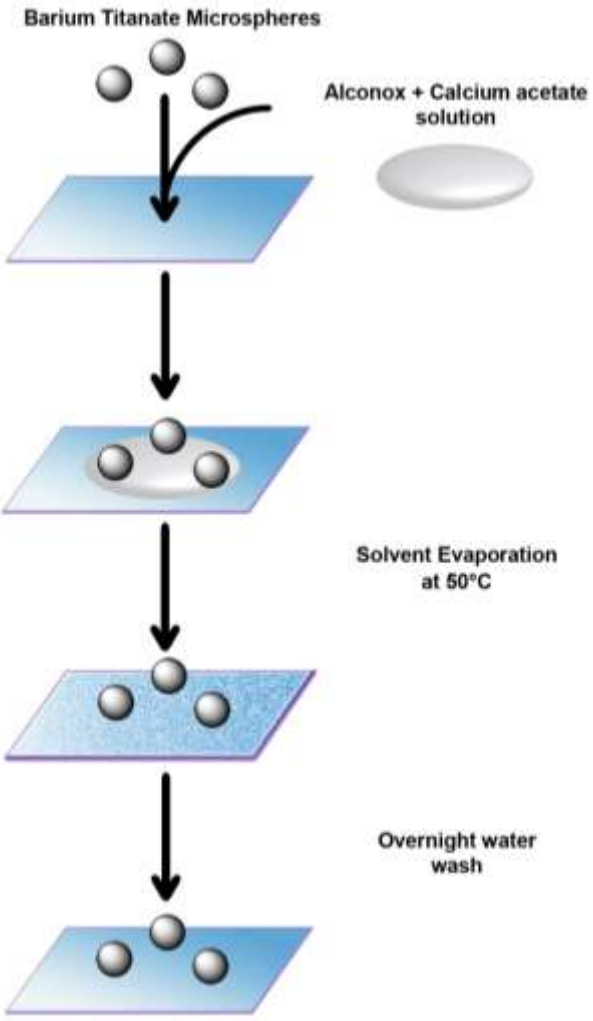


**Figure 5.2** – Schematic of the calcium-assisted procedure for immobilizing WGM microsphere resonators to a glass substrate. A drop containing 0.125% (v/v) Alconox and 0.125% (v/v) calcium acetate solution is placed along with a cluster of microspheres onto a clean glass substrate. The sample is then placed in a 50°C oven for 20 minutes. Evaporation of the solvent leaves a salt residue which is removed by bathing in deionized water overnight at room temperature, leaving a clean glass substrate with microspheres bound to the surface.

with 0.125% w/v calcium acetate (Fisher Scientific, Hampton, NH) and 0.125% w/v powdered detergent (Alconox Inc., White Plains, NY) in nanopure $H_2O$. As shown in **Fig.5.2**, approximately 100 uL of the bonding solution was placed on a clean glass cover slip (Fisher Scientific, Pittsburg, PA) and allowed to deprotonate the glass surface for ~5 minutes. Approximately 5 µL of the clean microspheres in PBS solution were transferred to the sample

slide and allowed to dry for 20 minutes at 50°C. The sample slide was washed thoroughly with nanopure $H_2O$ to remove any unbound spheres and excess salts from the surface prior to monolayer transfer.

### 5.3.2 - Lipid Transfer

Dioleoylphosphatidylcholine (DOPC) and ganglioside GM1 (GM1) were obtained at >99% purity (Avanti Polar Lipids, Alabaster, AL) and used without further purification. The fluorescent lipid probe, Texas-Red dihexadecanoyl-sn-glycero-3-phosphoethanolamine (TR-DHPE) (Life Technologies, Carlsbad, CA), was diluted in methanol to obtain appropriate working concentrations. DOPC/GM1 (95:5 mol%) solutions were prepared at 1 mg/mL concentrations in a 65:35 volume mixture of chloroform and methanol. Lipid mixtures prepared for WGM assays were further doped with 0.25 mol% TR-DHPE to enable WGM fluorescence imaging for the cholera toxin assay. Each lipid solution was doped with the appropriate TR-DHPE concentration for the dye study. Approximately 50 µL of the appropriate lipid solution was dispersed on a 18MΩ water subphase in a Langmuir-Blodgett trough (Type 611, Nima Technology, Coventry, England). The solvent was allowed to evaporate for at least 15 min prior to initiating compression/expansion cycles to anneal the film. Each monolayer was subjected to two compression/expansion cycles between surface pressures of 10 mN/m and 40 mN/m with the barrier rate held constant at 100 $cm^2$/min. Following the last expansion, the monolayers were compressed to 25 mN/m and held for ~10 min prior to transfer onto the substrate. Bilayers were transferred on to the immobilized glass microspheres at dipping velocity of 1 mm/min by the Langmuir-Blodgett/Langmuir-Schaeffer method resulting Y-type bilayers. All bilayers were transferred and imaged at 22°C.

### 5.3.3 - Assay Preparation

Prepared glass cover slips were fit into the custom flow cell. Refractive index matching fluid (n=1.514 immersion oil, Olympus, Center Valley, PA) was used between the prism surface and sample slide. A syringe pump (Harvard apparatus, Holliston, MA) was used to fill the flow cell chamber with a PBS solution (MP Biomedicals, Solon, OH). A second syringe pump and fluidic controller (Warner Instrument Corp., Hamden, CT) was used to inject aliquots of purified recombinant cholera toxin beta labeled with A555 (CTxB-A555) (Molecular Probes, Eugene, OR) into the flow chamber. Each injection was allowed in incubate in the flow chamber for 5 minutes before being flushed with PBS and imaged.

### 5.3.4 - TIR Fluorescence imaging

Fluorescence imaging assays of cholera toxin binding to supported bilayers of DOPC/GM1 utilized CTxB-A555 (Molecular Probes). Binding of the CTxB-A555 to the lipid bilayer was imaged with an inverted microscope (Olympus IX71) equipped with a 60x PlanAPO objective (1.45 NA, Olympus). The 514 nm line from an argon ion laser (Innova 90, Coherent Inc., Santa Clara, CA) was coupled into the microscope through the objective using a total internal reflection illumination configuration. Emission from the bound CTxB-A555 was collected with the same objective, filtered to remove the excitation light (Chroma), and imaged onto a cooled CCD (Coolsnap K4). Image collection was controlled with Slidebook software (Intelligent Imaging Innovations).

### 5.3.5 - WGM Fluorescence Imaging

The tunable output from a Vortex II TLB-6900 external cavity diode laser (New Focus, Santa Clara, CA) was directed into a Dove prism (Edmund Optics, Barrington, NJ), on which the

sample was mounted. Total internal reflection at the substrate interface creates an evanescent field, which was used to launch light into the immobilized microspheres. At a WGM resonance, an enhanced ring of fluorescence from TR-DHPE was observed from the microspheres, which were imaged from above. The fluorescence was collected through a 10X UMPlanFL (0.3 NA) objective (Olympus, Center Valley, PA), filtered to remove the residual excitation (Chroma, Bellows Falls, VT), and imaged onto a cooled CCD camera (Coolsnap K4, Roper Scientific, Tuscon, AZ). A LabView program controlled scanning of the laser system, which was synchronized with Slidebook image collection software (Intelligent Imaging Innovations, Denver, CO).

## 5.4 - Results and Discussion

### 5.4.1 – WGM Cholera Toxin Binding Assay with LB/LS Bilayer Coated Spheres

High index barium titanate ($BaTiO_3$) microspheres were bonded to glass substrates using the steps outlined schematically in **Fig. 5.2.** A glass substrate was first rubbed with a slurry of basic detergent (Alconox) containing 8.0 mM $Ca^{2+}$. The spheres were then deposited on the glass substrate and incubated at 50$^{o}$C for approximately 20 minutes until dry. The spheres, now bonded to the substrate, were incubated in 18 MΩ water overnight to remove the residual salts and unbound spheres from the substrate surface.

Conceptually, one can envision the divalent calcium ion as acting as a bridge between the negatively charged surface groups on the microspheres and substrate, thus leading to stable bond formation [26]. However, as the original report showed, a more complicated mechanism is almost certainly needed since other divalent cations do not lead to bond formation. Regardless of the mechanism, this approach does successfully immobilize $BaTiO_3$ spheres on the glass substrate. The bonding scheme outlined in **Fig. 5.2** uses a lower

temperature, which was found in the original study to lead to reversible bond formation. However, as will be shown, this gentler bonding method is more than sufficient to immobilize spheres for the assay employed in this report. Additionally, this immobilization method can be used to adhere dye functionalized spheres without loss of dye function. This is advantageous for the WGM imaging approach which uses fluorescence to detect sphere resonances.

Another advantage of the microsphere bonding scheme results from the flexibility inherent in this approach when designing assays. Immobilizing microsphere resonators onto a substrate opens new opportunities for functionalizing the resonators using techniques that are not compatible for use with free spheres. For example, Langmuir-Blodgett (LB) and related techniques offer extraordinary capabilities for creating highly ordered films on substrate surfaces. These techniques provide exquisite layer-by-layer control over film properties such as composition, packing, and constituent orientation which has generated interest in using this control to tailor assay properties [30, 31]. As illustrated in Fig. **5.3**, the LB method involves the transfer of films from an air-water interface onto a substrate surface using a dipping method. As suggested in **Fig. 5.3**, here we show that the bonded spheres are sufficiently immobilized to withstand LB film transfer, thus creating new opportunities for assay development using microsphere resonators.

To confirm that the immobilization procedure does not interfere with or degrade WGM resonances of the microspheres, fluorescence imaging experiments were first performed using LB films doped with a fluorescent marker. For these experiments, immobilized microspheres were coated with a DOPC bilayer containing 0.25 mol% TR-DHPE, transferred using the LB/LS method. The fluorescent lipid analog, TR-DHPE, was added to act as a fluorescent reporter of the WGM resonances. The immobilized spheres were mounted on a Dove prism, as shown in **Fig. 5.4**, where light from a tunable diode laser experiences total internal reflection at the

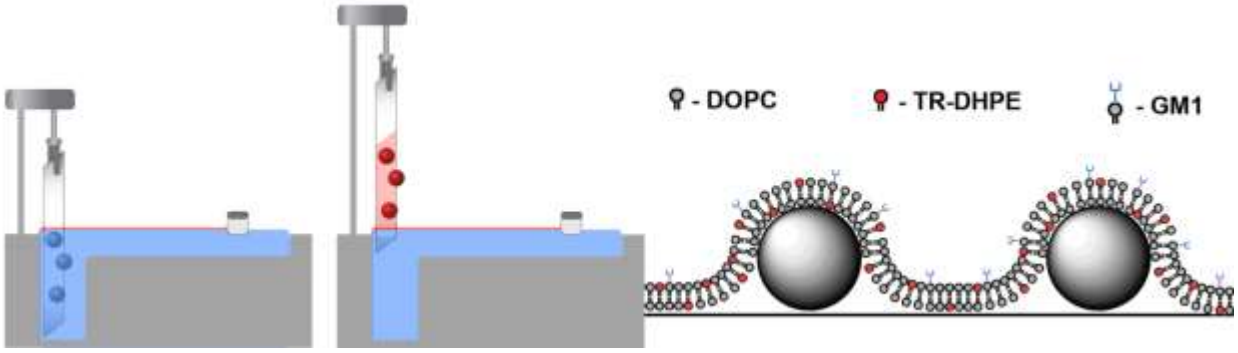


**Figure 5.3** – Schematic of the Langmuir-Blodgett trough used to transfer lipid films onto a substrate. A 50 uL aliquot of the lipid solution is dispersed on the water subphase and a moving barrier compresses the film to the desired surface pressure. A glass substrate with bonded microspheres is slowly pulled through the air-water interface, transferring a lipid monolayer onto the substrate surface. For these experiments, a second monolayer is transferred onto the first using the Langmuir-Schaffer technique, creating a bilayer as shown schematically in the right panel.

sample interface. As the wavelength of the diode laser was scanned, the associated evanescent field launches light into the immobilized spheres. WGM resonances are detected as an enhanced ring of fluorescence around the particular microsphere resonator, which is detected from above using fluorescence imaging. The fluorescence was collected and imaged onto a CCD camera as shown in **Fig. 5.4**.

**Figure 5.5** shows a typical series of fluorescence images taken on the same field of microspheres as the excitation wavelength from the tunable diode laser is scanned. These spheres have been immobilized onto the substrate surface using the scheme in **Fig. 5.1** and exhibit bright fluorescence rings indicative of WGM resonances. The excitation spectrum for each resonator can be extracted from a series of fluorescence images collected as a function of excitation wavelength. A typical excitation spectrum is shown in **Fig. 5.5**. The Q-factor calculated from this spectrum is 1.0 x $10^5$ which is comparable to measured Q-factors for

spheres resting on substrates through gravity alone. This demonstrates that the immobilization process has little effect on the quality of the WGM resonance.

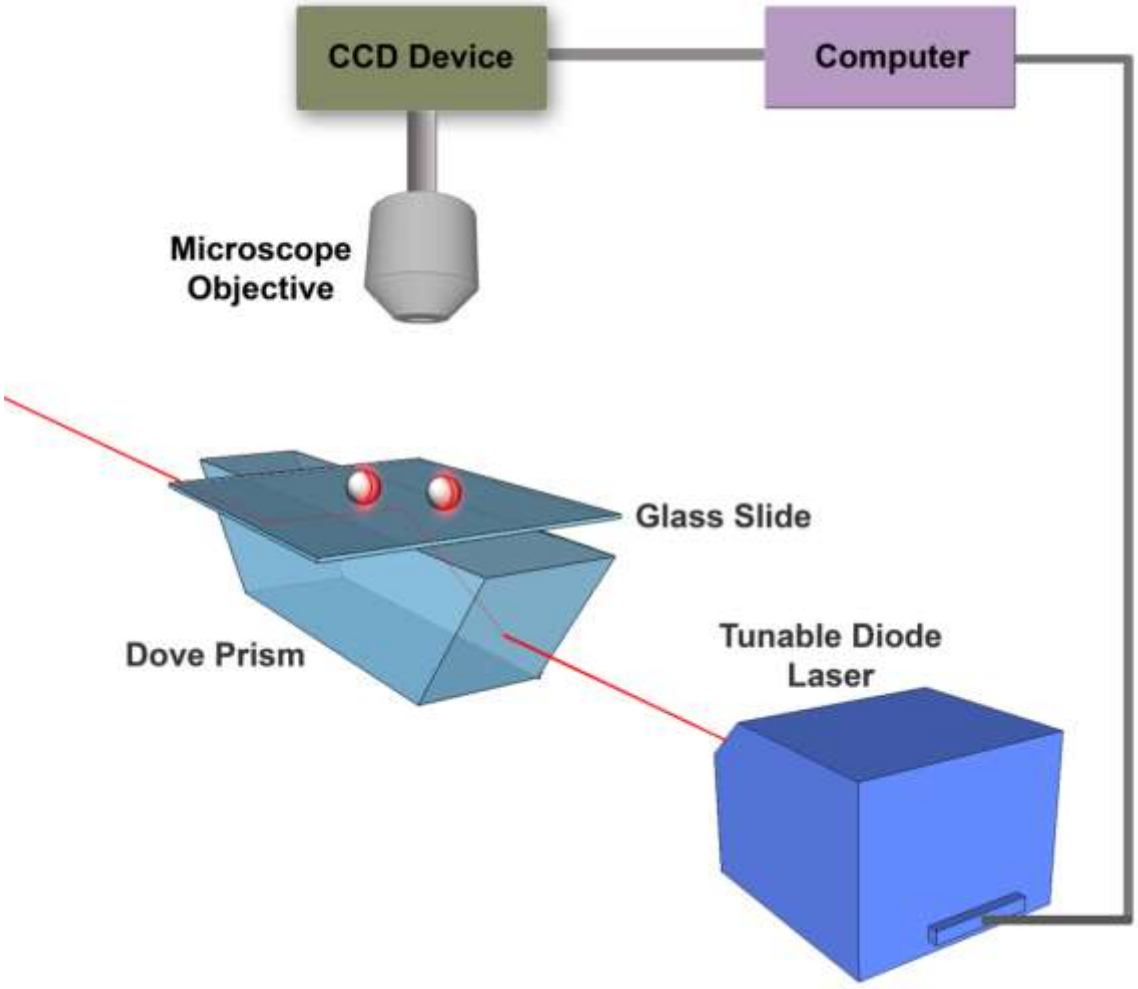


**Figure 5.4** – Schematic of the instrumentation used for the fluorescence imaging of WGM resonances. Light from a tunable diode laser is directed through a Dove prism, which creates an evanescent field at the substrate interface. The evanescent field couples light into the immobilized microspheres and WGM resonances are detected through fluorescence imaging of a dye marker located on their surface. As the excitation wavelength is tuned, an enhanced ring of fluorescence is observed around the spheres as a WGM resonance is reached. The fluorescence is collected and imaged onto a CCD camera.

Having shown that the immobilization procedure does not degrade resonator optical properties, the utility of membrane coated microspheres for bioassay development was explored. Bioassays require rapid fluid exchanges and the immobilized resonators need to maintain both close contact with the substrate surface and not reorient during these processes. To test the stability of the immobilized microspheres during rapid fluid exchanges, the flow cell in **Fig. 5.6** was fabricated.

The glass substrate supporting the immobilized microspheres rests on a rigid bottom plate that is notched to accept the Dove prism. An aluminum flow cell body that contains the solution inlet and outlet ports is sandwiched between the sample substrate and top coverslip using two silicone o-rings to form a water tight seal. The thickness of the flow cell body dictates the dead volume of the cell which is 500 uL. Screws connect a rigid top cover with the bottom PMMA plate and compress the o-rings. An image of the assembled flow cell is shown in **Fig. 5.6**.

Studies using the flow cell shown in **Fig. 5.6** indicate that the immobilized spheres remain stable at all flow rates studied (up to a maximum flow of 3 mL/min). This demonstrates that the bonding method described above results in resonators compatible with assay fluidics. As shown above, the resonator immobilization scheme does not degrade resonator optical properties while rigidly holding the spheres on the substrate surface under high flow rates. This approach, therefore, removes a significant barrier encountered when integrating microsphere resonators with the fluidics necessary for assay development using the WGM imaging method.

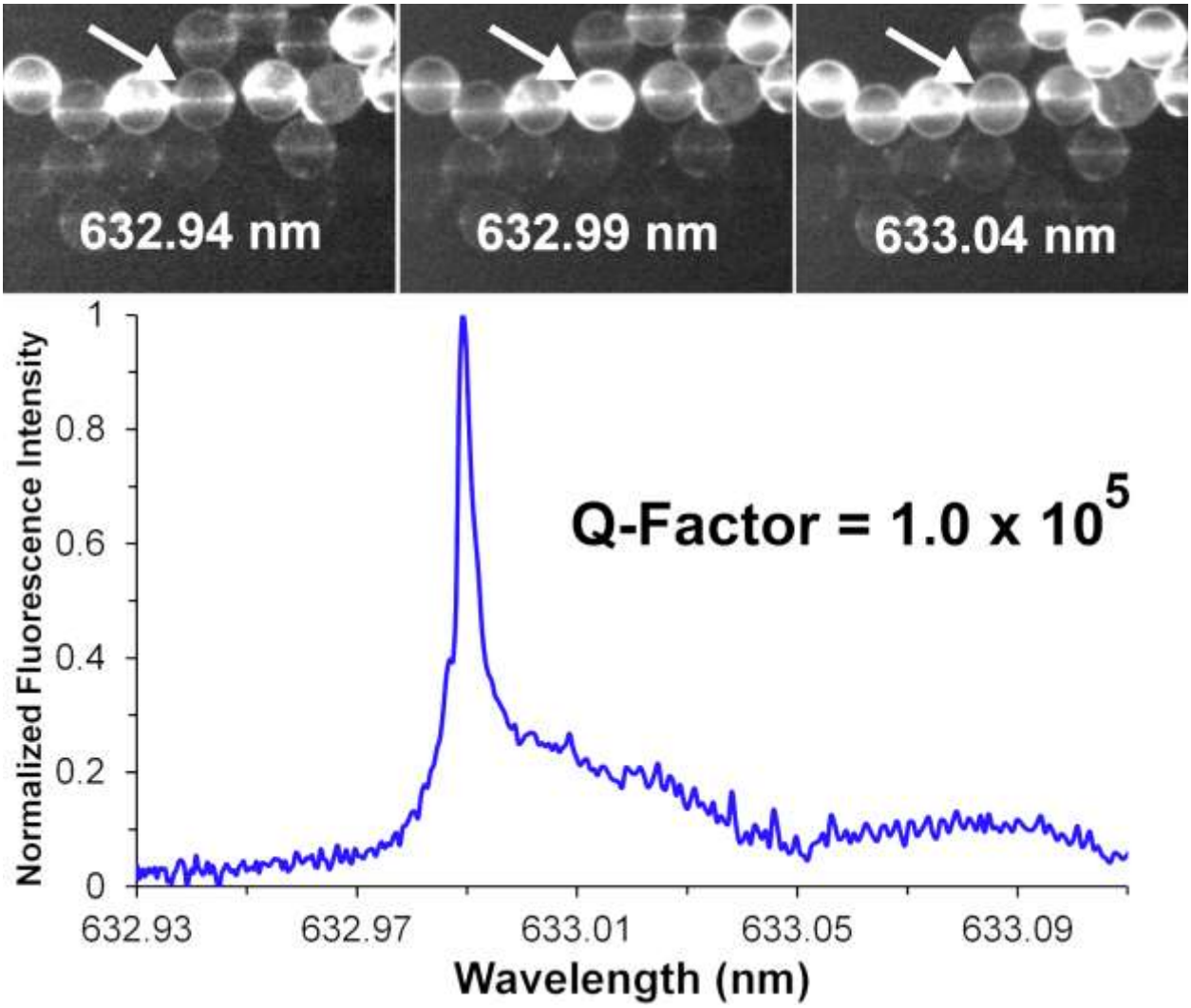


**Figure 5.5** – (top) Representative fluorescence images of 45 μm spheres extracted from a series of images taken as the wavelength of the diode laser is scanned between 632.93 nm and 633.10 nm. The arrow denotes a sphere that undergoes a large change in fluorescence, indicating a WGM resonance near 632.99 nm. (bottom) Excitation spectrum of the WGM resonance for the indicated sphere, extracted from the series of fluorescence images by integrating the emission from the sphere in each image.

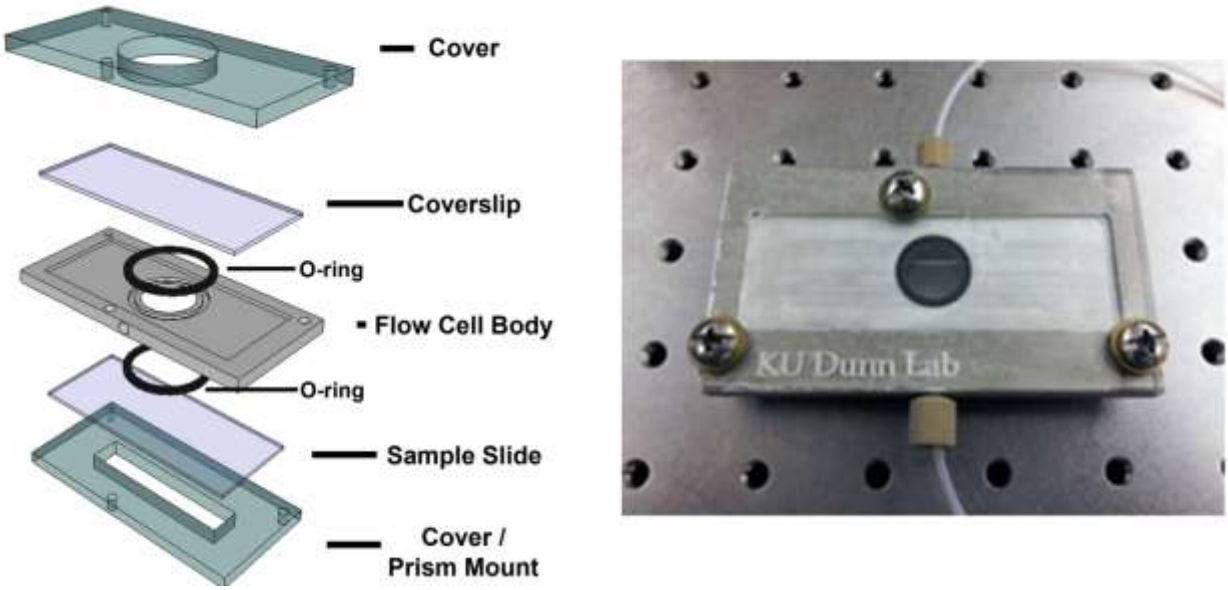


**Figure 5.6** – (left) Schematic of the flow cell used for fluidic exchange and WGM imaging. The bottom cover accepts the Dove prism used to launch light into the small resonators which are imaged from above through the transparent window. An image of the flow cell is shown on the right.

To illustrate this new capability, lipid films containing the ganglioside GM1 were transferred onto immobilized microsphere resonators to detect the presence of cholera toxin (CTx) using WGM imaging. CTx is secreted by *Vibrio cholera* and leads to the debilitating diarrhea associated with cholera infection. CTx is a 85 kDa protein containing one active alpha subunit and five binding beta subunits which bind GM1, an acidic glycosphingolipid found ubiquitously in the outer leaflet of cellular membranes [27]. The high affinity of CTx beta subunit (CTxB), a 11.4 kDa protein, for GM1 is considered a model for protein-sugar interactions with measured $K_d$ values ranging from nanomolar to picomolar depending on the particular system studied [29]. In this approach a 57 kDa non-toxic pentameric CTxB fluorescently labeled with Alexa 555 (CTxB-A555) was detected.

A monolayer of DOPC containing 5 mol% GM1 was transferred onto a microsphere/substrate platform at a surface pressure of 25 mN/m using the LB method. A

second monolayer at the same surface pressure and composition was deposited on the first using the Langmuir Schaeffer (LS) method, creating a bilayer covering the entire surface area of the substrate. At this surface pressure, both GM1 and the dye marker distribute homogeneously in the DOPC lipid film matrix. To confirm that the membranes incorporating GM1 were capable of CTxB binding, bulk fluorescence imaging of the bilayers were measured following the addition of fluorescently labeled CTxB-A555.

**Figure 5.7** presents fluorescence images of a DOPC/GM1 bilayer following increasing additions of CTxB-A555. The images are taken in the same region of the bilayer, which was allowed to react with the indicated dose of CTxB-A555 for 5 minutes, flushed with PBS buffer, and imaged. As seen in **Fig. 5.7**, exposure of the bilayer to increasing aliquots of CTxB-A555 leads to increased fluorescence intensity, as CTxB-A555 binds to the GM1. Control studies using substrates coated with pure DOPC bilayers, lacking GM1, exhibited constant fluorescence signals over the same CTxB-A555 dosing levels. This suggests that the increase in fluorescence observed arises from specific interactions between GM1 and the CTxB-A555.

Having confirmed that CTxB-A555 specifically binds to the GM1 in the transferred membranes, studies were carried out to explore the WGM response of the membrane coated microspheres. For this study, TR-DHPE was incorporated into the lipid bilayer at 0.25 mol% to provide a fluorescence marker for the WGM imaging. To ensure consistency with the bulk fluorescence studies, the fluorescently labeled CTxB-A555 was also used in these binding studies. However, long pass filters were inserted to remove any residual fluorescence from the A555 marker. Using the WGM fluorescence imaging approach outlined in **Fig. 5.4**, WGM excitation spectra were collected as a function of CTxB-A555 dose. **Figure 5.8** shows a typical

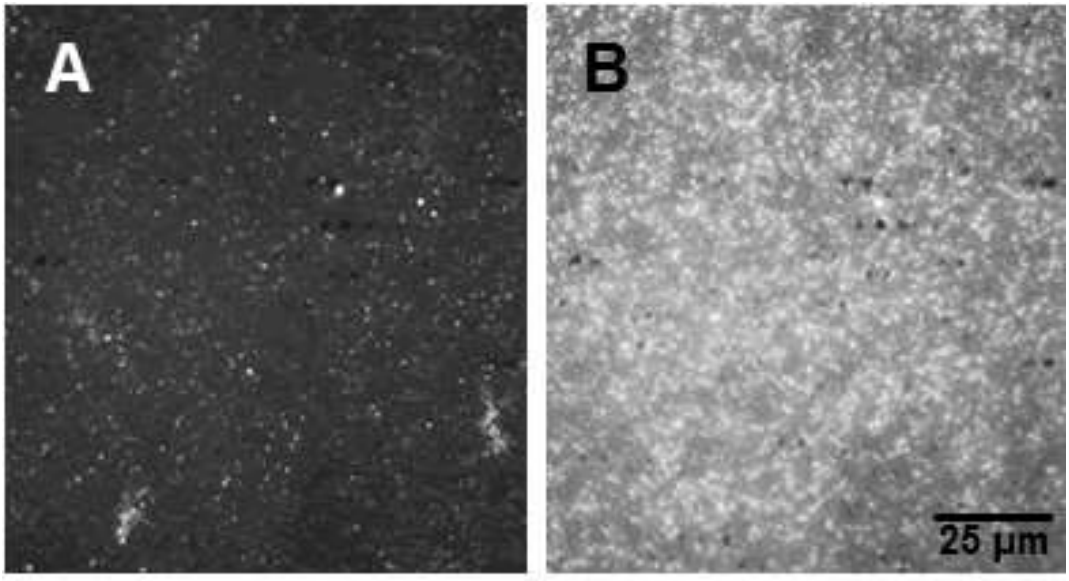


**Figure 5.7** – Bulk fluorescence assay of the binding of fluorescently labeled CTxB (CTxB-A555) to DOPC/GM1 bilayers transferred onto a glass substrate at 25 mN/m. Fluorescence images of the same region of the bilayer are shown following incubation with (A) 27.6 pM CTxB-A555 and (B) 110 pM CTxB-A555. The increase in fluorescence indicates specific binding of CTxB-A555 at GM1 sites in the bilayer. Control studies of bilayers composed of DOPC but lacking GM1 (not shown) do not show any significant fluorescence after incubation with CTxB-A555.

series of WGM excitation spectra collected as a function of CTxB-A555 concentration. Prior to the addition of CTxB-A555, this particular microsphere resonator had a WGM resonance centered at 632.98 nm with a Q-factor of $1.0 \times 10^5$. With the addition of 2.8 pM CTxB-A555, the peak red-shifts 6.33 pm as CTxB-A555 binds to the GM1/DOPC bilayer on the sphere surface which changes the effective refractive index around the resonator (Eq. 1). The peak continues to red shift as additional CTxB-A555 is added as shown in **Fig. 5.8**.

The results in **Fig. 5.8** are summarized by the binding curve shown in **Fig. 5.9**. **Figure 5.9** plots the WGM resonance shifts as a function of CTxB-A555 concentration, exhibiting the classic binding curve shape expected. The binding curve saturates at approximately $4.0 \times 10^{-11}$ M CTxB-A555 and fitting the curve yields a measured $K_d$ value of $1.5 \times 10^{-11}$. This value is in the range of the reported values ($7.3 \times 10^{-10}$ to $4.6 \times 10^{-12}$) measured using surface plasmon resonance [28, 29].

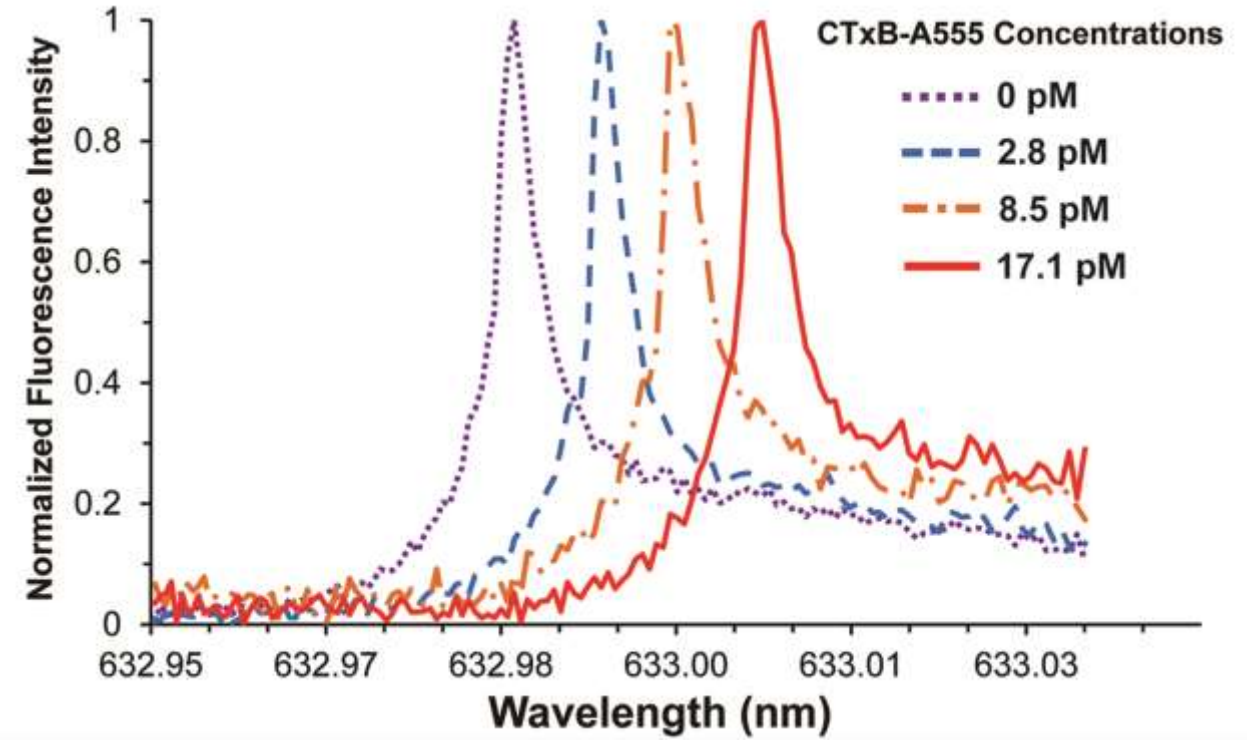


**Figure 5.8** – Representative WGM excitation spectra extracted from the same microsphere resonator at four different CTxB-A555 concentrations. Specific binding of CTxB-A555 to the GM1 containing bilayer coated around the microsphere, changes the effective refractive index and shifts the WGM resonance.

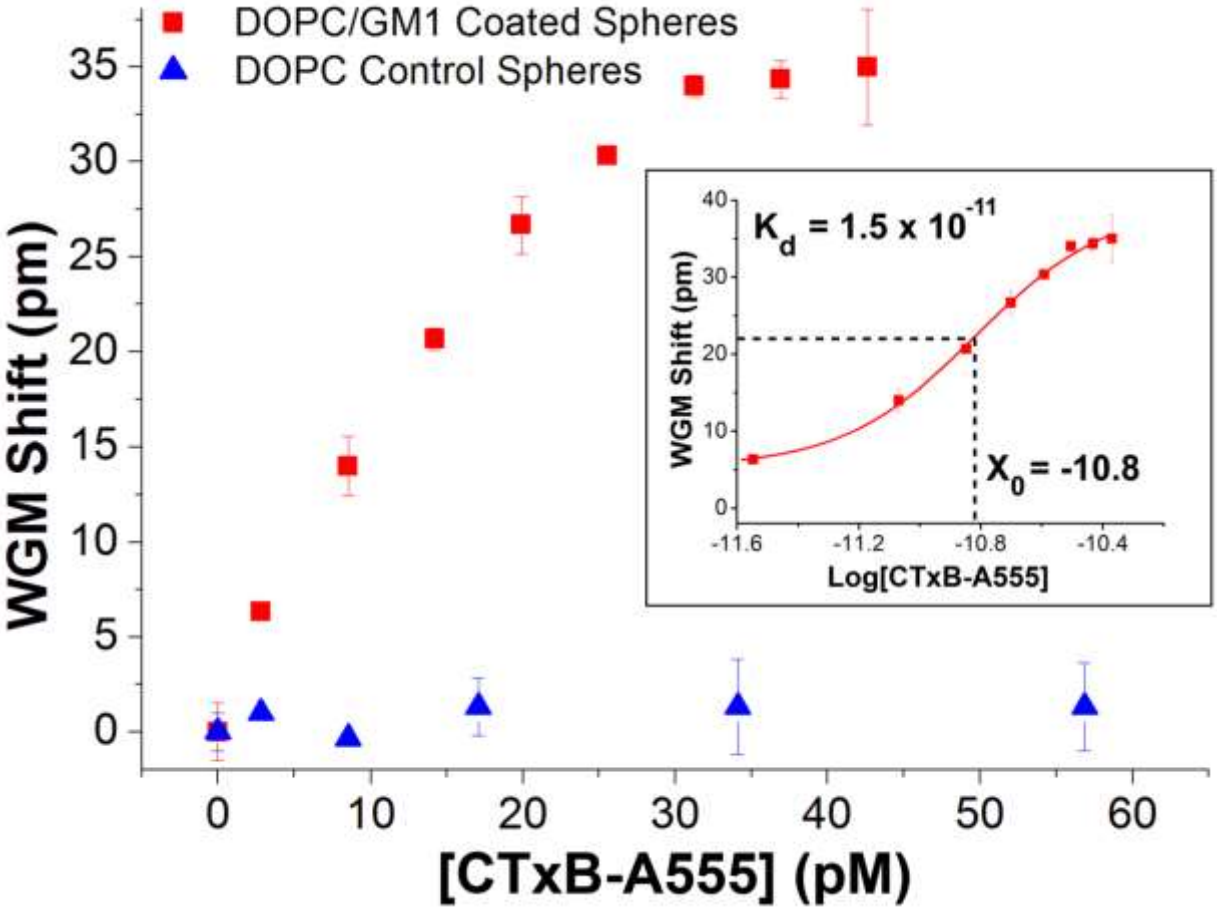


**Figure 5.9** – CTxB-A555 binding curves measured by tracking shifts in the WGM resonance with CTxB-A555 concentration. For resonators coated with DOPC bilayers incorporating GM1 (red squares) the binding curve shows a saturation response with a detection limit of 3.3 pM. This is compared with control studies using spheres coated with pure DOPC bilayers (blue triangles), which show negligible shifts with CTxB-A555 addition. The inset shows a log plot of the data from which a $K_d$ of 1.5 x $10^{-11}$ is calculated, which is consistent with literature values.

These measurements show that microspheres can be efficiently immobilized on glass substrates using the calcium bonding method with no loss in optical performance. The spheres remain stable under fluid exchange and the bond is sufficiently strong to enable lipid film transfer onto their surface using the LB/LS technique. Using bilayers incorporating GM1 transferred onto the spheres, we show that WGM fluorescence imaging measurements can quantify CTxB-A555 binding with picomolar detection limits. These studies, therefore, illustrate

the utility of the calcium bonding approach for integrating high-Q microsphere resonators with the fluidics necessary for assay development. The simple immobilization procedure does not require expensive equipment or elaborate fabrication processes, thus making the approach generally applicable. This, therefore, removes a significant barrier for the development of sensitive, multiplexed biosensors using the superior optical properties of high-Q microsphere resonators.

### 5.4.2 – Assessment of Dye Loading Influence on WGM Resonator Performance

Model membranes as coatings for WGM resonators can not only serve as a matrix for capture material in biosensing applications, but also can provide a tool for fundamental investigations of resonator performance. As shown in **Eq. 5.2**, there are several factors which can contribute to the loss of light from the resonant cavity. Introducing a fluorescent dye to the resonant surface provides a useful mechanism for imaging WGM resonances. However, as these fluorophores absorb energy from the resonant cavity, they potentially limit Q-factor and resonator performance. The compositional control provided by model membrane techniques allows each immobilized sphere on the glass substrate to be reliably coated with a film of known dye concentration. Therefore, with this method we can assess the effect of fluorophore absorbance on resonator performance.

Similar to the binding assay studies, glass microspheres were immobilized on a glass substrate with the calcium bonding method described in **Fig. 5.2**. A DOPC monolayer doped with a known dye concentration was then deposited by LB transfer the substrate. The WGM excitation spectrum of at least 20 microspheres coated with each dye concentration were then measured using the method outlined in **Fig. 5.5**. From these spectra, the Q-factor of each sphere was measured and tabulated in **Fig. 5.10**.

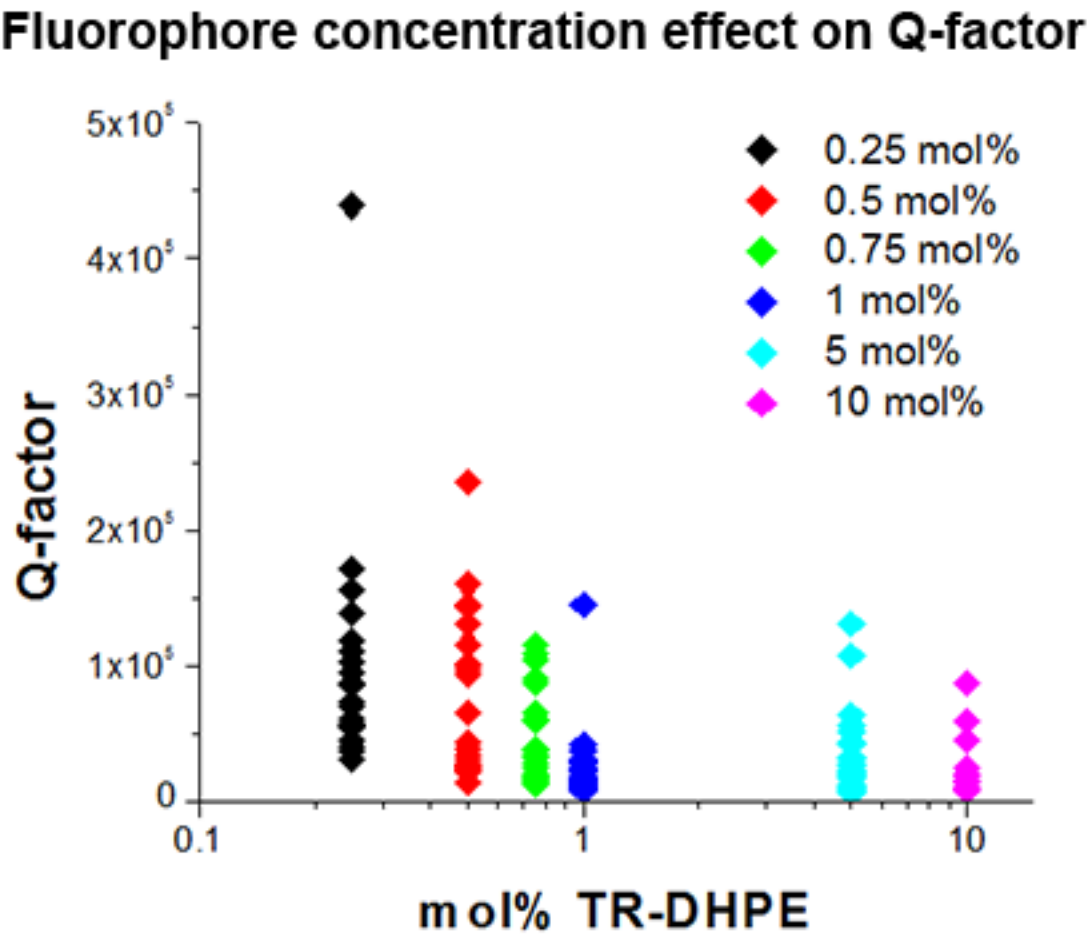


**Figure 5.10** – Q-factor dependence of WGM resonators coated in lipid film containing a fluorescent dye is shown as a function of dye concentration within the film. By reducing the dye, the average and maximum attainable Q-factor is increased.

**Figure 5.10** shows that as the dye concentration is reduced from 10 mol% TR-DHPE to 0.25 mol% TR-DHPE the average and highest attainable Q-factor increases. Decreasing the dye concentration on the resonator surface, reduces losses of light from the absorbing dye on the surfare. This leads to improved Q-factors and improved performance in sensing applications. At TR-DHPE concentrations below 0.25% reliably measuring excitation spectra from these bound microspheres became exceedingly difficult due to lack of signal. Factors influencing Q-factor value have previously been described:

$$Q_o = \frac{2\pi n_s}{\alpha\lambda} \qquad \textbf{Eq. 5.3}$$

where the intrinsic Q-factor ($Q_0$) of a resonator is a function of the refractive index of the sphere ($n_s$), linear attenuation of light in the cavity (α), and the resonant wavelength of light (λ) [32]. While there is considerable noise in the measurements shown in **Fig 5.10**, it is evident from the data that as expected reducing absorption of surface bound molecules through lowing bound dye content resulted in improved Q-factor. As seen in the data set in **Fig. 5.10** it is difficult to distinguish whether Q-factor responds linearly with dye concentration. However, as shown in Eq 5.3, Q-factor is inversely proportional to linear attenuation. Therefore, future WGM imaging applications which employ fluorescence as a readout mechanism should limit dye coverage of microspheres in order to conserve resonator performance.

### 5.6 - Conclusion

High index glass microspheres were immobilized onto glass substrates using a calcium-assisted bonding method. The bonding method was shown not to degrade the optical properties of the immobilized resonators which was confirmed through characterization of resonator Q-factors. The immobilized resonators were stable over the flow rates necessary for assay development and amenable to lipid film transfer using the Langmuir-Blodgett and Langmuir-Schaeffer methods. Bilayers transferred on to immobilized spheres using the sequential transfer of monolayers of DOPC doped with 5 mol% GM1 were fabricated to detect CTxB-A555 which binds to GM1. CTxB-A555 binding to GM1 was characterized by measuring shifts in the WGM resonance. Analysis of the resulting binding curves yields a measured $K_d$ of $1.5 \times 10^{-11}$ which is consistent with previous SPR measurements. The measured detection limit of 3.3 pM is competitive with other approaches and the small size of the microspheres reduces

the detection footprint and amount of material needed. The calcium bonding method, therefore, is shown to lead to stably immobilized resonators that are compatible with the fluidics necessary for assay development. This removes a significant barrier for integrating microsphere resonators with assay fluidics for WGM detection. Additionally, membrane coated microspheres allowed for an assessment of fluorescent dye effect on resonator performance demonstrating that dye usage should be limited in order to minimize the adverse effect it has on Q-factor and sensing performance. With the superior optical properties of these bound microspheres there are several new opportunities for cost effective assay development and deployment.

*This chapter has been adapted in part from previously published work: Kim, D. C., K. P. Armendariz, and R. C. Dunn. 2013. Integration of microsphere resonators with bioassay fluidics for whispering gallery mode imaging. Analyst 138:3189-3195.*

## 5.6 - References


1. Overington, J. P., B. Al-Lazikani, and A. L. Hopkins. 2006. How many drug targets are there? Nat. Rev. Drug Discov. 5:993-996.

2. Taylor, A. D., Q. Yu, S. Chen, J. Homola, and S. Jiang. 2005. Comparison of E. coli O157:H7 preparation methods used for detection with surface plasmon resonance sensor. Sens. Act. B: Chem.107:202-208.

3. Silin, V., H. Weetall, and D. J. Vanderah. 1997. SPR Studies of the Nonspecific Adsorption Kinetics of Human IgG and BSA on Gold Surfaces Modified by Self-Assembled Monolayers (SAMs). J. Colloid Interf. Sci. 185:94-103.

4. Revell, D. J., J. R. Knight, D. J. Blyth, A. H. Haines, and D. A. Russell. 1998. Self-Assembled Carbohydrate Monolayers: Formation and Surface Selective Molecular Recognition. Langmuir 14:4517-4524.

5. Love, J. C., L. A. Estroff, J. K. Kriebel, R. G. Nuzzo, and G. M. Whitesides. 2005. Self-Assembled Monolayers of Thiolates on Metals as a Form of Nanotechnology. Chem. Rev. 105:1103-1170.

6. Vollmer, F., and S. Arnold. 2008. Whispering-gallery-mode biosensing: label-free detection down to single molecules. Nat. Meth. 5:591-596.

7. Gorodetsky, M. L., and V. S. Ilchenko. 1999. Optical microsphere resonators: optimal coupling to high-Q whispering-gallery modes. J. Opt. Soc. Am. B 16:147-154.

8. Knight, J. C., G. Cheung, F. Jacques, and T. A. Birks. 1997. Phase-matched excitation of whispering-gallery-mode resonances by a fiber taper. Opt. Lett. 22:1129-1131.

9. Vollmer, F., and L. Yang. 2012. Label-free detection with high-Q microcavities: a review of biosensing mechanisms for integrated devices. Nanophotonics. 267.

10. Soria, S., S. Berneschi, M. Brenci, F. Cosi, G. Nunzi Conti, S. Pelli, and G. C. Righini. 2011. Optical Microspherical Resonators for Biomedical Sensing. Sensors 11:785-805.

11. Fan, X. D., I. M. White, S. I. Shopova, H. Y. Zhu, J. D. Suter, and Y. Z. Sun. 2008. Sensitive optical biosensors for unlabeled targets: A review. Anal. Chim. Acta. 620:8-26.

12. Huckabay, H. A., and R. C. Dunn. 2011. Whispering gallery mode imaging for the multiplexed detection of biomarkers. Sens. Actuators, B 160:1262-1267.

13. Arnold, S., M. Khoshsima, I. Teraoka, S. Holler, and F. Vollmer. 2003. Shift of whispering-gallery modes in microspheres by protein adsorption. Opt. Lett. 28:272-274.

14. Vollmer, F., D. Braun, A. Libchaber, M. Khoshsima, I. Teraoka, and S. Arnold. 2002. Protein detection by optical shift of a resonant microcavity. Appl. Phys. Lett. 80:4057-4059.

15. Vollmer, F., S. Arnold, D. Braun, I. Teraoka, and A. Libchaber. 2003. Multiplexed DNA Quantification by Spectroscopic Shift of Two Microsphere Cavities. Biophys. J. 85:1974-1979.

16. Huckabay, H. A., S. M. Wildgen, and R. C. Dunn. 2013. Label-free Detection of Ovarian Cancer Biomarkers Using Whispering Gallery Mode Imaging. Biosens. Bioelectron. 138, 3189-3195.

17. Li, X., Z. Zhang, S. Qin, T. Wang, F. Liu, M. Qiu, and Y. Su. 2009. Sensitive label-free and compact biosensor based on concentric silicon-on-insulator microring resonators. Appl. Opt. 48:F90-94.

18. Qavi, A. J., and R. C. Bailey. 2010. Multiplexed detection and label-free quantitation of microRNAs using arrays of silicon photonic microring resonators. Angew. Chem., Int. Ed. 49:4608-4611, S4608/4601-S4608/4621.

19. Chiasera, A., Y. Dumeige, P. Feron, M. Ferrari, Y. Jestin, G. N. Conti, S. Pelli, S. Soria, and G. C. Righini. 2010. Spherical whispering-gallery-mode microresonators. Laser Photonics Rev. 4:457-482.

20. Vollmer, F., S. Arnold, and D. Keng. 2008. Single virus detection from the reactive shift of a whispering-gallery mode. Proc. Natl. Acad. Sci. U.S.A. 105:20701-20704.

21. Washburn, A. L., M. S. Luchansky, A. L. Bowman, and R. C. Bailey. 2009. Quantitative, label-free detection of five protein biomarkers using multiplexed arrays of silicon photonic microring resonators. Anal. Chem. 82:69-72.

22. Fan, X., I. M. White, H. Zhu, J. D. Suter, and H. Oveys. 2007. Overview of novel integrated optical ring resonator bio/chemical sensors. Proc. SPIE 64520M-64520M.

23. Gorodetsky, M. L., A. A. Savchenkov, and V. S. Ilchenko. 1996. Ultimate Q of optical microsphere resonators. Opt. Lett. 21:453-455.

24. Vahala, K. J. 2003. Optical microcavities. Nature 424:839-846.

25. Mazzei, A., S. Götzinger, L. d. S. Menezes, V. Sandoghdar, and O. Benson. 2005. Optimization of prism coupling to high-Q modes in a microsphere resonator using a near-field probe. Optics Comm. 250:428-433.

26. Allen, P. B., and D. T. Chiu. 2008. Calcium-Assisted Glass-to-Glass Bonding for Fabrication of Glass Microfluidic Devices. Anal. Chem. (Washington, DC, U. S.) 80:7153-7157.

27. Reed, R. A., J. Mattai, and G. G. Shipley. 1987. Interaction of Cholera-Toxin with Ganglioside Gm1 Receptors in Supported Lipid Monolayers. Biochemistry 26:824-832.

28. MacKenzie, C. R., T. Hirama, K. K. Lee, E. Altman, and N. M. Young. 1997. Quantitative analysis of bacterial toxin affinity and specificity for glycolipid receptors by surface plasmon resonance. J. Biol. Chem. 272:5533-5538.

29. Kuziemko, G. M., M. Stroh, and R. C. Stevens. 1996. Cholera toxin binding affinity and specificity for gangliosides determined by surface plasmon resonance. Biochemistry 35:6375-6384.

30. Davis, F., and S. P. J. Higson. 2005. Structured thin films as functional components within biosensors. Biosens. Bioelectron. 21:1-20.

31. Girard-Egrot, A., and L. Blum. 2007. Langmuir-Blodgett Technique for Synthesis of Biomimetic Lipid Membranes. Nanobiotech. Biomimetic Membranes. D. Martin, editor. Springer US. 23-74.

32. Gorodetsky, M. L., and V. S. Ilchenko. 1999. Optical microsphere resonators: optimal coupling to high-Q whispering-gallery modes. J. Opt. Soc. Am. B 16:147-154.

# Chapter 6: Improving label-free biosensor assay metrics through addressing antibody orientation and decreasing nonspecific adsorption

## 6.1 - Introduction

Recently there has been an increasing interest in the scientific community to develop improved and more versatile biosensing platforms for a broad range of applications. These applications range from medical diagnostics [1, 2] and drug discovery [3] to environmental monitoring[4] and remote sensing for chemical and biological warfare agents [5, 6]. The majority of biosensing formats employ an antigen capture material bound to a substrate which transduces antigen binding into a measurable signal. There are numerous types of capture materials, such as antibodies [7, 8], nucleic acids [9-11], and imprinted polymers [12]. Of these, immunoassays, which employ antibodies as the capture material, are perhaps the most prevalent and well-studied biosensing systems. Immunoassays are routinely deployed for use in clinical diagnostics, therapeutic drug monitoring, and drug discovery [3, 4, 7, 13]. Label-free biosensing platforms, such as surface plasmon resonance (SPR) [14, 15], quartz crystal microbalances (QCM) [16], and whispering gallery mode (WGM) resonators [8, 17, 18], have further expanded the viability of immunoassay techniques by eliminating the requirement of analyte labeling for detection and quantification.

However, label-free immunoassays are not without their disadvantages. First, antibodies often lose their activity and fail to bind the target analyte once they are immobilized on a substrate [7, 19, 20]. As such, there has been significant research effort directed toward improving antibody immobilization protocols to promote a higher percentage of active antibodies following immobilization. Second, it is imperative to suppress nonspecific absorption of proteins and other biological material to the surface of label-free sensors [21]. While nonspecific

adsorption is an issue for all immunoassay platforms, it is particularly important for label-free techniques as all binding events to the sensor surface are detected. Again, to address this issue, numerous studies have been dedicated to developing methods which can reduce nonspecific binding to sensor surfaces. In this chapter, we report two methods to address each of the issues separately.

### 6.1.1 – Immobilized Antibody Activity

The most common techniques for antibody immobilization can be broadly grouped in to three categories including physical adsorption, covalent binding, and affinity-based interactions [19, 20, 22]. An overview of these immobilization methods is provided in **Table 6.1**, where several of the common techniques and their important attributes are highlighted.

**Table 6.1 - Antibody Immobilization Chemistries** Table adapted from Ref. #[22]

| Immobilization Chemistry | Surface Chemistry | Attachment Site | Advantages | Disadvantages |
|---|---|---|---|---|
| Adsorption | **Polystyrene**<br>Polyacrylamide<br>Poly-L-lysine<br>Amino<br>Agarose | **Hydrophobic Interactions**<br>Electrostatic Interactions<br>Hydrogen Bonding | **Ease of Use** | **Random orientations** |
| Covalent Binding | Maleimide | Thiol | **Stable binding**<br>Simple immobilization | Can require antibody pretreatment<br>**Random orientations possible** |
| | Hydrazine | Cardohydrate | | |
| | **Succinimidyl ester**<br>Epoxide<br>Aldehyde | **Primary Amine** | | |
| Affinity Based | **Protein A** or G | **Fc region** | **Directed orientations** | Low specificity<br>Antibody migration<br>Specific for certain antibody classes |
| | Streptavidin | Biotin | | |
| | Nickel<br>Copper<br>Nickel-nitrilotriacetic acid | Histidine Tag | | |
| | Glutathione | Gst Tag | | |

Traditionally, the issue of antibody inactivity upon immobilization has been studied with binding capacity assays, which assume increased binding capacity is the result of producing sensors with a greater density of active antibodies. While binding capacity measurements are a useful tool for comparing different immobilization protocols, they do not provide insight as to why certain protocols produce more efficient binding surfaces. This is complicated by the fact that there are several factors, such as antibody orientation and denaturation, which contribute to antibody inactivity on a surface [3, 7, 20, 22]. **Figure 6.1** illustrates these issues. Antibody orientation is a typical consideration as it is clearly advantageous to direct the binding region of the antibody toward the sample matrix rather than the immobilization substrate. While antibody orientation is obviously important, it is also essential to prevent the antibodies from becoming denatured once bound to the surface. This most often occurs through nonspecific adsorption of the antibody to the sensor substrate.

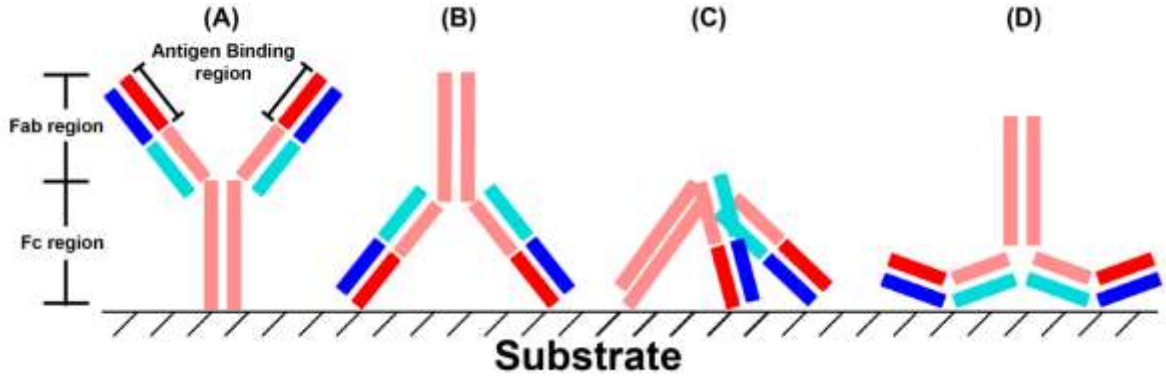


**Figure 6.1** – A schematic diagram of antibodies immobilized on a solid substrate is shown above. Each antibody consists of two heavy chains and two light chains shown in red and blue, respectively. The two antigen binding regions of each antibody are highlighted above within the Fab region of each antibody. Antibody immobilization to a substrate is shown in the idealized manner in (A), where the antigen binding regions are directed toward the sample matrix. Antibody activity can be hindered following immobilization when the antibody is oriented such that the antigen binding region is hidden from the sample matrix, as shown in (B). Antibody activity can also be inhibited due to denaturation of the antibody following immobilization, as depicted in (C) and (D).

Physical adsorption is one of the most routine and easily implemented methods for antibody immobilization. In fact, the majority of 96-well plate ELISA platforms utilize this method as antibodies readily adsorb to the polystyrene wells [7, 19, 23]. However, physical adsorption is an inherently random process and offers no control over immobilized antibody orientation. Moreover, the immobilization of the antibodies to the surface is primarily driven by hydrophobic interactions, which can result in antibody denaturation as well as desorption under certain conditions. This leads to low binding efficiency of antibodies immobilized through nonspecific adsorption, which is typically reported at ~10% [7, 19, 20, 24]. Therefore, physical adsorption protocols are usually not considered for high performance biosensing platforms, which are pursuing low detection limits through highly active sensor surfaces.

Therefore, there are several immobilization protocols which attempt to selectively direct the Fab region, or antigen binding region, of the antibody toward the sample matrix and away from the substrate surface. Both covalent attachment and affinity binding methods offer some degree of orientation control for antibody immobilization [20, 22]. However, these techniques are not always reliable when trying to design a general protocol which can properly orient antibodies of various classes. As shown in **Table 6.1**, covalent methods can result in random antibody orientations when multiple attachment sites are available within the amino acid sequence [25]. Also, affinity based methods are only applicable for certain antibody classes and can suffer from long term stability issues [20]. Therefore, it would be advantageous to supplement binding capacity measurements with a technique which can provide information which can relate antibody structure and orientation to function for the evaluation of antibody immobilization protocols. As such, the defocused imaging approach for measuring single molecule orientations discussed in previous chapters offers a unique opportunity to supplement current techniques and provide further insight regarding this particular issue.

### 6.1.2 – Methods for Investigating Immobilized Antibody Activity and Orientation

Given the popularity of immunoassay-based approaches for biosensing applications, there have been several studies directed toward measuring antibody activity and orientation. As mentioned above, antibody binding capacity assays are a common method for comparing various immobilization protocols. This method compares the sensor response from analyte of interest binding immobilized antibodies on the sensor surface, which have been adhered through different attachment strategies [25-27]. These tests are simple to perform, however, no direct information regarding antibody orientation is provided. Therefore, other methods are utilized to gain insight regarding the orientation of immobilized antibodies.

Previous methods which have been employed to measure antibody orientations include neutron reflection [28-30], atomic force microscopy (AFM) [29, 31], and time-of-flight secondary ion mass spectrometry (TOF-SIMS) [32]. Studies employing neutron reflection have been used to measure the density of protein on a surface as a function of distance from the surface [29-31]. This density information is then used to infer the absolute orientation of immobilized antibodies. There are several drawbacks with this approach, however. These measurements are difficult and costly to perform. TOF-SIMS studies have been employed to examine the exposed amino acids on sensor surfaces [32]. These residues are compared to the known amino acids sequence of the immobilized antibody in order to infer antibody orientation. This approach has demonstrated the potential to directly observe antibody orientation in dry samples. However, the TOF-SIMS method is not applicable to samples in solution, which detracts from its value. Furthermore, both neutron reflection and TOF-SIMS techniques provide an ensemble average view of antibody structure, which may mask heterogeneities within the bound protein layer. AFM studies have been used to provide topographical measurements of surface-bound proteins to approximate the antibody orientations [29, 31]. This method provides the advantage of sufficient resolution to allow for the measurement of individual proteins.

However, AFM measurements have shown that protein orientations can be distorted by tip-protein interactions [31]. Moreover, these measurements are difficult to perform on samples in solution and suffer from relatively low throughput [29]. Therefore, while these approaches can infer or provide approximate antibody orientations, it is evident that new methods are needed to directly measure antibody orientations in solution.

### 6.1.3 – Single Antibody Orientations via Defocused Single Molecule Imaging

The method for single molecule orientation measurements via defocused fluorescence imaging discussed in previous chapters provides a promising new tool for evaluating antibody orientation for various immobilization protocols. This technique provides several attributes which will be advantageous for evaluating immobilization strategies for antibodies. The defocused single molecule fluorescence method is compatible with dry samples as well as samples is in solution [33]. Additionally, this method provides orientation measurements of individual molecules within the sample, which allows the heterogeneous structure of the sample to be observed [33-38]. The fundamental method for measuring the single orientation is thoroughly discussed in Chapter 2 and, thus, not reiterated here. While this approach will prove to be a promising new tool for evaluating antibody orientation, there are several issues which must be addressed in order to develop a useful test system for antibodies.

Similar to the studies of molecular orientations within membranes, a critical requirement for antibody measurements will be the identification of a useful single molecule fluorescent probe. For membrane studies, utilizing a fluorescent lipid analog with the fluorophore located along the acyl tail proved to be a sensitive marker of membrane order [35, 36]. However, the development of a suitable single antibody probe has been more challenging. The most important and problematic issue for developing a single antibody probe is the need to rigidly

attach a fluorescent marker to the antibody of interest. Without rigid dye attachment to the antibody scaffold, single molecule measurements of dye orientation cannot be correlated to antibody orientation and are, thus, inconsequential. Methods to achieve rigid dye attachment to antibodies are discussed below.

It would seem that the most straight-forward method for creating a fluorescent antibody marker for these studies would be to covalently link a small molecule dye to the antibody. There are numerous dyes and labeling protocols for antibody labeling; however, most of these methods result in single site attachment of dye to the antibody [39]. With only a single site of attachment, the bound dye will experience some orientational freedom relative to the antibody. Therefore, covalent methods without bidentate attachment of the fluorescence probe are not considered candidates for these single molecule experiments.

While the majority of covalent attachment methods result in single-site dye attachment, there have been dyes developed which attach rigidly to specific sites along protein sequences. Biarsenical-tertacysteine probes, commonly known as FlAsH and ReAsH tags, form stable complexes with unique amino sequences [40, 41]. These probes have been valuable for several studies, such as, fluorescence resonance energy transfer (FRET) [42] and chromophore-assisted light inactivation (CALI) [43, 44] experiments. The target amino acid sequence (Cys – Cys- Pro – Gly – Cys – Cys), called a tretracysteine tag (TC-tag), rarely appears in endogenous proteins and can be genetically inserted within a protein of interest as a site for dye attachment [41]. The FlAsH/ReAsH probes utilize the high-affinity interaction of arsenic for the thiol groups within these cysteine residues. An advantage provided by these probes is that they are only fluorescent once bound to the TC-tag, thereby significantly reducing the issue of background fluorescence from unbound probes [41]. The binding scheme for FlAsH/ReAsH probes is shown in **Fig 6.2**.

In general, these FlAsH/ReAsH tags provide tremendous promise for labeling genetically engineered proteins for single molecule orientation investigations. Unfortunately, these tags are less useful for labeling antibodies. Antibodies are complex glycoproteins, which are transcribed from several exons within the genome[45]. As shown in **Fig 6.3**, each antibody is composed of a pair of heavy chains consisting of three constant domains ($C_H1$, $C_H2$, $C_H3$) and a variable domain ($V_H1$) and a light chain consisting of a constant domain ($C_L$) and variable domain ($V_L$). Significant diversity in antibody structure is required for immune response to bind various antigens within biological systems. Much of the diversity is derived from the fact that genes encoding for the various parts of each of the variable domains are contained on different gene exons[45]. Further diversity is gained from combining different variable regions with various constant regions, mixing various heavy and light chains, and somatic mutation[45]. In total there are ~$10^{10}$ possible combinations for antibody structure and each B-cell, which is responsible for immune response, only expresses a single unique antibody on its surface[7].

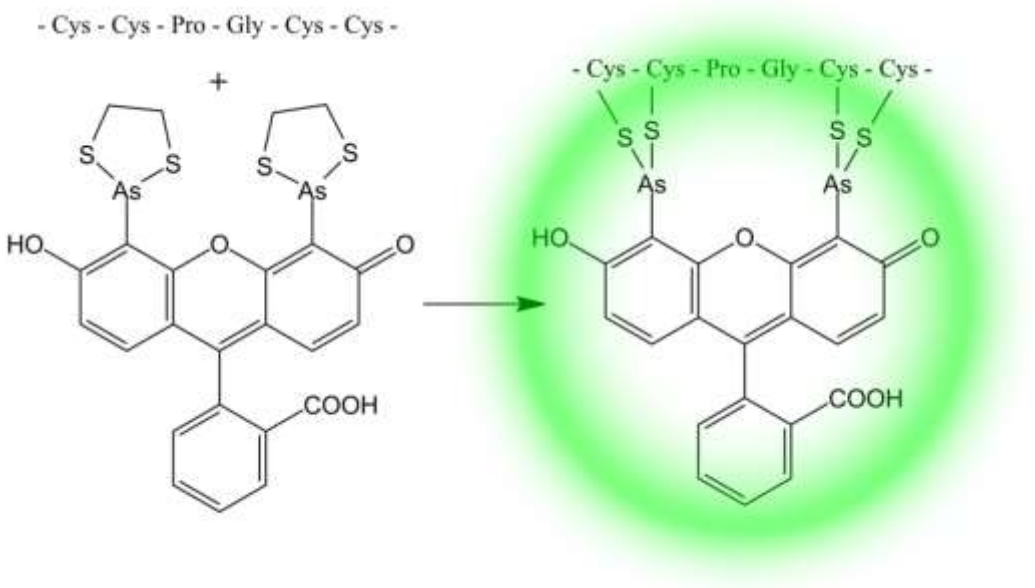


**Figure 6.2** - Biarsenical-tertacysteine probes, such as FlAsH shown above, form stable complexes with genetically engineered amino acids sequences, called a tretracysteine tag (TC-tag). The target TC-tag (Cys – Cys- Pro – Gly – Cys – Cys) is relatively rare in endogenous proteins, making it useful to targeting a specific protein in a complex matrix. Upon binding the TC-tag the FlAsH probe becomes fluorescent.

Therefore, it becomes difficult to identify the exons responsible for creating a particular antibody. It would be even more difficult to attempt genetically alter the genes responsible for a particular antibody in order to accept a FlAsH/ReAsH tag. While genetic engineering of antibody fragments for research and pharmaceutical purposes has been increasing recently, engineering full antibodies has remained a challenge [46-48]. Therefore, as a general scheme for investigating antibody orientations with FlAsH/ReAsH tags appears to be of limited utility.

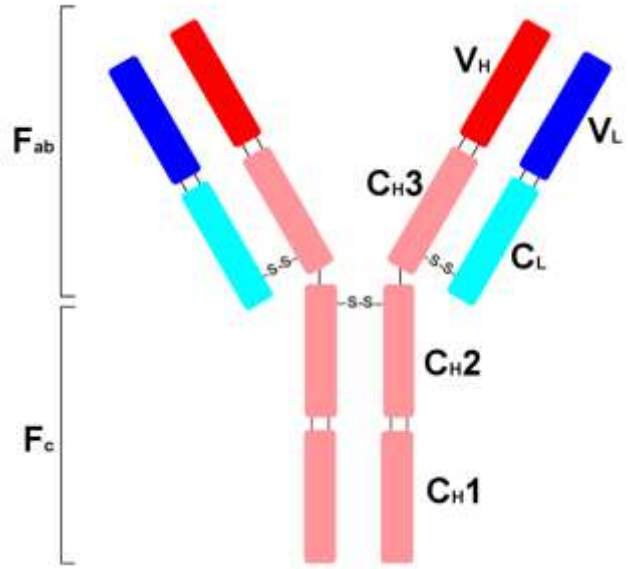


**Figure 6.3** - The schematic structure of an IgG antibody is depicted above. The antibody is composed of a pair of heavy chains and a pair of light chains shown in red and blue, respectively. Each chain consists of constant (C) and variable (V) regions as shown above. The antigen binding region, or Fab region, consists of one heavy and one light chain, while the crystallizable region, or Fc region, consists of two heavy chains.

Fortunately, an alternative approach for generating label antibodies for single molecule orientation measurements using antibodies raised with specificity against fluorescence dyes has substantial promise. These antibodies treat the fluorescent dye as an antigen and bind them rigidly within the antigen binding site of the antibody [49-51]. While these antibodies provide rigid attachment of dye, this attachment often comes at the cost fluorescence quenching due to collisional quenching, static quenching, or a combination of both [52]. Collisional quenching

occurs due to the dissipation of excitation energy upon collisions, while static quenching occurs as the result of the ground state fluorophore forming a non-fluorescent complex with a quencher. Many antibody dye pairs have high reported quenching rates of 90% or greater [49]. Therefore, an antibody/dye pair with significantly lower quenching rates will be required to attempt single molecule fluorescence measurements. Thus, an anti-fluorescein IgG antibody, 4-4-20, with the fluorescein analog, fluo-3, with a lower reported quenching rate, ~32%, will be investigated as a model system for antibody orientation measurements [49].

The 4-4-20 antibody offers several other advantages as model system for preliminary investigation of antibody orientations. This particular antibody has been well studied and a crystal structure of the Fab region of 4-4-20 with bound fluorescein has been reported and is available in the Protein Data Bank (PDB ID: 1FLR) [48, 53-58]. This crystal structure with bound fluorescein, shown in **Fig. 6.4**, allows the orientation of the Fab region to be extrapolated from the measurable dye orientation [53]. While the 4-4-20 antibody has been shown to quench fluorescein fluorescence by ~93% [49], this antibody demonstrates cross reactivity with fluorescein analogs [54, 56]. As mentioned above, the fluo-3 analog of fluorescein, shown in **Fig. 6.5**, has lower reported quenching when bound to the 4-4-20 antibody at ~32% [49]. Thus, we have begun preliminary investigations of antibody orientations using the 4-4-20/fluo-3 complex as a model system.

### 6.1.4 – Limiting Nonspecific Binding in Label-free Biosensor Assays

Considering that many of the label-free techniques discussed above are being designed for clinical diagnostic applications, it is apparent that these techniques will be required to perform in complicated biological matrices, such as whole blood, serum, and urine. These types of sample matrices can contain high concentrations of proteins, nucleic acids, and salts;

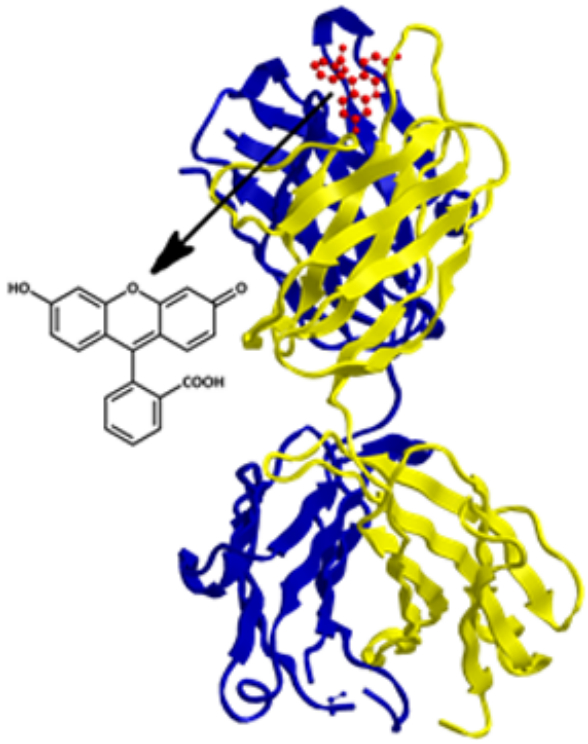


**Figure 6.4** – The crystal structure of the Fab fragment IgG antibody 4-4-20 with bound fluorescein is shown above (PDB ID: 1FLR) [53]. Within the ribbon view, the heavy chain is displayed in blue, the light chain in yellow, and the bound fluorescein dye in red.

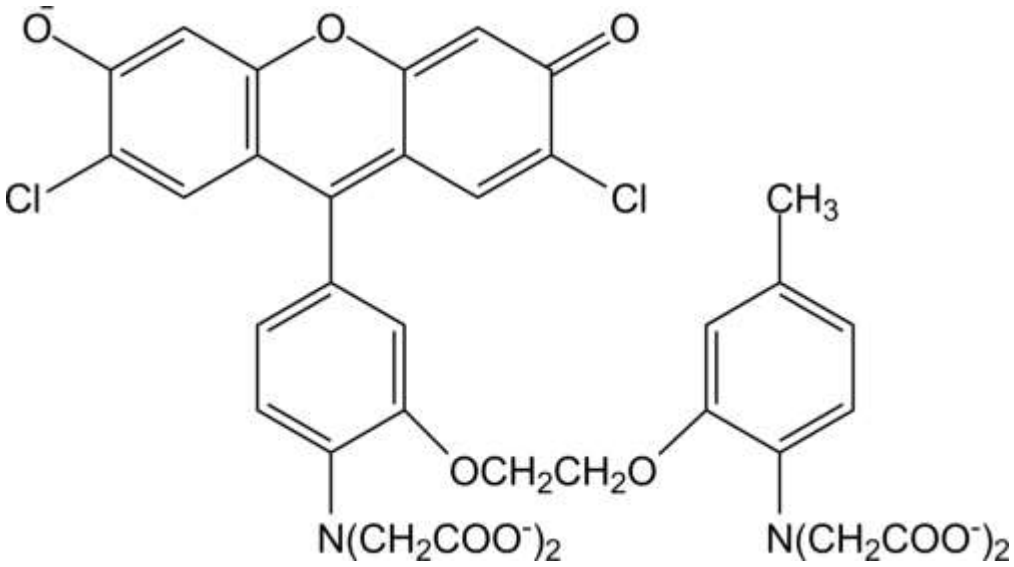


**Figure 6.5 –** The structure fluo-3, a fluorescein analog, is provided above.

furthermore, these concentrations can complicate specific analyte detection. Considering that label-free techniques provide a response to any binding event to the sensor surface, it is imperative to reduce undesired binding events. In complicated biological matrices this can become a daunting task. As such, several protocols and blocking methods have been developed to reduce nonspecific binding events to biosensor surfaces.

One of the most common blocking methods pretreats the sensor surfaces with Bovine Serum Albumin (BSA), a well-known, sticky protein [59]. The goal of this technique is to populate the sites on the sensor surface where nonspecific adsorption can occur prior to exposing the sensor to the sample matrix. More complicated protein mixtures are commercially available and have been shown in some studies to be more efficient at reducing nonspecific absorption [59]. Another promising alternative for reducing nonspecific adsorption on sensor surfaces utilizes polyethylene glycol (PEG) polymer coatings. Several studies have demonstrated that these PEG polymers can be used to create self-assembled monolayers (SAMs), which have been shown to reduce nonspecific binding to sensor surfaces [60, 61].

While these self-assembled PEG monolayers have proven to be a valuable tool for reducing nonspecific adsorption in label-free biosensing applications, the SAM method of creating monolayers offers less control in terms of packing density of membrane components relative to Langmuir-Blodgett (LB) / Langmuir-Schaffer (LS) methods [62]. Therefore, it would be advantageous to utilize LB/LS methods for depositing PEG coatings on a sensor surface to determine the optimal packing density of PEG monomers needed for reducing nonspecific binding in a controlled system. Fortunately, with the growing interest in PEG coatings, there are now synthetic lipid analogs that are commercially available which have been modified to incorporate a PEG polymer [63]. Therefore, here we report the initial findings of LB/LS deposition of these PEGylated lipids for reducing nonspecific adsorption. The chemical structure of the PEGylated lipid employed in these studies is shown in **Fig. 6.6**.

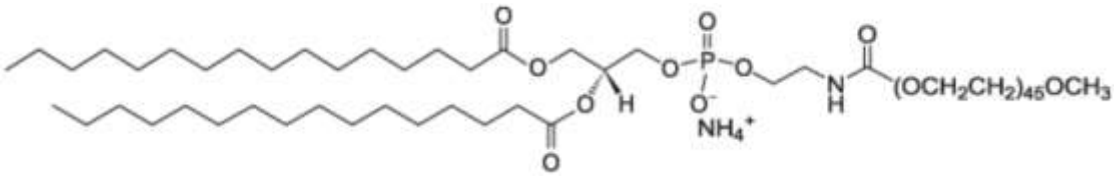


**Figure 6.6** – The chemical structure of DPSE-PEG2000 (DSPE-PEG), a PEG functionalized lipid, is shown above.

## 6.2 – Materials and Methods

### 6.2.1 – 4-4-20 Antibody / Fluo-3 Preparation and Immobilization

Monoclonal antibody 4-4-20 (Life Technologies, Grand Island, NY) and Fluo-3 (Life Technologies) were obtained and used without further purification. Excess Fluo-3 was complexed to the 4-4-20 antibody by incubation in PBS buffer for 2 hours at room temperature. Unbound fluo-3 was then filtered by dialysis using a 3 kD molecular weight cut off filter (Thermo Scientific, Rockford, IL). Dialysis was repeated until fluorescence could no longer be observed in the dialysate. The purified 4-4-20/Fluo-3 complex was then immobilized to glass cover slips for single molecule orientation analysis. Immobilization protocols included nonspecific adsorption and attachment through Protein A affinity. Nonspecific adsorption was achieved by incubation of the 4-4-20/Fluo-3 complex with the substrate for 2 hours. Protein A attachment was achieved by pretreatment of the substrate with Protein A (Thermo Scientific, Waltham, MA) for 2 hours, washing, and incubation with antibody/dye complex for an hour. All immobilization procedures were carried out at room temperature.

### 6.2.2 – Single Antibody Orientation Measurements via Defocused Imaging

Immobilized 4-4-20/Fluo-3 complexes were imaged using a total internal reflection fluorescence microscope (TIRF-M) (Olympus IX71, Center Valley, PA) equipped with a 100x, 1.45 NA objective (Achromat, Olympus). The 514nm line from an argon ion laser (Coherent Innova 90, Santa Clara, CA) was directed through half-wave and quarter-wave plates (Newport, Irvine, CA) to select for p-polarized excitation before being coupled into the microscope. Excitation was directed through the objective with the optics defocused ~500nm and fluorescence was collected, filtered, and imaged on a cooled CCD camera (Retiga 1300, Q Imaging, Surrey, BC, Canada). Image collection was controlled with Slidebook software (Version 4.2.0.3, Intelligent Imaging Innovations, Denver, CO). For both dry samples and samples in PBS solution, individual captures were integrated over 200 ms. The resulting single molecule emission patterns were analyzed with MATLAB (Natick, MA).

### 6.2.3 – PEGylated Bilayers Generated via LB/LS Deposition

Dipalmitoylphosphatidyethanolamine (DPPE), Dioleoylphosphatidylcholine (DOPC), Distearoylphosphoethanolamine-N-[methoxy(polyethylene glycol)-2000 (DSPE-PEG), Distearoylphosphoethanolamine-N-[poly(ethylene glycol)2000-N'-carboxyfluorescein] (DSPE-PEG-fl) ) (Avanti Polar Lipids, Alabaster, AL) were obtained at >99% purity and used without further purification. Each lipid and lipid analog was diluted in 50/50 (v/v) methanol/chloroform to obtain appropriate working concentrations, ~1mg/ml. For monolayer fluorescence studies, DOPC/PEG-2000 solutions were prepared at the required molar ratio and doped with 0.5% PEG-2000-fl. For bilayers utilized in the fluorescence and WGM assays, DPPE monolayers were first deposited to the glass substrate by LB deposition at 35 mN/m. A subsequent

monolayer containing DOPC/PEG-2000 was deposited to this substrate via LS deposition at 30 mN/m to create Y-type bilayers.

Monolayers were created in a Langmuir-Blodgett (LB) trough (Type 611, Nima Technology, Coventry, England) by dispersing approximately 50 µL of the appropriate lipid solution on an 18MΩ water subphase. The solvent was allowed to evaporate for at least 15 min prior to initiating compression/expansion cycles to anneal the film. Each monolayer was subjected to two compression/expansion cycles between surface pressures of 35 mN/m and 2 mN/m. The barrier rate during these cycles was held at 100 $cm^2$/min. Following the last expansion, the monolayers were compressed to the desired target pressure and held for ~10 min prior to transfer onto a solid substrate. LB monolayers were transferred onto clean slides and glass slides with immobilized glass microsphere in a headgroup down arrangement using a dipping velocity of 5 mm/min. LS monolayers were transferred to DPPE coated slides by lightly contacting the substrate to a subsequent DOPC/PEG-2000 monolayer at approximately a 5º angle. The substrate was then slowly lifted from the water interface at a dipping velocity of 3 mm/min. All monolayers were transferred and imaged at 22 °C.

### 6.2.4 – Microsphere Immobilization

High refractive index (n = 1.9), barium titanate ($BaTiO_3$) glass microspheres (53 µm diameter, Mo-Sci, Rolla, MO) were cleaned in a 5% Contrad solution. The spheres were rinsed in an ethanol/water (30/70 v/v) solution, then a PBS solution, and stored in PBS until use. A glass bonding solution was prepared with 0.125% w/v calcium acetate (Fisher Scientific, Hampton, NH) and 0.125% w/v powdered detergent (Alconox Inc., White Plains, NY) in nanopure $H_2O$. Approximately 100 uL of the bonding solution was placed on a clean glass cover slip (Fisher Scientific, Hampton, NH) and allowed to deprotonate the glass surface for ~5 minutes. Approximately 5 µL of the clean microspheres in PBS solution were transferred to the

sample slide and allowed to dry for 20 minutes at 50 °C. The sample slide was washed thoroughly with nanopure $H_2O$ to remove any unbound spheres and excess salts from the surface.

### 6.2.5 – Fluorescence Imaging

Fluorescence imaging of the microstructure within DOPC/PEG-2000/PEG-2000-fl monolayers was acquired with an inverted microscope (Olympus IX71) equipped with a 100x PlanAPO objective (1.45 NA, Olympus). The 514 nm line from an argon ion laser (Innova 90, Coherent Inc.) was coupled into the microscope through the objective using a total internal reflection illumination configuration. Emission from the fluorescent lipid analog DSPE-PEG2000-fl was collected with the same 100x objective and imaged on a cooled CCD camera (Coolsnap K4, Roper Scientific, Tuscon, AZ). Image collection with 200ms integration time was controlled with Slidebook software (Intelligent Imaging Innovations).

Imaging for the fluorescence binding assays was completed on an inverted microscope (Zeiss axiovert135TV, Thornwood, NY) equipped with a 10x UMPlanFL objective (Olympus). The 488 nm and 647 nm line from a krypton/argon ion laser (Innova 70 spectrum, Coherent Inc., Santa Clara. CA) was directed through a dove prism to achieve evanescent wave excitation at the sample surface. Fluorescence from the sample was collected by the objective viewing through the dove prism, filtered at the appropriate wavelength (488LP/647LP, Chroma), and collected on a cooled CCD (Coolsnap K4). Image collection with 250 ms integration time was controlled with Slidebook software (Intelligent Imaging Innovations). The power density of the excitation spot on the sample surface was held constant by using a constant illumination intensity at each wavelength and a micromanipulator controlled focusing lens.

### 6.2.6 – Fluorescence Binding Assays

Investigations of specific binding and nonspecific adsorption to glass surfaces were accomplished utilizing fluorescently labeled streptavidin-Alexa633 (SA-633, Life Technologies) and BSA-Alexa488 (BSA-488, Life Technologies), respectively. Immobilized glass microspheres on glass slides were treated with various lipid coatings produced by the LB/LS method discussed in **Section 6.2.3**. Each sample was contained within a rubber gasket (Grace Bio-Labs, Bend, OR) adhered to the slide and incubated in 800ul of PBS buffer. Each sample was then incubated with 20 ul of 0.1 mg/ml SA-633 and 50 ul of 0.1 mg/ml BSA-488 for 15 minutes. The samples were then washed 3 times with 800ul of PBS buffer. Simultaneous binding of SA-633 and BSA-488 were measured by their fluorescence intensity. At least 3 background images and 5 images after the washing procedure were collected from various locations containing microspheres on the sample surface. Data analysis was performed in Photoshop CS3, where the average intensity of microspheres within the illumination area was calculated at each wavelength.

### 6.2.7 – WGM Assays of Serum Proteins

Barium-titinate glass microspheres with a 53 um diameter were obtained from Mo-Sci Corp. (Rolla, MO). These spheres were functionalized with Alexa-633 succinimidyl ester (Invitrogen, Carlsbad, CA). StartingBlock blocking solution was obtained from Thermo Scientific (Rockford, IL). Human Ab serum, PBS, and all other reagents were obtained from Fisher Scientific (Hampton, NH), unless otherwise noted.

Glass microspheres were prepared for use in WGM assays by soaking in a 10% Contrad-70 solution in nanopure water for one hour. These spheres were triply rinsed with nanopure, then incubated in 30% hydrogen peroxide solution for one hour. These spheres were

then rinsed with nanopure water, ethanol, and toluene, then tumbled overnight in 6% APTES in toluene to form an amine terminated surface. The spheres were then washed with toluene, ethanol, and PBS buffer. To attach the Alexa-633 fluorescent dye to the spheres, samples were subsequently tumbled for 2 hr in 6% glutaraldehyde solution in PBS and triply rinsed with PBS, then incubated overnight with Alexa-633 succinimidyl ester to covalently link the dye to the sensor surface. These spheres were washed with PBS and refrigerated until used.

Functionalized glass microspheres were immobilized to glass slide using the calcium bonding procedure outline above in **Section 6.2.4**. These glass substrates were then subjected to various surface treatments for blocking nonspecific adsorption. For PEG coatings, PEGylated lipid bilayers were deposited onto the surface using the LB/LS technique outlined above in **Section 6.2.3**. These samples were then enclosed in perfusion chambers (Grace Bio-Labs, Bend, OR) and incubated in PBS. For protein incubation methods, each sample was enclosed in a perfusion chamber and incubated in 10% of appropriate protein solution in PBS for 1 hour. These samples were then washed thoroughly with PBS.

WGM measurements were performed with a tunable Vortex II TLB-6900 external cavity diode laser (New Focus, Santa Clara, CA). Laser excitation was directed into a Dove prism (Edmund Optics, Barrington, NJ), on which the sample was mounted. Total internal reflection at the substrate interface creates an evanescent field, which was used to launch light into the immobilized microspheres. At a WGM resonance, an enhanced ring of fluorescence from Alexa-633 was observed from the microspheres, which were imaged from above. The fluorescence was collected through a 10X UMPlanFL (0.3 NA) objective (Olympus), filtered (Chroma), and imaged onto a cooled CCD camera (Coolsnap K4). A LabView program controlled scanning of the laser system, which was synchronized with Slidebook image collection software (Intelligent Imaging Innovations).

Serum protein nonspecific adsorption to these prepared samples was quantified by WGM resonance shift upon subjecting each sample to increasing serum concentrations. WGM resonances from spheres within each sample were recorded prior to the first injection. After a 10 minute incubation period following each serum injection, the WGM resonance spectra were acquired again for each sphere. Data analysis of the WGM response to nonspecific adsorption was performed using LabView (National Instruments Corp., Austin, TX) and Origin 6 (Microcal Software Inc., Northampton, MA) software.

## 6.3 – Results and Discussion

### 6.3.1 – Single Antibody Orientations

In previous studies we have validated the use of single molecule orientation measurements via defocused single molecule imaging for investigations of membrane structure[33-38]. These studies have demonstrated that measurements with acyl-linked fluorescent lipid analogs can elucidate structural perturbations within the membrane at the molecular level. While these have been valuable for contributing to the understanding of membrane structure, here we seek to utilize the single molecule orientation approach to investigate the orientation of antibodies bound to a solid substrate. The orientation of immobilized antibodies is of great interest due to the prevalence of immunoassay techniques which suffer loss of sensitivity due to inactive antibodies. Therefore, here we present preliminary findings of a model test system for investigating antibody orientations with single molecule orientation measurements via defocused fluorescence imaging.

For the development of a model test system for investigating antibody orientations we employed a fluorescein analog, Fluo-3, bound to monoclonal antibody 4-4-20. The 4-4-20

antibody was raised with specificity for fluorescein; however, it also experiences affinity for fluorescein analogs, such as Fluo-3 [49, 54, 56]. When bound to the 4-4-20 antibody, fluorescein experiences quenching rates greater than 90% [49]. Achieving single molecule fluorescence measurements with this dye complex is, thus unrealistic. Therefore, Fluo-3 was employed for these studies due to its significantly lower quenching rates upon complexing with 4-4-20 and its compatibility with single molecule imaging [49] .

The 4-4-20/Fluo-3 complex was allowed to bind in PBS buffer and then purified by dialysis. This complex was then immobilized to glass coverslips by physical adsorption and through affinity to Protein A. Following immobilization, the incubation solution was removed and the samples were imaged using the defocused TIRF approach described in detail in **Chapter 2**. A representative image of the defocused emission patterns observed when imaging the 4-4-20/Fluo-3 complex is shown in **Fig. 6.6**. Orientation measurements of this complex in both dry and wet samples were obtained and are discussed below.

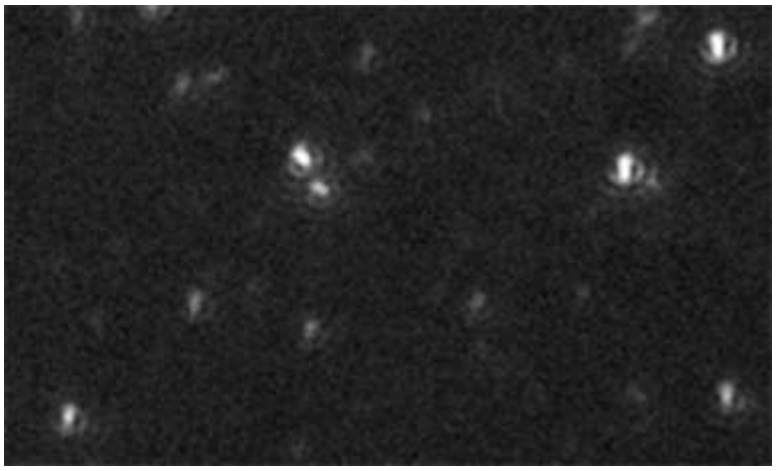

**Figure 6.6** – A representative defocused single molecule fluorescence image of purified 4-4-20/Fluo-3 is shown above. Even when bound to the antibody, fluorescence from individual Fluo-3 molecules can be observed with sufficient a signal to noise ratio to allow for orientation measurements.

Initial studies of 4-4-20/Fluo-3 orientation on glass substrates were performed on dried samples. Within this study, the molecular orientation of 4-4-20/Fluo-3 immobilized through nonspecific adsorption and Protein A were compared. The single molecule emission pattern mapping methods discussed in **Chapter 2** were utilized to measure the three-dimensional orientation of each molecule observed within each image. A histogram compiling the observed polar angle (Φ) from each 4-4-20/Fluo-3 complex observed within these samples is shown in **Fig. 6.7**.

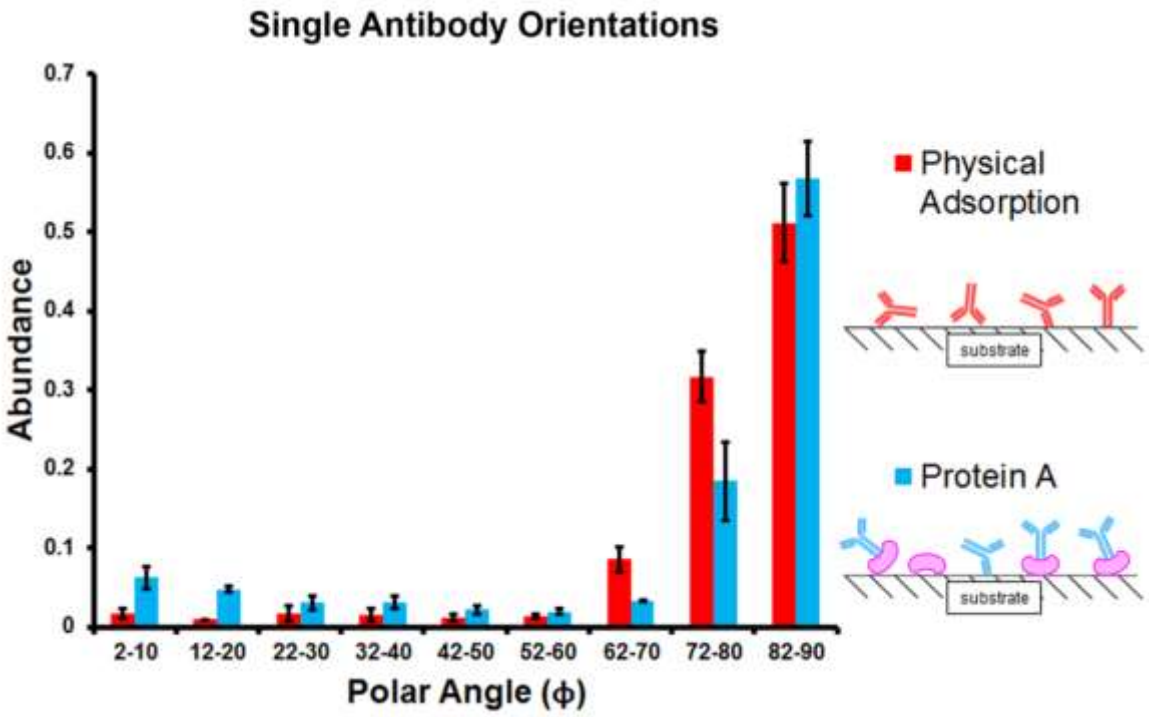


**Figure 6.7** – A tilt angle histogram of the observed molecular orientations of dry 4-4-20/Fluo-3 complexes measured by defocused fluorescence imaging is shown above. As shown in the schematic illustration on the right, physical adsorption and Protein A immobilization strategies are compared. While correlation of total antibody or Fab region orientation to observed Fluo-3 orientation is speculative with these preliminary results, the data above does suggest that there is a statistical difference in the 4-4-20/Fluo-3 complex orientation with each immobilization protocol. Orientation measurements of at least 300 individual molecules for 3 separate samples using each immobilization protocol were used to populate the histogram above.

The results displayed in **Fig. 6.7** should be should be interpreted cautiously given the following considerations. First, while the 4-4-20/Fluo-3 complex can be utilized to correlate orientational changes of the antibody, the observed tilt angle of the Fluo-3 emission dipole orientation should not be used to determine the absolute orientation of the overall antibody or Fab fragment. While the 4-4-20/fluorescein system has been studied extensively and crystal structure of this bound complex has been reported, as shown in **Fig. 6.4**, a crystal structure for the 4-4-20/Fluo-3 complex has not been reported[53]. Although the reduced quenching efficiency is a major positive attribute of the 4-4-20/Fluo-3 complex, this reduction in quenching efficiency also suggests Fluo-3 maybe bind differently within the 4-4-20 antibody. Therefore, even though it is assumed that Fluo-3 and fluorescein bind in a similar manner to the 4-4-20 antibody, a crystal structure is needed to support this assumption. Second, more robust purification methods should be employed to ensure each observed emission pattern is from a bound 4-4-20/Fluo-3 complex. Finally, similar to alternative methods for investigating antibody orientations, measurements of dried samples are less relevant than samples in solution for immunoassay applications.

Albeit with these considerations, there are still interesting conclusions to be drawn from the results shown in **Fig. 6.7**. Shown in the tilt angle histogram is a statistically relevant deviation in upright oriented fluorophores. While, we hesitate to suggest that this represents a greater abundance of 4-4-20/Fluo-3 complexes with outward facing Fab regions when immobilized though Protein A attachment, we are confident these results suggest there is a measurable difference in orientation of 4-4-20/Fluo-3 complex when immobilized by these two procedures.

Even though dried samples are less relevant for immunoassay applications, utilizing dry samples is advantageous in terms of imaging defocused emission patterns. The refractive index difference between the glass substrate and the sample matrix affects the single molecule

fluorescence coupling angle through the sample interface and into the objective. As detailed in Chapter 2, it is through deviations in this fluorescence coupling angle through the sample interface that allow single molecule orientations to be measured. Reducing this refractive index difference by placing the sample in solution requires that a greater defocus distance is used to effectively image single molecule emission patterns. This has two adverse effects for imaging single molecule orientations. First, increasing the defocusing distance results is spreading the emission pattern from a single molecule over a greater area on the imaging plane. This reduces the signal-to-noise ratio and can make emission pattern mapping more difficult. Second, through numerous experimental measurements of single molecule orientations in membranes and of 4-4-20/Fluo-3, we have found that acceptable defocus distance for single molecule orientations is polar angle (Φ) dependent. For dry samples, the acceptable defocus distance for molecular orientations of polar angles at the two extremes (Φ = 0º and 90º) overlap significantly, thereby easing demands on the imaging system. Unfortunately, in under-water samples, which require greater defocus distances, the overlapping acceptable defocus distance is much smaller. This makes acquiring images which capture emission patterns of all molecular orientations within a sample significantly more difficult.

In spite of the increased imaging difficulty, we were able demonstrate the single molecule orientations of 4-4-20/Fluo-3 complexes in solution, as shown in **Fig. 6.8**. By capturing time-lapsed defocused images of 4-4-20/Fluo-3 complexes bound through Protein A we were able to observe the dynamic motion of these complexes. As shown in **Fig. 6.8**, the rotation of a single complex can be observed in the upper left (A) of the series of images. Also observed within these images were a static complex (D) and a complex with dynamics on a faster time than the image integration time (B).

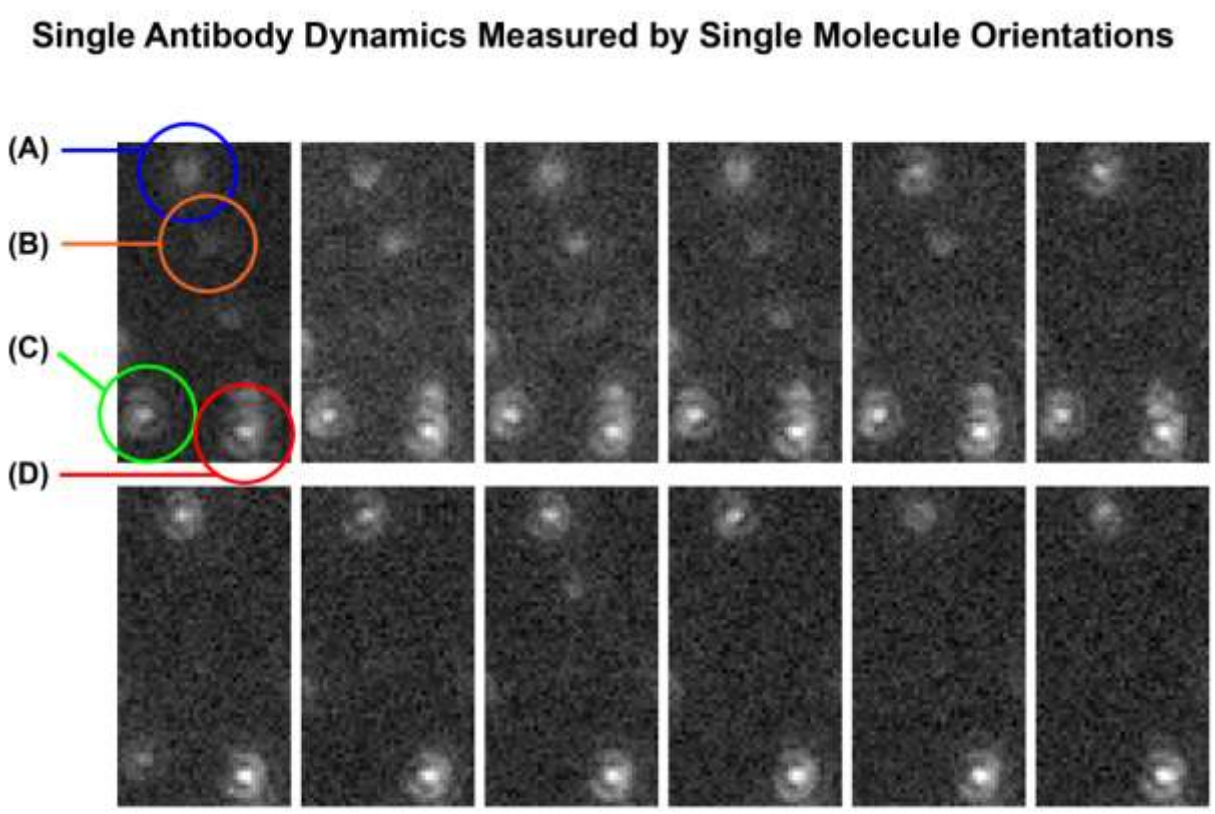


**Figure 6.8** – Images from a time-lapse capture of defocused emission patterns from 4-4-20/Fluo-3 immobilized to a glass substrate through Protein A attachment in an underwater sample are shown above. Each capture was completed with a 200ms integration and 100 ms dead time. Within this series of images, the dynamic motion of a single 4-4-20/Fluo-3 complex can be observed in (A). Additionally, a complex which is moving on a faster time scale than the integration rate and photobleaching can be observed in (B) and (C), respectively. Finally, a static single molecule in the bottom right of the image can be observed in (D).

As with the orientation measurements of dry samples, we hesitate to correlate the observed Fluo-3 orientation to overall antibody or Fab fragment orientation when using the 4-4-20/Fluo-3 system. As such, we cannot yet reliably conclude which observed molecular orientations will correspond to increased antibody activity. We hypothesize that it may be the dynamic molecules such as those observed in **Fig. 6.8**, which have the freedom to explore greater dimensional space within the sample matrix may be the most effective at binding their target analyte. Thus, the results presented in **Figs. 6.7** and **6.8** provide promise for utilizing

defocused single molecule orientation for studies of antibodies on solid substrates. The ability to not only observe molecular orientations of 4-4-20/Fluo-3 in samples in solution, but also to measure the dynamic nature of the molecule make this approach a promising new alternative for investigating the relationship between antibody orientation and binding affinity.

### 6.3.2 – PEGylated LB/LS Bilayers for Reduced Nonspecific Adsorption in Biosensors

Several previous studies of self-assembled monolayers (SAMs) have demonstrated the use of membrane films as a coating for biosensors for the specific analyte detection and reducing nonspecific absorption [60-62, 64]. The SAM approach is valuable for coating biosensor surfaces because it can easily deposit monolayers to several types of surfaces with high control of monolayer composition [61]. With these attributes, studies employing polyethylene glycol (PEG) SAMs on biosensor surfaces report significantly reduced nonspecific binding to these surfaces when a high surface density of PEG is achieved to create a polymer brush [61, 65].

The reduction in nonspecific adsorption of these PEG films is attributed to the formation of a water cushion between the surface and the sample matrix. This water cushion is formed due to PEG containing repetitive hydrogen bond acceptors within its polymer chain. Non-specific adsorption, which is driven by surface-protein attraction, is essentially avoided by incurring an osmotic penalty for inserting a protein within the PEG monomers [66]. With these reports there has been considerable interest to achieve an optimal PEG coating for blocking nonspecific adsorption by altering the PEG polymer brush though augmenting the PEG chain length and concentration within SAMs [65, 67]. However, it seems clear that control of packing density within the PEG polymer brush is a key attribute for limiting nonspecific adsorption.

While the self-assembled method for monolayer production has several positive attributes, control of monomer surface density in SAMs is limited.

In the study discussed in Chapter 5, we demonstrated the use of lipid bilayers deposited by the LB/LS method for the specific detection of Cholera toxin with label-free WGM biosensors [68]. With PEG functionalized lipid analogs (PEGylated lipids) now being commercially available, here we report the use LB/LS deposition methods to easily control packing density of PEG monomers within lipid film coatings for sensors surfaces.

Initial studies of membrane structure were performed using fluorescence microscopy in order to ensure uniform and complete surface coverage of the PEG polymer which is required for blocking nonspecific adsorption. A series of DOPC/DSPE-PEG LB monolayers doped with 0.5% of a fluorescent PEGylated lipid analog, DSPE-PEG-fl, were deposited on to glass substrates at 30 mN/m and imaged with an inverted fluorescence microscope. Representative images of monolayers containing various DSPE-PEG concentrations in DOPC are shown in **Fig. 6.9**. As shown in **Fig 6.9**, monolayers containing ≤25 mol% DSPE-PEG exhibit relatively uniform coverage of DSPE-PEG-fl within the monolayer. The formation of microdomains lacking PEG with these monolayers can begin to be observed at 33 mol% DSPE-PEG and more clearly observed at 50 mol% DSPE-PEG. It should also be noted, there are small bright regions within the monolayer containing 5 mol% DSPE-PEG, which suggests some aggregation of the DSPE-PEG-fl dye within the monolayer. Fluorescent images of PEGylated bilayers were also acquired to ensure the monolayer microstructure structure observed in **Fig 6.9** was maintained in bilayer films. These bilayers images confirmed similar structure to that displayed in the monolayers shown in **Fig. 6.9**.

Previous studies of SAMs suggest there is a minimum PEG monomer concentration required to reduce nonspecific adsorption [69]. These findings correspond with the concept that the formation of polymer brush of PEG monomers is required for effective blocking of protein

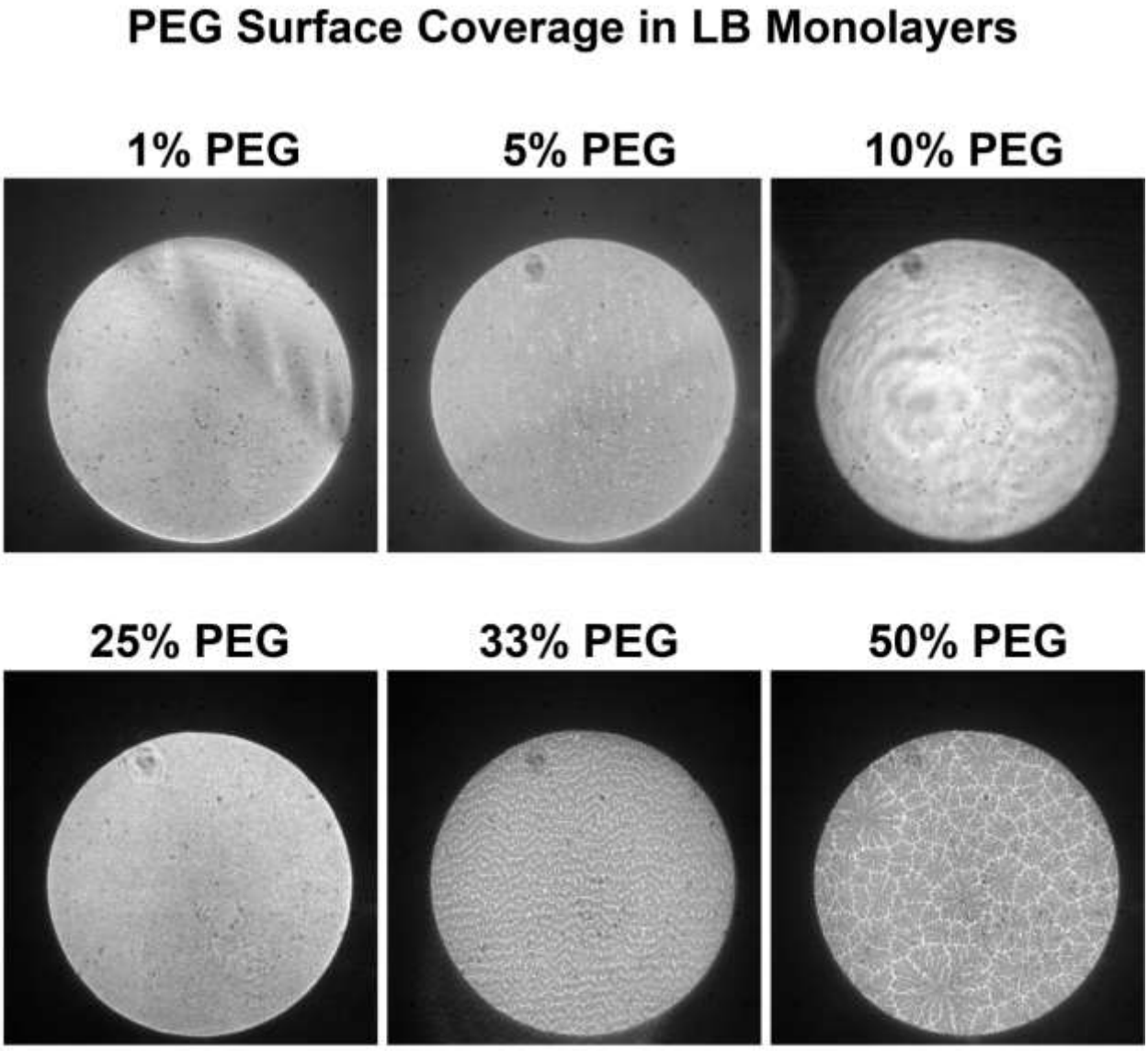


**Figure 6.9** – Fluorescence images of DOPC/DSPE-PEG monolayers doped with 0.5% DSPE-PEG-fl deposited at 30 mN/m by LB transfer to glass slides are shown above. The formation of microscopic domain phases becomes apparent at DSPE-PEG concentrations ≥33 mol%. Each image was captured over a 200 ms integration period with 100x magnification. The scale for each image is ~130x130 μm.

adsorption to a surface. Thus, a minimum concentration of DSPE-PEG is also expected to be required for blocking with LB/LS bilayers as well. Also, as suggested from the images shown in **Fig. 6.9**, at higher concentrations of DSPE-PEG the formation of microscopic membrane domains result in nonuniform coverage of PEG monomers on the substrate. Therefore, this data suggests that there will be an optimal concentration of DSPE-PEG in the outer leaflet of LB/LS bilayers deposited at 30 mN/m for reducing nonspecific adsorption.

As discussed above, bilayers deposited onto glass slides were created by first depositing a DPPE monolayer with the LB method. DPPE was employed for the bottom monolayer in order to create a stable and reproducible hydrophobic film on the glass substrate. A subsequent monolayer containing DOPC/DSPE-PEG was then applied to this substrate with the LS method to create a lipid bilayer. Bilayers created with this procedure were applied to glass substrates with immobilized microsphere resonators in order to test nonspecific adsorption of proteins to sensor surfaces.

Initial tests of specific and nonspecific binding of proteins to bilayer coated microspheres were completed using fluorescence imaging of labeled streptavidin and bovine serum albumin, respectively. Each of these proteins was purchased labeled with Alexa series dyes which are easily spectrally separated. The absorption and emission spectra of the fluorescent labels employed in this study, Alexa-488 and Alexa-633, are shown in **Fig. 6.10** [70]. Thus, bovine serum albumin labeled with Alexa-488 (BSA-488) and streptavidin labeled with Alexa-633 (SA-633) were employed to measure nonspecific adsorption and specific binding to biotin, respectively.

Each lipid coated slide with immobilized glass microspheres was incubated in PBS buffer spiked with 5.9 μg/ml BSA-488 and 2.4 μg/ml SA-633 for 15 minutes. Each slide was then

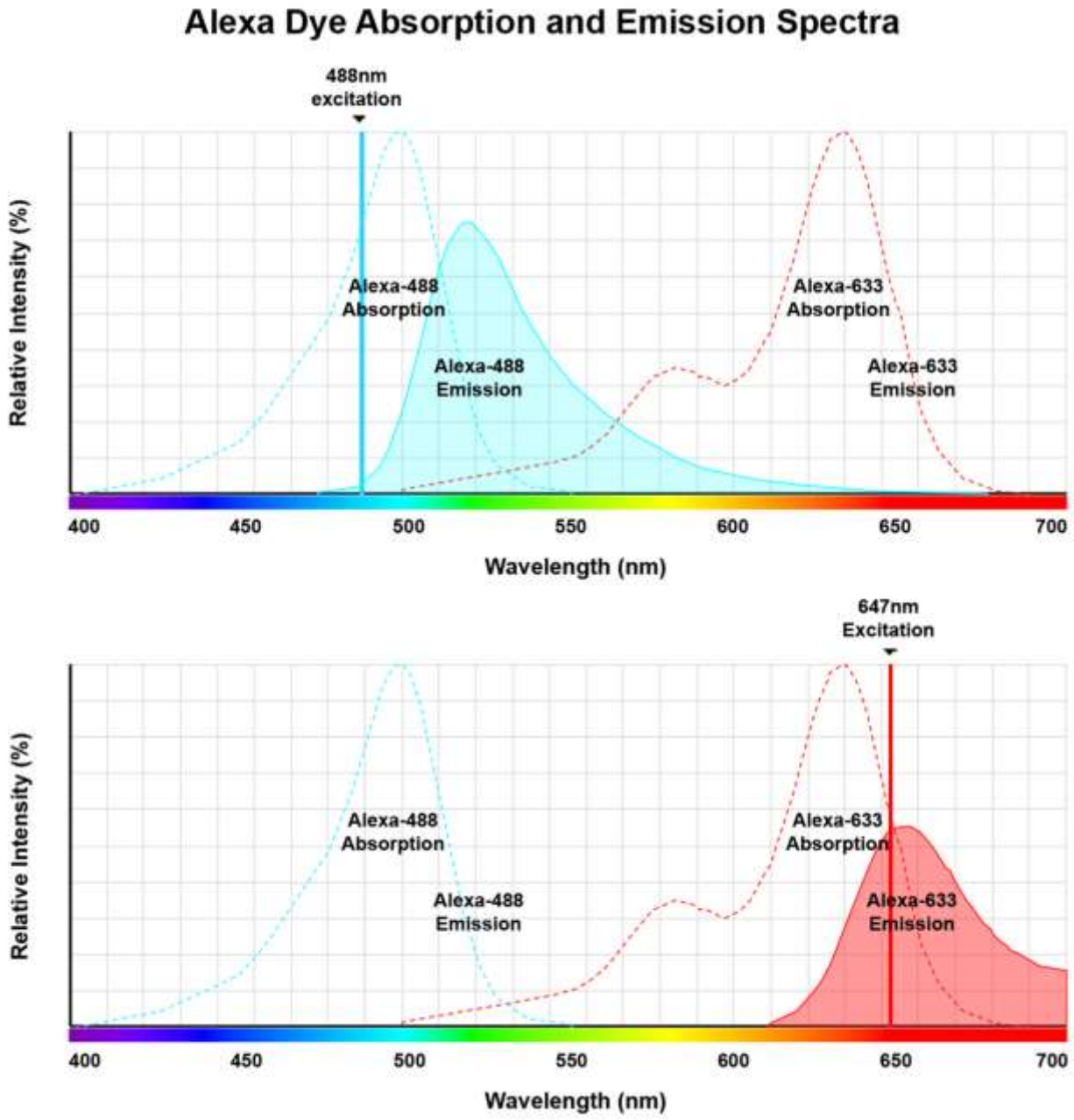


**Figure 6.10 –** Absorption and emission spectra of Alexa-488 and Alexa-633 are shown with 488 nm (above) and 647 nm (below) excitation lines.

rinsed with PBS in triplicate and imaged with total internal reflection fluorescence microscopy. Total internal reflection evanescent wave excitation was employed to excite fluorophores bound the sample surface while limiting background fluorescence from the bulk solution. Each sample was imaged with both 488 nm and 647 nm excitation lines from an Ar/Kr ion laser to separately quantify BSA-488 and SA-633 bound to the surface. The fluorescence response from bound fluorophores was performed by measuring the average intensity from at least 10 microspheres from several different areas on the sample surface. BSA-488 and SA-633 protein binding to these immobilized glass microspheres quantified by fluorescence intensity is shown in **Fig. 6.11**. DOPC and DOPC/DSPE-PEG bilayers were utilized to compare nonspecific binding of BSA to the slide surface. Additionally, a bilayer containing biotin labeled lipid analog, DSPE-PEG-biotin, was used to demonstrate that while PEG can be utilized to reduce nonspecific adsorption, specific binding through affinity-based interactions can be maintained with these bilayer coatings.

The results displayed in **Fig. 6.11** demonstrate the reduction of nonspecific adsorption to glass microspheres coated in bilayers containing DSPE-PEG as measured by fluorescence intensity of BSA-488. These results also suggest there is an optimal packing density, or concentration of PEG monomers deposited at 30mN/m, near 10% DSPE-PEG for maximum blocking of nonspecific adsorption. This agrees with the findings from the fluorescence studies of PEG surface coverage, shown in **Fig. 6.9**. The fluorescence binding assay, shown in **Fig. 6.11,** reveals that nonspecific adsorption of BSA is reduced for 10 mol% DSPE-PEG bilayers relative to 25% DSPE-PEG bilayers. Indications for reduced nonspecific binding in the surface coverage fluorescence measurement are not evident until domain phases are clearly seen at ≥33% DSPE-PEG. This discrepancy is likely do to the resolution limits of optical microscopy. It is possible the initial formation of these domains occur at DSPE-PEG concentrations <33 mol% but are not resolvable by optical microscopy. In addition to monitoring nonspecific

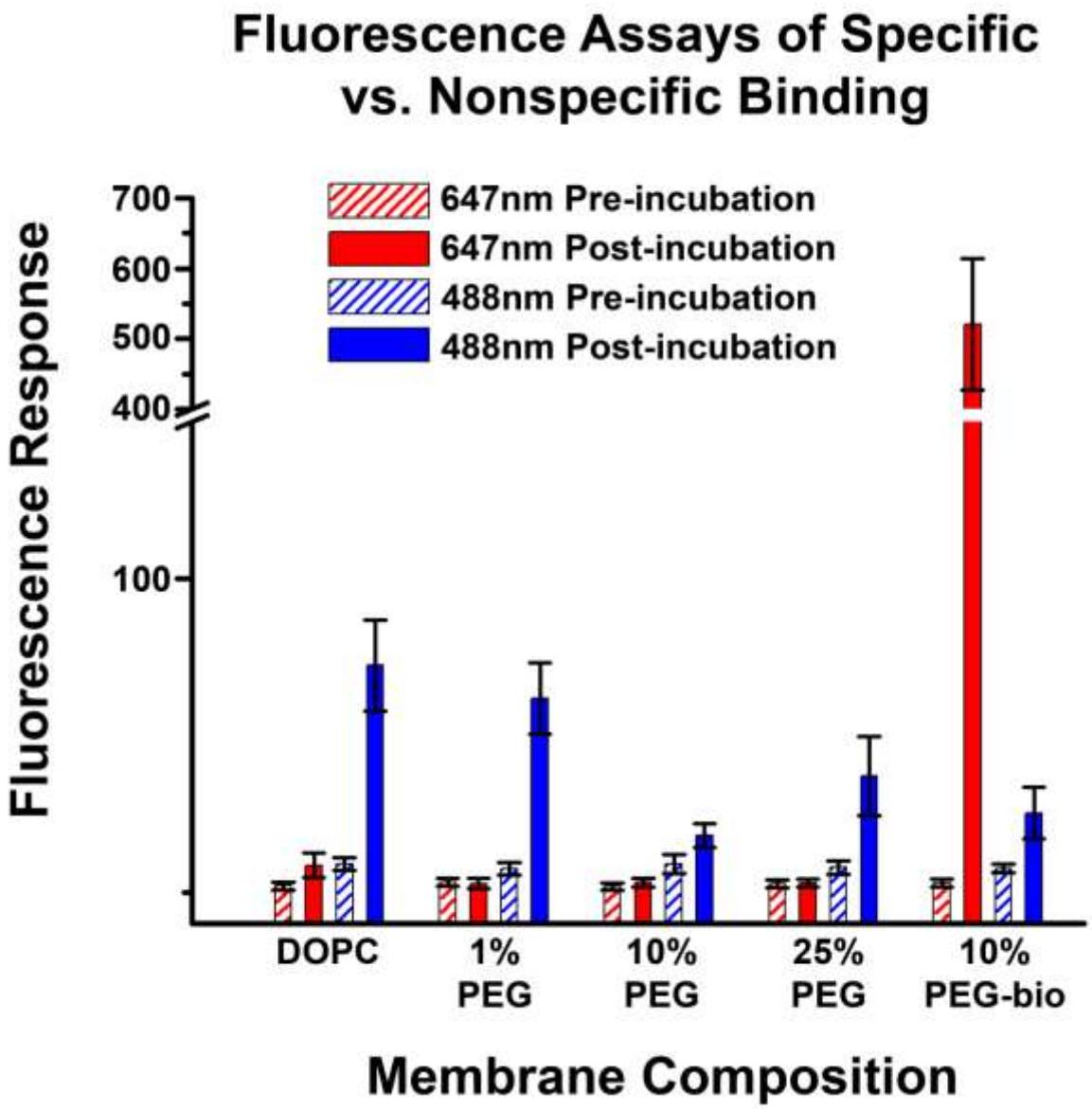


**Figure 6.11** – The fluorescence response due to binding of labeled streptavidin and BSA to the glass microspheres coated with various lipid bilayers is shown above. The striped bar of each color represents the pre-incubation response and the solid bar of each color represents the fluorescence response after incubation and washing. Specific binding was monitored utilizing streptavidin-Alexa-633 (SA-633) which has affinity biotin labeled surfaces. Nonspecific protein adsorption was examined with bovine serum albumin-Alexa-488 (BSA-488). As shown is **Fig. 6.10**, these dyes are separately excited with 488 nm and 647 nm Kr/Ar laser lines and easily spectrally separated. Each sample was incubated with 2.4 μg/ml SA-633 and 5.9 μg/ml BSA-488 for 15 minutes then washed in triplicate. Multiple fluorescence images were acquired with both excitation lines prior to and following incubation with SA-633 and BSA-488. The average fluorescence intensity from at least 10 separate spheres for each sample type is shown above with the standard deviation displayed in the error bars.

adsorption with BSA-488, these fluorescence binding assays utilized SA-633 to measure specific binding of streptavidin to biotinylated surfaces. As shown in **Fig. 6.11**, all bilayers lacking a biotin-linked lipid analog resulted in a negligible fluorescence response. In contrast, bilayers containing 10 mol% DSPE-PEG-biotin demonstrated a clear response from specific binding of SA-633. Therefore, this data demonstrates the utility of PEGylated bilayers for reducing nonspecific adsorption of proteins to glass surface while maintaining the specific binding capabilities required for coatings in biosensor applications.

In order to further examine the potential of DSPE-PEG bilayer coatings for reducing nonspecific adsorption in label-free biosensors, a series of WGM microsphere resonators were treated with standard and PEGylated lipid blocking protocols then incubated with increasing concentrations of serum proteins. Several traditional methods and PEGylated lipid methods for reducing nonspecific adsorption were compared. These methods include no pretreatment, pre-incubation with Starting block solution, pre-incubation with serum, coating with a DPPC bilayer, coating with a 1% DSPE-PEG in DOPC bilayer, coating with a 5% DSPE-PEG in DOPC bilayer, coating with a 10% DSPE-PEG in DOPC bilayer, and coating with a 25% DSPE-PEG in DOPC bilayer. The resulting binding curve of serum protein to these treated glass surfaces measured by WGM resonance response is shown in **Fig. 6.12**. The data displayed in **Fig. 6.12** represents the average response from at least 4 WGM resonators for each type of surface treatment with the standard deviation displayed with the error bars. For clarity, the same data is displayed in **Fig. 6.13**, where bilayer blocking methods are compared in the upper graph and traditional methods are compared to the optimal bilayer method compared in the lower graph.

As discussed in **Chapter 5**, WGM resonators are label-free refractive index sensors which function through the continuous total internal reflection of discrete wavelengths of light in a circular dielectric medium. Light evanescently coupled into these WGM resonators can be

efficiently trapped when the wavelength of light is an integer multiple of the distance circumnavigated around the resonator [2, 17, 71-74]. Under these conditions, constructive interference leads to WGM resonances given by:

$$\lambda_r = \frac{2\pi r n_{eff}}{m} \qquad \textbf{Eq. 6.1}$$

where $\lambda_r$ is the resonant wavelength, r is the radius of the resonator, $n_{eff}$ is the effective refractive index, and m is an integer that indexes the mode number [72, 73]. The key relationship which is exploited for sensing purposes is the dependence of the resonant wavelength on the effective refractive index at the resonator surface. Due to this relationship, binding events resulting in changes in local refractive index can be detected through measuring shifts in the WGM resonant wavelength.

For bioassays, binding events of proteins and other biological material to the sensor increases the local refractive at resonator surface and shifts the resonant wavelength to longer wavelengths. However, it should be noted that increasing protein concentration results in a corresponding increase of the refractive index of the bulk solution as well. Therefore, the WGM response data presented in **Figs. 6.12** and **6.13** is plotted as a function of the bulk refractive index due to increasing serum protein concentration. As expected, each sample of microsphere resonators responds to increasing bulk refractive index changes through a shift to longer resonant wavelengths. Furthermore, this data shows that the WGM response of unblocked microspheres and several of the treated microspheres is non-linear with respect to bulk refractive index changes. The drastic initial shifts in WGM resonant wavelength observed for these samples is, therefore, explained by nonspecific adsorption of protein to resonator surfaces resulting in local refractive index changes as opposed to bulk refractive index changes. Thus,

the data displayed in **Fig 6.12** reveals a clear reduction in serum protein nonspecific adsorption for several of the blocking protocols employed in this study relative to untreated samples.

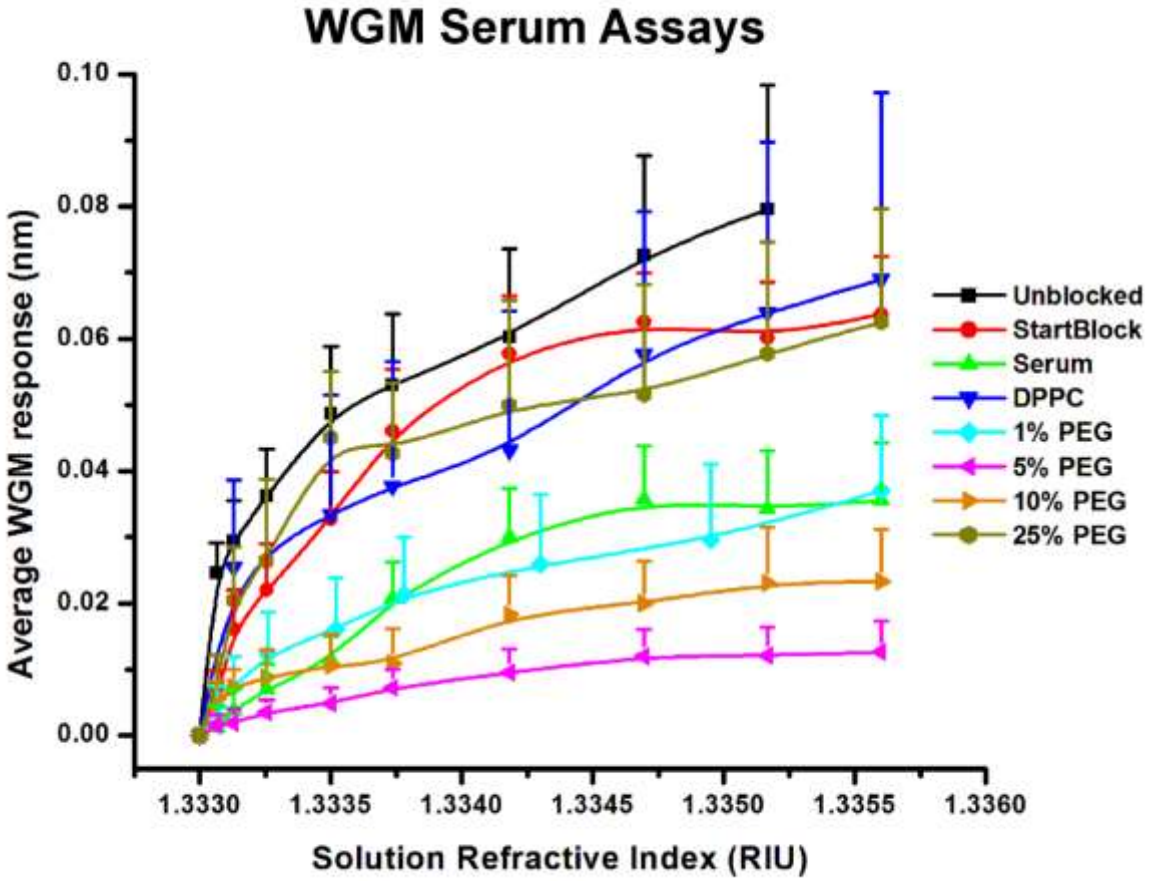


**Figure 6.12** – Binding curves of nonspecific adsorption of serum proteins to glass surfaces are measured with WGM microspheres resonators. Several protocols for reducing nonspecific adsorption are compared including unblocked (black squares, N=9), pre-incubation with Starting block solution (red circles, N=9), pre-incubation with serum (upward green triangles, N=4), DPPC bilayer coating (downward blue triangles, N=7), 1% DSPE-PEG in DOPC bilayer coating (teal diamonds, N=6), 5% DSPE-PEG in DOPC bilayer coating (leftward pink triangles, N=12), 10% DSPE-PEG in DOPC bilayer coating (rightward orange triangle, N=8), and 25% DSPE-PEG in DOPC bilayer coating (gold circles, N=9). These results demonstrate bilayers containing ~5% PEG are the optimal coating tested for reducing nonspecific adsorption in biosensing applications.

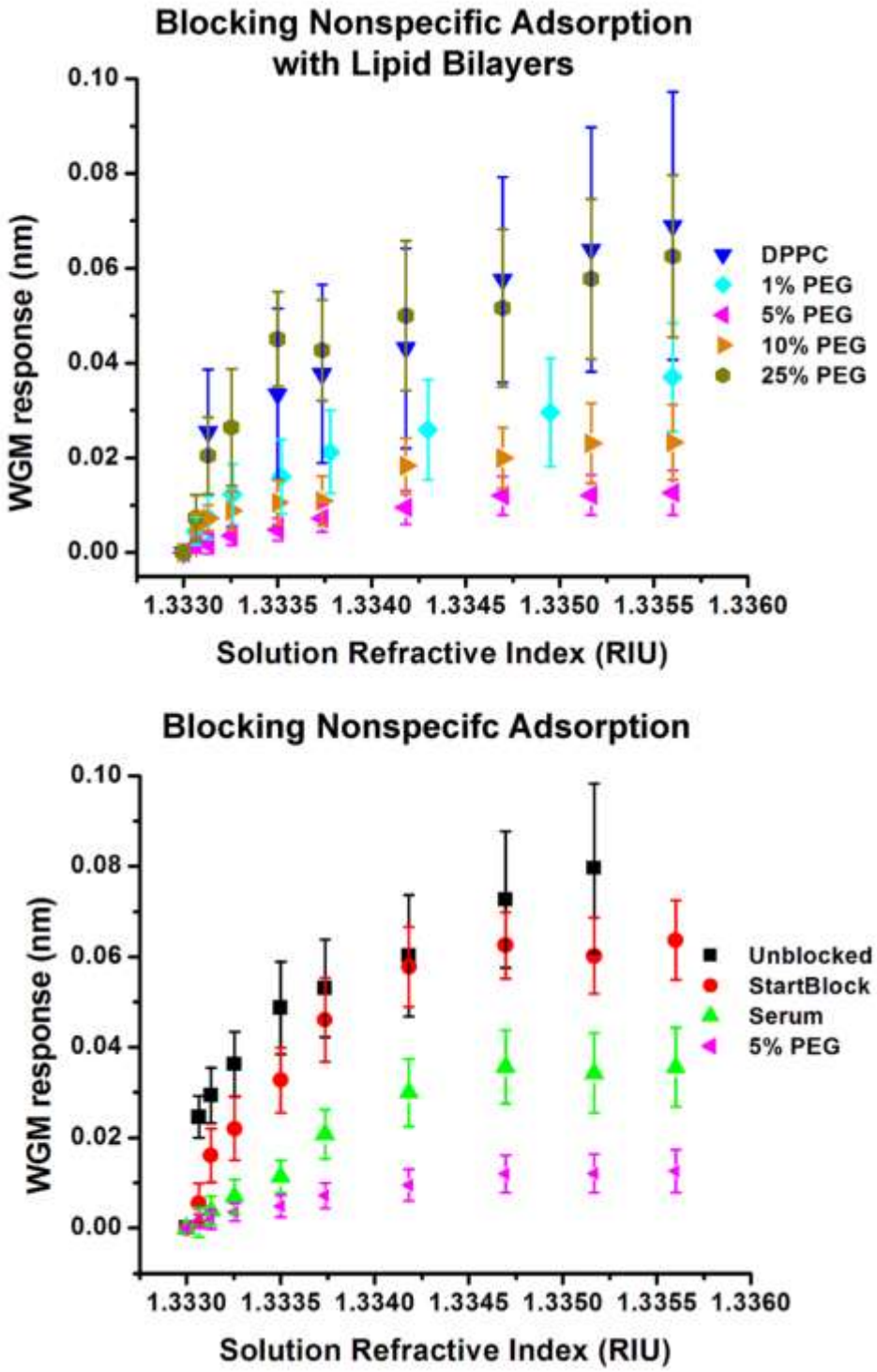


**Figure 6.13** – Assays of WGM response to the presence of human serum proteins. For clarity the binding curves shown in **Fig. 6.12** are categorized above. A comparison of PEGylated bilayer methods (top) demonstrates the 5% DSPE-PEG in DOPC at 30 mN/m results in the greatest reduction of nonspecific adsorption of serum proteins. Furthermore, this PEGylated bilayer is also shown to reduce nonspecific binding to WGM resonators more effectively than traditional blocking methods (bottom).

As shown in **Fig. 6.13 (top)**, various LB/LS bilayer lipid coatings for blocking nonspecific adsorption of serum proteins are compared. As mentioned above, each of the WGM resonators responses to increases in bulk refractive index through shifts to longer resonant wavelengths regardless of surface treatment. However, WGM responses from resonators with certain bilayer coating suggest evidence of greater nonspecific adsorption to serum proteins to the sensor surfaces than others. For example, WGM sensors with DPPC and DOPC/DSPE-PEG (75:25) bilayer coatings indicate a significantly greater response to refractive index increases than WGM sensors with DOPC/DSPE-PEG (95:5) and DOPC/DSPE-PEG (90:10) bilayer coatings. Evidence of nonspecific binding in these WGM sensors with DPPC and DOPC/DSPE-PEG (75:25) bilayer coatings is suggested by the non-linear and greater overall response of WGM sensors. With these criteria, the data displayed in **Fig. 6.13 (top)** suggests DOPC/DSPE-PEG (95:5) is the optimal bilayer composition tested for reducing nonspecific adsorption for WGM glass microspheres.

**Figure 6.13 (bottom)** compares the optimal LB/LS bilayer coating, DOPC/DSPE-PEG (95:5) at 30 mN/m, to traditional methods for blocking nonspecific adsorption. From the WGM response to increasing serum concentrations, the PEGylated bilayer coating demonstrates a significantly greater reduction in nonspecific adsorption of serum proteins to WGM sensor surfaces. Again, this can be observed through the non-linear and greater overall response of WGM sensors pretreated with StartingBlock and serum protein solutions. Therefore, these results further illustrate the potential of PEG coatings for limiting nonspecific adsorption, which is a vital attribute for label-free biosensor approaches.

## Conclusions

With the increasing popularly of label-free biosensors approaches for various research applications, there has been further interest to develop more efficient sensing surfaces. For immunoassay approaches this translates to developing immobilization protocols which maintain antibody activity upon immobilization to sensor surfaces. An additional requirement which is vital for label-free sensors, in particular, is to simultaneously reduce nonspecific adsorption to these sensor surfaces in order to ensure specific detection of the analyte of interest. Therefore, here we have presented several studies to further address these problematical issues.

Antibody orientation has long been of interest for immunoassay techniques as antibody activity can be inhibited if the active site of the antibody is hidden from the sample matrix. Therefore, various immobilization protocols have been developed to promote active antibody orientations. Unfortunately, there is a lack of techniques which can provide accurate measurements of immobilized antibody orientation which can be related to antibody activity at relevant sample conditions. Therefore, here the preliminary findings from a single molecule fluorescence approach for measuring antibody orientation are presented. While the 4-4-20/Fluo-3 model system requires further modification and control studies to allow for the correlation of fluorophore to antibody orientation, the findings from these studies demonstrate the potential utility of the defocused single molecule imaging approach for measuring antibody orientations in relevant sample conditions. These studies have shown a difference in observed orientations for antibodies immobilized through physical adsorption and Protein A affinity in dry samples. Additionally, these studies have demonstrated the ability to measure antibody orientations of samples in buffer, which is significantly more relevant for bioassay applications. Furthermore, the ability to observe immobilized antibodies in buffer has also allowed us to capture the dynamic motion of these antibodies with time-lapsed imaging. Therefore, the

defocused single molecule imaging approach should be a promising tool for further investigation of immobilized antibody orientations and activity.

Nonspecific adsorption in another common obstacle faced by immunoassay techniques, and is a particularly important issue for label-free biosensors. The primary of advantage provided by label-free biosensors is that the attachment of a label is not required for analyte detection. However, this attribute is also related to one of the most difficult challenges faced by label-free approaches. Any binding event, specific or not, can elicit a response from the label-free sensor. Therefore, it is imperative to promote specific binding interactions while eliminating nonspecific ones. The largest culprit in terms of nonspecific binding events is a result of nonspecific adsorption of proteins to the sensor surface. As such, numerous blocking protocols have been developed and tested to reduce nonspecific absorption. One of the more promising approaches has utilized self-assembled PEG polymer coatings. Other approached have shown that packing density of PEG monomers within these coatings to be a crucial variable which can augment the blocking efficiency of these coatings. While packing density within the PEG polymers is difficult to control with self-assembled monolayer methods, Langmuir deposition methods provide simple control of monomer surface density though surface pressure control during deposition.

Therefore, here we have presented a method for creating controllable PEG coating for biosensor surfaces by LB/LS bilayer deposition of PEGylated lipid conjugates. Uniform surface coverage of the PEG coatings was confirmed with fluorescence imaging studies of membrane microstructure. Fluorescence binding assays were utilized to simultaneously tests specific and nonspecific binding to bilayer treated sensors with labeled proteins. Finally, WGM assays of nonspecific adsorption of serum proteins were used to evaluate various membrane and traditional methods for blocking nonspecific adsorption. These results suggest there is an optimal packing density of PEG monomer for blocking nonspecific adsorption which can be

achieved with a DOPC/DSPE-PEG (95:5) bilayer deposited at 30 mM/m. In conclusion, the LB/LS method provides considerable promise for creating optimized PEG coating for label-free sensor applications.

## 6.5 - References


1. Lequin, R. M. 2005. Enzyme Immunoassay (EIA)/Enzyme-Linked Immunosorbent Assay (ELISA). Clinical Chemistry 51:2415-2418.

2. Washburn, A. L., L. C. Gunn, and R. C. Bailey. 2009. Label-Free Quantitation of a Cancer Biomarker in Complex Media Using Silicon Photonic Microring Resonators. Anal Chem 81:9499-9506.

3. Luppa, P. B., L. J. Sokoll, and D. W. Chan. 2001. Immunosensors—principles and applications to clinical chemistry. Clinica Chimica Acta 314:1-26.

4. Gerard, M., A. Chaubey, and B. D. Malhotra. 2002. Application of conducting polymers to biosensors. Biosensors and Bioelectronics 17:345-359.

5. Iqbal, S. S., M. W. Mayo, J. G. Bruno, B. V. Bronk, C. A. Batt, and J. P. Chambers. 2000. A review of molecular recognition technologies for detection of biological threat agents. Biosensors and Bioelectronics 15:549-578.

6. Lim, D. V., J. M. Simpson, E. A. Kearns, and M. F. Kramer. 2005. Current and Developing Technologies for Monitoring Agents of Bioterrorism and Biowarfare. Clinical Microbiology Reviews 18:583-607.

7. Wild, D. 2001. The Immunoassay handbook. Nature Pub. Group, London.

8. Huckabay, H. A., S. M. Wildgen, and R. C. Dunn. 2013. Label-free detection of ovarian cancer biomarkers using whispering gallery mode imaging. Biosensors & bioelectronics 45:223-229.

9. Song, S., L. Wang, J. Li, C. Fan, and J. Zhao. 2008. Aptamer-based biosensors. TrAC Trends in Analytical Chemistry 27:108-117.

10. Vollmer, F., S. Arnold, D. Braun, I. Teraoka, and A. Libchaber. 2003. Multiplexed DNA Quantification by Spectroscopic Shift of Two Microsphere Cavities. Biophysical Journal 85:1974-1979.

11. Tyagi, S., and F. R. Kramer. 1996. Molecular beacons: Probes that fluoresce upon hybridization. Nature biotechnology 14:303-308.

12. Haupt, K., and K. Mosbach. 2000. Molecularly Imprinted Polymers and Their Use in Biomimetic Sensors. Chemical reviews 100:2495-2504.

13. Valdes, R., S. A. Jortani, and M. Gheorghiade. 1998. Standards of laboratory practice: cardiac drug monitoring. Clinical Chemistry 44:1096-1109.

14. Anker, J. N., W. P. Hall, O. Lyandres, N. C. Shah, Z. Jing, and R. P. Van Duyne. 2008. Biosensing with plasmonic nanosensors. Nature Materials 7:442-453.

15. Homola, J. 2008. Surface Plasmon Resonance Sensors for Detection of Chemical and Biological Species. Chemical reviews 108:462-493.

16. Marx, K. A. 2003. Quartz Crystal Microbalance: A Useful Tool for Studying Thin Polymer Films and Complex Biomolecular Systems at the Solution−Surface Interface. Biomacromolecules 4:1099-1120.

17. Luchansky, M. S., and R. C. Bailey. 2011. High-Q Optical Sensors for Chemical and Biological Analysis. Anal Chem 84:793-821.

18. Huckabay, H. A., and R. C. Dunn. 2011. Whispering gallery mode imaging for the multiplexed detection of biomarkers. Sensor Actuat B-Chem 160:1262-1267.

19. Herron JN, W. H.-K., Janatová V, Durtschi JD, Caldwell KD, Christensen DA, Chang I-N, Huang S-C. 2003. Orientation and Activity of Immobilized Antibodies. In Biopolymers at Interfaces. M. M, editor. Marcel Dekker, New York. 115-163.

20. Jung, Y., J. Y. Jeong, and B. H. Chung. 2008. Recent advances in immobilization methods of antibodies on solid supports. Analyst 133:697-701.

21. Zhu, H. Y., P. S. Dale, C. W. Caldwell, and X. D. Fan. 2009. Rapid and Label-Free Detection of Breast Cancer Biomarker CA15-3 in Clinical Human Serum Samples with Optofluidic Ring Resonator Sensors. Anal Chem 81:9858-9865.

22. Seurynck-Servoss, S. L., C. L. Baird, K. D. Rodland, and R. C. Zangar. 2007. Surface chemistries for antibody microarrays. Front Biosci-Landmrk 12:3956-3964.

23. Sigma-Aldrich. ELISA protocols.

24. Štefanová, I., V. Hořejši, I. J. Ansotegui, W. Knapp, and H. Stockinger. 1991. GPI-Anchored Cell-Surface Molecules Complexed to Protein Tyrosine Kinases. Science 254:1016-1019.

25. Vijayendran, R. A., and D. E. Leckband. 2000. A Quantitative Assessment of Heterogeneity for Surface-Immobilized Proteins. Anal Chem 73:471-480.

26. Lu, B., M. R. Smyth, and R. O'Kennedy. 1996. Tutorial review. Oriented immobilization of antibodies and its applications in immunoassays and immunosensors. Analyst 121:29R-32R.

27. Kausaite-Minkstimiene, A., A. Ramanaviciene, J. Kirlyte, and A. Ramanavicius. 2010. Comparative Study of Random and Oriented Antibody Immobilization Techniques on the Binding Capacity of Immunosensor. Anal Chem 82:6401-6408.

28. Xu, H., J. R. Lu, and D. E. Williams. 2006. Effect of Surface Packing Density of Interfacially Adsorbed Monoclonal Antibody on the Binding of Hormonal Antigen Human Chorionic Gonadotrophin. The Journal of Physical Chemistry B 110:1907-1914.

29. Xu, H., X. Zhao, C. Grant, J. R. Lu, D. E. Williams, and J. Penfold. 2006. Orientation of a Monoclonal Antibody Adsorbed at the Solid/Solution Interface: A Combined Study Using Atomic Force Microscopy and Neutron Reflectivity. Langmuir 22:6313-6320.

30. Xu, H., X. Zhao, J. R. Lu, and D. E. Williams. 2007. Relationship between the Structural Conformation of Monoclonal Antibody Layers and Antigen Binding Capacity. Biomacromolecules 8:2422-2428.

31. San Paulo, A., and R. García. 2000. High-Resolution Imaging of Antibodies by Tapping-Mode Atomic Force Microscopy: Attractive and Repulsive Tip-Sample Interaction Regimes. Biophysical Journal 78:1599-1605.

32. Wang, H., D. G. Castner, B. D. Ratner, and S. Jiang. 2004. Probing the Orientation of Surface-Immobilized Immunoglobulin G by Time-of-Flight Secondary Ion Mass Spectrometry. Langmuir 20:1877-1887.

33. Huckabay, H. A., and R. C. Dunn. 2011. Hydration Effects on Membrane Structure Probed by Single Molecule Orientations. Langmuir 27:2658-2666.

34. Armendariz, K. P., and R. C. Dunn. 2013. Ganglioside influence on phospholipid films investigated with single molecule fluorescence measurements. J Phys Chem B 117:7959-7966.

35. Armendariz, K. P., H. A. Huckabay, P. W. Livanec, and R. C. Dunn. 2012. Single molecule probes of membrane structure: Orientation of BODIPY probes in DPPC as a function of probe structure. Analyst 137:1402-1408.

36. Livanec, P. W., and R. C. Dunn. 2008. Single-molecule probes of lipid membrane structure. Langmuir 24:14066-14073.

37. Livanec, P. W., H. A. Huckabay, and R. C. Dunn. 2009. Exploring the effects of sterols in model lipid membranes using single-molecule orientations. J Phys Chem B 113:10240-10248.

38. Song, K. C., P. W. Livanec, J. B. Klauda, K. Kuczera, R. C. Dunn, and W. Im. 2011. Orientation of fluorescent lipid analogue BODIPY-PC to probe lipid membrane properties: insights from molecular dynamics simulations. J Phys Chem B 115:6157-6165.

39. Johnson, I. a. S. M. 2010. The Molecular Probes Handbook - Chapter 1 - Fluorophores and Their Amine-Reactive Derivatives. 11th ed.:11-96.

40. Griffin, B. A., S. R. Adams, and R. Y. Tsien. 1998. Specific covalent labeling of recombinant protein molecules inside live cells. Science 281:269-272.

41. Griffin, B. A., S. R. Adams, J. Jones, and R. Y. Tsien. 2000. Fluorescent labeling of recombinant proteins in living cells with FlAsH. Method Enzymol 327:565-578.

42. Martin, B. R., B. N. Giepmans, S. R. Adams, and R. Y. Tsien. 2005. Mammalian cell-based optimization of the biarsenical-binding tetracysteine motif for improved fluorescence and affinity. Nature biotechnology 23:1308-1314.

43. Marek, K. W., and G. W. Davis. 2002. Transgenically Encoded Protein Photoinactivation (FlAsH-FALI): Acute Inactivation of Synaptotagmin I. Neuron 36:805-813.

44. Tour, O., R. M. Meijer, D. A. Zacharias, S. R. Adams, and R. Y. Tsien. 2003. Genetically targeted chromophore-assisted light inactivation. Nature biotechnology 21:1505-1508.

45. Tonegawa, S. 1983. Somatic generation of antibody diversity. Nature 302:575-581.

46. Clackson, T., H. R. Hoogenboom, A. D. Griffiths, and G. Winter. 1991. Making antibody fragments using phage display libraries. Nature 352:624-628.

47. Knappik, A., L. Ge, A. Honegger, P. Pack, M. Fischer, G. Wellnhofer, A. Hoess, J. Wölle, A. Plückthun, and B. Virnekäs. 2000. Fully synthetic human combinatorial antibody libraries (HuCAL) based on modular consensus frameworks and CDRs randomized with trinucleotides. J Mol Biol 296:57-86.

48. Bedzyk, W. D., K. M. Weidner, L. K. Denzin, L. S. Johnson, K. D. Hardman, M. W. Pantoliano, E. D. Asel, and E. W. Voss, Jr. 1990. Immunological and structural characterization of a high affinity anti-fluorescein single-chain antibody. J Biol Chem 265:18615-18620.

49. Johnson, I. a. S. M. 2010. The Molecular Probes Handbook - Section 7.2 Anti-dye and Anti-Hapten Antibodies.272-276.

50. Lopatin, D. E., and E. W. Voss, Jr. 1971. Fluorescein. Hapten and antibody active-site probe. Biochemistry 10:208-213.

51. Lukacs, G. L., O. D. Rotstein, and S. Grinstein. 1991. Determinants of the phagosomal pH in macrophages. In situ assessment of vacuolar H(+)-ATPase activity, counterion conductance, and H+ "leak". Journal of Biological Chemistry 266:24540-24548.

52. Watt, R. M., and E. W. Voss, Jr. 1977. Mechanism of quenching of fluorescein by anti-fluorescein IgG antibodies. Immunochemistry 14:533-551.

53. Whitlow, M., A. J. Howard, J. F. Wood, E. W. Voss, Jr., and K. D. Hardman. 1995. 1.85 A structure of anti-fluorescein 4-4-20 Fab. Protein engineering 8:749-761.

54. Bedzyk, W. D., J. N. Herron, A. B. Edmundson, and E. W. Voss, Jr. 1990. Active site structure and antigen binding properties of idiotypically cross-reactive anti-fluorescein monoclonal antibodies. J Biol Chem 265:133-138.

55. Boder, E. T., K. S. Midelfort, and K. D. Wittrup. 2000. Directed evolution of antibody fragments with monovalent femtomolar antigen-binding affinity. Proc Natl Acad Sci U S A 97:10701-10705.

56. Swindlehurst, C. A., and E. W. Voss, Jr. 1991. Fluorescence measurements of immune complexes of Mab 4-4-20 with isomeric haptens. Biophys J 59:619-628.

57. Denzin, L. K., G. A. Gulliver, and E. W. Voss, Jr. 1993. Mutational analysis of active site contact residues in anti-fluorescein monoclonal antibody 4-4-20. Molecular immunology 30:1331-1345.

58. Herron, J. N., X. M. He, M. L. Mason, E. W. Voss, Jr., and A. B. Edmundson. 1989. Three-dimensional structure of a fluorescein-Fab complex crystallized in 2-methyl-2,4-pentanediol. Proteins 5:271-280.

59. Scientific, T. Blocking and Washing.

60. Silin, V., H. Weetall, and D. J. Vanderah. 1997. SPR Studies of the Nonspecific Adsorption Kinetics of Human IgG and BSA on Gold Surfaces Modified by Self-Assembled Monolayers (SAMs). Journal of Colloid and Interface Science 185:94-103.

61. Senaratne, W., L. Andruzzi, and C. K. Ober. 2005. Self-Assembled Monolayers and Polymer Brushes in Biotechnology: Current Applications and Future Perspectives. Biomacromolecules 6:2427-2448.

62. Du, H., P. Chandaroy, and S. W. Hui. 1997. Grafted poly-(ethylene glycol) on lipid surfaces inhibits protein adsorption and cell adhesion. Biochimica et Biophysica Acta (BBA) - Biomembranes 1326:236-248.

63. Avanti Polar Lipid, I. 2013. Avanti Lipodomics Products.

64. Elbert, D. L., and J. A. Hubbell. 1996. Surface Treatments of Polymers for Biocompatibility. Annual Review of Materials Science 26:365-294.

65. Gudipati, C. S., C. M. Greenlief, J. A. Johnson, P. Prayongpan, and K. L. Wooley. 2004. Hyperbranched fluoropolymer and linear poly(ethylene glycol) based amphiphilic crosslinked networks as efficient antifouling coatings: An insight into the surface compositions, topographies, and morphologies. Journal of Polymer Science Part A: Polymer Chemistry 42:6193-6208.

66. Halperin, A., G. Fragneto, A. Schollier, and M. Sferrazza. 2007. Primary versus ternary adsorption of proteins onto PEG brushes. Langmuir 23:10603-10617.

67. Zhu, B., T. Eurell, R. Gunawan, and D. Leckband. 2001. Chain-length dependence of the protein and cell resistance of oligo(ethylene glycol)-terminated self-assembled monolayers on gold. Journal of biomedical materials research 56:406-416.

68. Kim, D. C., K. P. Armendariz, and R. C. Dunn. 2013. Integration of microsphere resonators with bioassay fluidics for whispering gallery mode imaging. Analyst 138:3189-3195.

69. Marsh, D., R. Bartucci, and L. Sportelli. 2003. Lipid membranes with grafted polymers: physicochemical aspects. Biochim Biophys Acta 1615:33-59.

70. Inc., L. T. Fluorescence SpectraViewer.

71. Vollmer, F., and S. Arnold. 2008. Whispering-gallery-mode biosensing: label-free detection down to single molecules. Nature Methods 5:591-596.

72. Gorodetsky, M. L., and V. S. Ilchenko. 1999. Optical microsphere resonators: optimal coupling to high-Q whispering-gallery modes. J. Opt. Soc. Am. B 16:147-154.

73. Knight, J. C., G. Cheung, F. Jacques, and T. A. Birks. 1997. Phase-matched excitation of whispering-gallery-mode resonances by a fiber taper. Opt. Lett. 22:1129-1131.

74. Vollmer, F., and L. Yang. 2012. Label-free detection with high-Q microcavities: a review of biosensing mechanisms for integrated devices. In Nanophotonics. 267.

# Chapter 7 – Future Directions

## 7.1 – Introduction

As shown in chapters 3 and 4 and previous studies of single molecule orientations, acyl-linked fluorescent lipid analogs have proven to be a useful tool for investigating molecular level structure in model membranes. These studies have demonstrated that this technique can elucidate structural perturbations due to changes in surface pressure, the addition of additives such as cholesterol and ganglioside GM1, and ambient humidity levels[1-6]. The study in Chapter 4 presents evidence for the formation of nanometric domains resembling lipid rafts in binary DPPC/GM1 monolayers. It would be advantageous to employ more complex and more accurate raft model systems. Additionally, the study of these complex lipid raft model systems would be aided by utilizing a fluorescent lipid analog which can report structural perturbations from within condensed membrane regions. In addition to studies of membrane structure, single molecule orientation studies of antibody measurements would be improved with further studies of the 4-4-20/Fluo-3 complex. Once optimized, this antibody system would be able to be implemented to assess the relationship between antibody orientation and binding efficiency for various immobilization chemistries.

In addition to these single molecule structure studies, further advancements of lipid coatings for sensor surfaces could provide several advantages. As established in chapters 5 and 6, Langmuir-Blodgett/Langmuir-Schaffer (LB/LS) lipid membranes demonstrated the ability to incorporate recognition elements for the specific detection of analytes[7]. Furthermore, lipid bilayers containing polyethylene glycol (PEG) functionalized lipids have been shown to reduce nonspecific binding to sensor surfaces. Therefore, combining these attributes provides tremendous promise for the development of a general blocking protocol which can

simultaneously reduce nonspecific binding and incorporate detection elements of the users' choosing.

### 7.2 – Lipid Raft Models and New Single Molecule Probes

The results from single molecule studies of DPPC/GM1 monolayers in Chapter 4 suggest the formation of nanometric domains, which cannot be resolved by bulk fluorescence microscopy. Ultimately, these findings suggest the need for further investigation of membrane systems which more accurately model lipid rafts. Traditionally, models of lipid rafts employ lipid mixtures containing cholesterol and sphingolipids, as these lipid components are enriched in detergent resistant membrane fractions[8, 9]. Therefore, single molecule orientation studies of lipid structure should be implemented with model membrane systems which contain biologically relevant concentrations of major membrane components, such as DPPC, DOPC, cholesterol, and sphingomyelin. While further single molecule orientation studies of more complicated lipid mixtures should provide greater understanding of membrane molecular level structure, it is important to gradually build up the complexity of these model systems in order to understand the structural influence of each membrane component. Therefore, our previous single molecule studies of cholesterol and GM1 influence on DPPC membrane structure provides a foundation for studying these more complicated lipid raft models[1, 5]. In addition to investigating more complex models of lipid rafts, it would be informative to utilize lipid raft models which include raft proteins, such as T-cell antigen receptors or glycosylphosphatidylinositol (GPI) anchored proteins. These models would provide insight as to whether the protein components of lipid rafts affect lipid structure throughout the membrane.

While more accurate lipid raft models will be an important part of understanding raft formation and structure, it is also important to consider the lipid probe employed to study these systems. As discussed in previous chapters, acyl-linked fluorescent lipid analogs have proven to be a useful tool for investigations of lipid structure within model membranes[1-6]. Similar to the majority of fluorescent lipid analogs, these probes preferentially partition with expanded, or more fluid, membrane phases. However, with the considerable interest in probing lipid raft structure, it would be advantageous to employ a single molecule probe which partitions within these condensed membrane regions. A probe partitioning with these condensed regions would offer greater sensitivity to raft formation as well as report structural perturbations from within lipid rafts. While, most fluorescent lipid analogs partition with expanded lipid phases, there are reports of a cholesterol analog with an attached BODIPY fluorophore that exhibits condensed phase partitioning[10]. The structure of the cholesterol-BODIPY probe is shown in **Fig. 7.1**. Condensed phase partitioning of this cholesterol-BODIPY probe is demonstrated by comparison to a well-known expanded phase lipid probe, Texas Red - dihexadecanoyl-phosphoethanolamine (TR-DHPE), shown in **Fig 7.2**. Therefore, a condensed phase probe for future single molecule orientation studies may be able to provide insight for a greater understanding of how individual raft components affect lipid raft formation and structure.

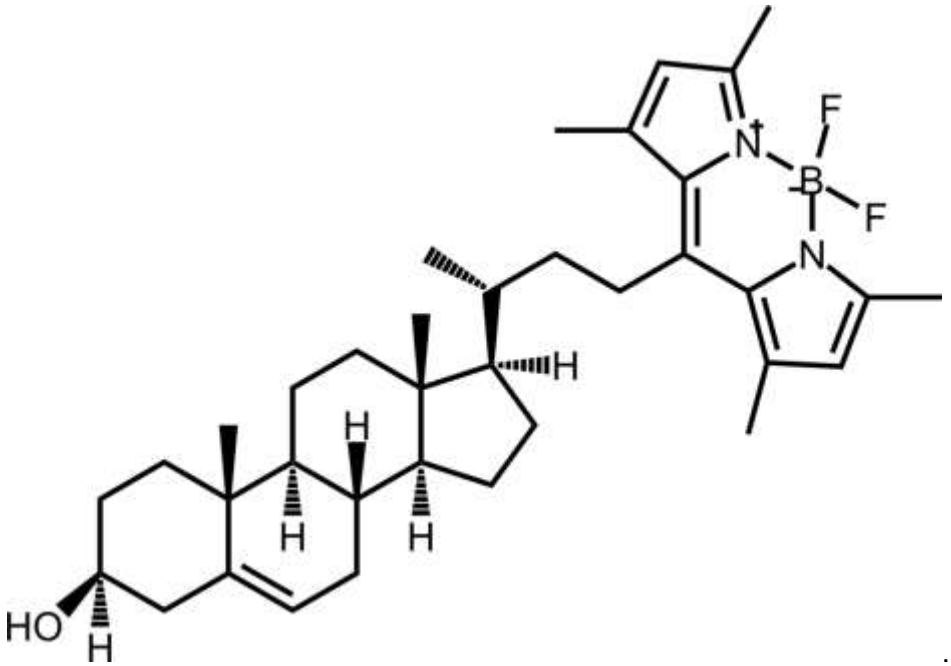


**Figure 7.1** – Chemical structure of a fluorescent cholesterol analog, cholesterol-BODIPY. This particular fluorescent lipid analog exhibits preferential partitioning for condensed lipid phases[11].

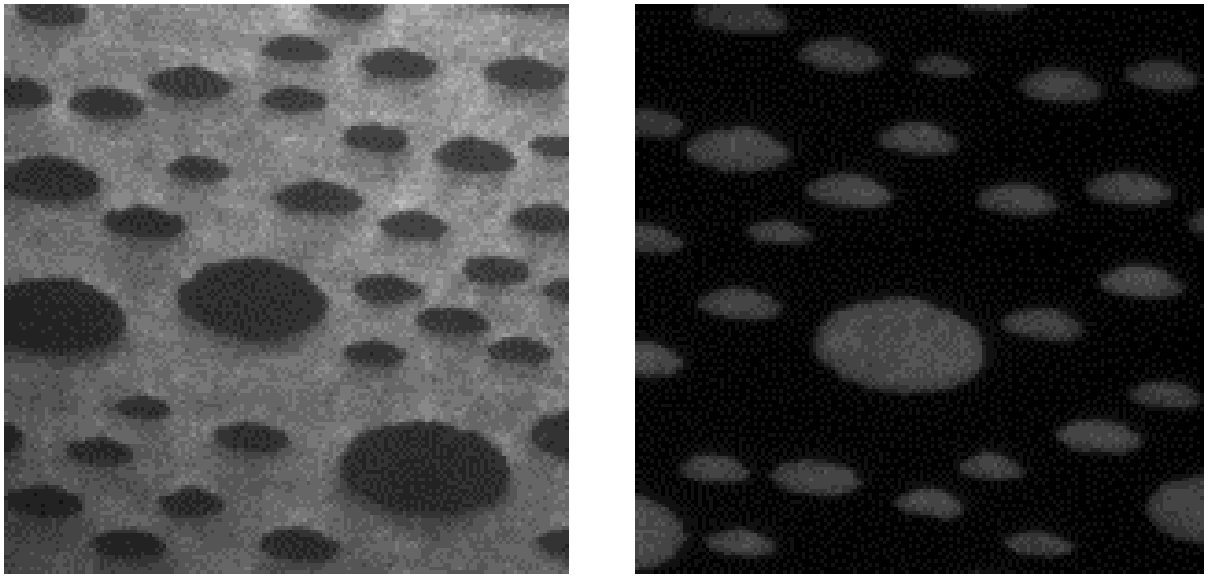

**Figure 7.2** – Fluorescence images of LB monolayers of DPPC / DOPC / cholesterol (1:1:0.1 mol%) containing a particular fluorescent lipid analog. The film on the left contains Texas Red – DHPE which marks the expanded (more fluid) phases within the monolayer. On the right, the film contains a BODIPY-linked cholesterol analog, shown in **Fig 7.1**, which partitions into condensed phases within the membrane. [Image captured by Brittany DeWitt, unpublished data]

### 7.3 – Antibody Orientations and Immobilization Strategies

As addressed in Chapter 6, there are several improvements and control studies needed in order to reliably correlate single molecule fluorescence emission patterns to overall antibody or Fab fragment orientation. The most relevant study needed is a crystal structure determination of the 4-4-20/Fluo-3 complex in order to allow for direct measurements of antibody orientations. With this information further single molecule orientation studies of immobilization protocols will be able to elucidate the link between antibody orientation and binding efficiency. Utilizing this system, traditional and new antibody immobilization protocols can be evaluated.

A recently developed immobilization which shows promise utilizes a conserved nucleotide binding site (NBS) in the Fab region on all antibody isotypes. This site, shown in **Fig. 7.3,** exhibits a low μM affinity for indole-3-butyric acid, which can be covalently cross-linked to the NBS through exposure to UV light[12]. Previous studies utilizing this immobilization procedure have demonstrated higher antibody activity and improved antigen detection efficiency[12]. Further studies of immobilization strategies utilizing this binding site may provide a general protocol for improved immunoassay performance.

There has been some past interest to employ Langmuir deposition techniques to control antibody orientations on substrates[13, 14]. However, a routine protocol promoting advantageous antibody orientations is currently unavailable. Using the NBS may provide a site of attachment for antibodies and lipid analogs. Covalently linking an antibody to a lipid analog would then provide a test system for orienting antibodies on sensor surfaces utilizing the control of surface density afforded by Langmuir deposition techniques. Therefore, we feel the development of lipid analog functionalized with indole-3-butyric acid would offer an exciting new tool for creating oriented antibody surfaces.

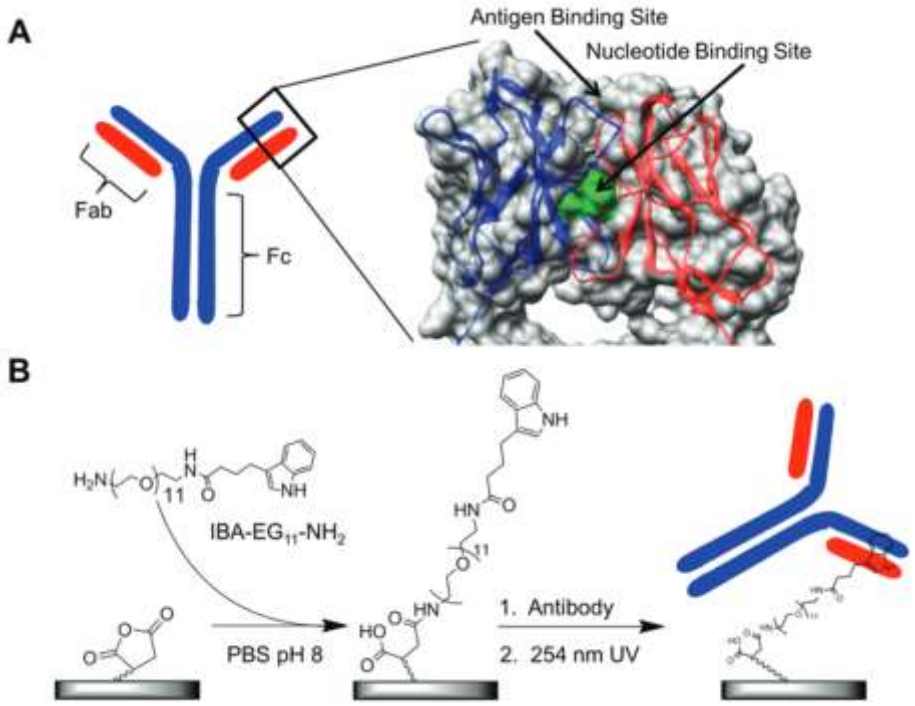


**Figure 7.3 –** The structure of the nucleotide binding site (NBS) within the Fab region of all antibody isotypes is shown above in A. This site has a low μM affinity for indole-3-butyric acid. By functionalizing a substrate with indole-3-butyric acid through a PEG linker, as shown in B, antibodies can be bound the substrate. These antibodies can then be covalently linked to substrate through this site by exposure to UV light. Figure used with permission from Ref #[12].

## 7.4 – Developing a General Protocol for Label-Free Sensor Coatings

The lipid coated sensor studies discussed in Chapters 5 and 6 have proved that LB/LS bilayer coatings are useful for both the specific detection of analytes and reducing nonspecific adsorption of serum proteins with PEGylated lipids. The natural extension from these studies is the development of a general protocol for sensor functionalization that incorporates both attributes afforded by bilayer coatings.

A general protocol can be accomplished with biotin terminated PEGylated lipids and streptavidin linked antibodies. As illustrated by the studies in Chapter 6, DOPC/DSPE-PEG bilayers deposited at 30 mN/m demonstrated a significant reduction in nonspecific adsorption of

serum proteins. Additionally, the fluorescence binding study within Chapter 6 demonstrated that specific binding to LB/LS PEGylated surfaces can be maintained. A scheme for specific detection of various analytes is illustrated in **Fig. 7.4**. In this scheme, biotin terminated PEGylated lipids are employed to both reduce nonspecific adsorption and provide a site for specific attachment of streptavidin. For detecting a specific analyte of interest, streptavidin linked antibodies are bound to the surface through biotin/streptavidin linkage. Commercially available labeling kits for streptavidin linkage allow any monoclonal antibody to be modified to specifically attach to the biotin terminated PEG surfaces[15]. With this scheme, the analyte of interest can be selectively detected by employing a monoclonal antibody with specificity for the analyte of interest.

The PEGylated lipid approach of generating active sensor surfaces discussed above provides other potential benefits as well. The approach outlined in **Fig. 7.4**, would allow label-free biosensors to not only measure analyte binding but also quantify antibody loading on sensor surfaces. This would provide an *in situ* tool for measuring the binding capacity of the attached antibodies. A further advantage potentially provided by this approach is reduced antibody denaturation upon immobilization. As discussed in Chapter 6, the two main reasons for loss of antibody activity upon immobilization are improper antibody orientation and denaturation[16-19]. Considering the main positive attribute provided by the PEGylated lipid approach is a reduction in nonspecific adsorption of proteins to the sensor surface, nonspecific adsorption resulting in antibody denaturation should also be reduced by this approach. Precedence for this approach has been previously reported through the use of a polymer coating to improve antibody activity[20]. Furthermore, this study demonstrated the use of Protein A on top to these polymer surface to properly orient antibodies toward the sample matrix and further increase antibody activity. Therefore, we feel the use of PEGylated lipid surfaces provides tremendous promise as coatings for future label-free biosensing applications.

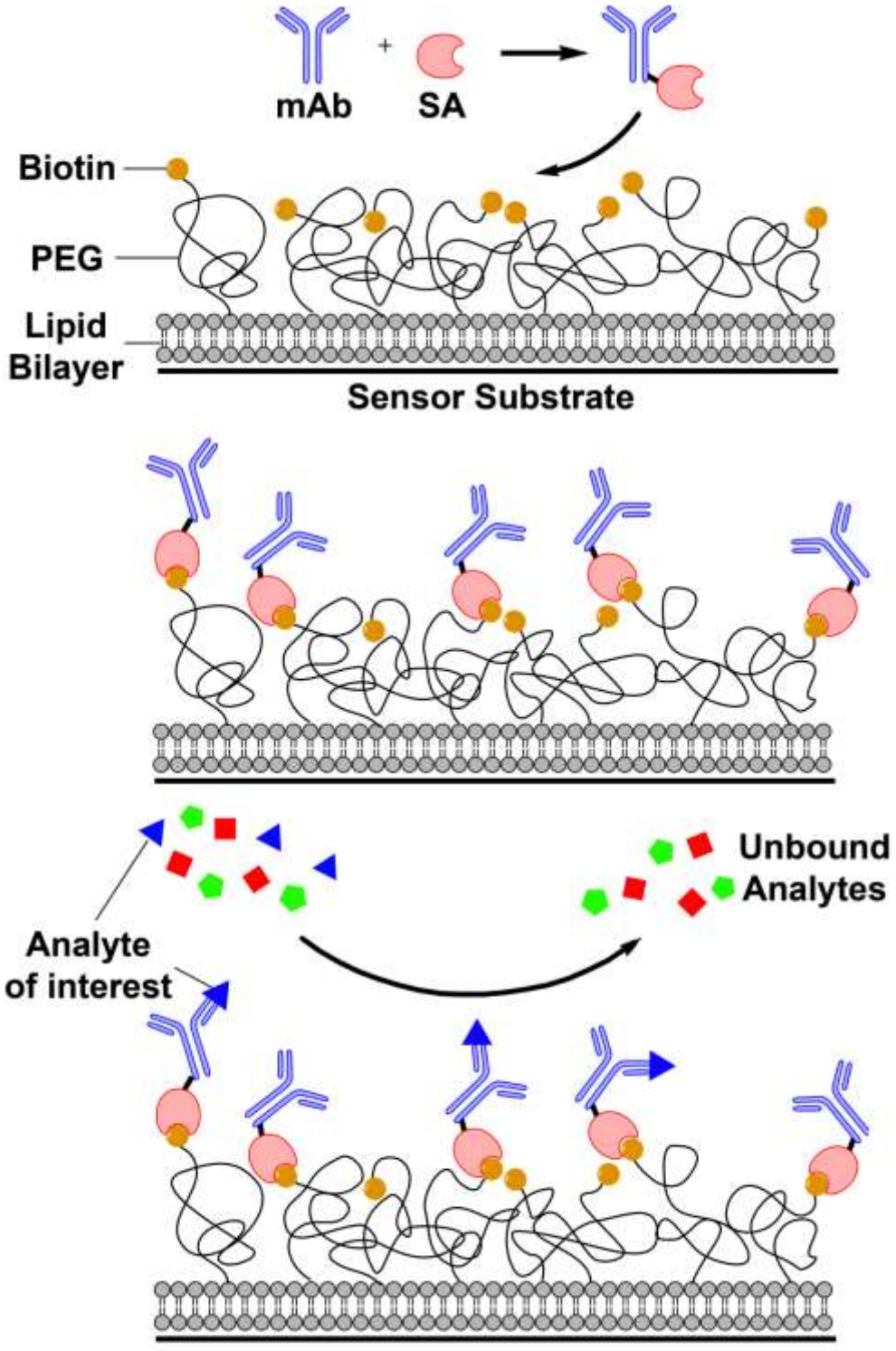


**Figure 7.3** – A general detection platform for reducing nonspecific adsorption and specific analyte detection for label-free biosensors. Monoclonal antibodies (mAbs) are covalently bound to streptavidin (SA), then incubated with the sensor surface which is coated in a biotin terminated PEG bilayer. Antibody/streptavidin complexes bound to the surface through biotin affinity are then used to specifically bind the analyte of interest.

## 7.5 - References


1. Armendariz, K. P., and R. C. Dunn. 2013. Ganglioside influence on phospholipid films investigated with single molecule fluorescence measurements. J Phys Chem B 117:7959-7966.

2. Armendariz, K. P., H. A. Huckabay, P. W. Livanec, and R. C. Dunn. 2012. Single molecule probes of membrane structure: Orientation of BODIPY probes in DPPC as a function of probe structure. Analyst 137:1402-1408.

3. Huckabay, H. A., and R. C. Dunn. 2011. Hydration Effects on Membrane Structure Probed by Single Molecule Orientations. Langmuir 27:2658-2666.

4. Livanec, P. W., and R. C. Dunn. 2008. Single-molecule probes of lipid membrane structure. Langmuir 24:14066-14073.

5. Livanec, P. W., H. A. Huckabay, and R. C. Dunn. 2009. Exploring the effects of sterols in model lipid membranes using single-molecule orientations. J Phys Chem B 113:10240-10248.

6. Song, K. C., P. W. Livanec, J. B. Klauda, K. Kuczera, R. C. Dunn, and W. Im. 2011. Orientation of fluorescent lipid analogue BODIPY-PC to probe lipid membrane properties: insights from molecular dynamics simulations. J Phys Chem B 115:6157-6165.

7. Kim, D. C., K. P. Armendariz, and R. C. Dunn. 2013. Integration of microsphere resonators with bioassay fluidics for whispering gallery mode imaging. Analyst 138:3189-3195.

8. Simons, K., and E. Ikonen. 1997. Functional rafts in cell membranes. Nature 387:569-572.

9. Sonnino, S., L. Mauri, V. Chigorno, and A. Prinetti. 2007. Gangliosides as components of lipid membrane domains. Glycobiology 17:1R-13R.

10. Ariola, F. S., Z. Li, C. Cornejo, R. Bittman, and A. A. Heikal. 2009. Membrane Fluidity and Lipid Order in Ternary Giant Unilamellar Vesicles Using a New Bodipy-Cholesterol Derivative. Biophysical Journal 96:2696-2708.

11. Avanti Polar Lipid, I. 2013. Avanti Lipodomics Products.

12. Alves, N. J., T. Kiziltepe, and B. Bilgicer. 2012. Oriented Surface Immobilization of Antibodies at the Conserved Nucleotide Binding Site for Enhanced Antigen Detection. Langmuir 28:9640-9648.

13. Dubrovsky, T., A. Tronin, and C. Nicolini. 1995. Determination of Orientation of the Igg Molecules in Immobilized Langmuir Monolayers by Means of Binding with Fragment Specific Antiimmunoglobulin Antibodies. Thin Solid Films 257:130-133.

14. Tronin, A., T. Dubrovsky, G. Radicchi, and C. Nicolini. 1996. Optimisation of IgG Langmuir film deposition for application as sensing elements. Sensor Actuat B-Chem 34:276-282.

15. Abcam. Streptavidin Conjugation Kit.

16. Jung, Y., J. Y. Jeong, and B. H. Chung. 2008. Recent advances in immobilization methods of antibodies on solid supports. Analyst 133:697-701.

17. Wild, D. 2001. The Immunoassay handbook. Nature Pub. Group, London.

18. Luppa, P. B., L. J. Sokoll, and D. W. Chan. 2001. Immunosensors—principles and applications to clinical chemistry. Clinica Chimica Acta 314:1-26.

19. Seurynck-Servoss, S. L., C. L. Baird, K. D. Rodland, and R. C. Zangar. 2007. Surface chemistries for antibody microarrays. Front Biosci-Landmrk 12:3956-3964.

20. Tajima, N., M. Takai, and K. Ishihara. 2011. Significance of Antibody Orientation Unraveled: Well-Oriented Antibodies Recorded High Binding Affinity. Anal Chem 83:1969-1976.